



Universiteit
Leiden
The Netherlands

Automated planning approaches for non-invasive cardiac valve replacement procedures from CT angiography

Gao, X.; Gao X.

Citation

Gao, X. (2017, November 7). *Automated planning approaches for non-invasive cardiac valve replacement procedures from CT angiography*. *ASCI dissertation series*. Retrieved from <https://hdl.handle.net/1887/57132>

Version: Not Applicable (or Unknown)

License: [Licence agreement concerning inclusion of doctoral thesis in the Institutional Repository of the University of Leiden](#)

Downloaded from: <https://hdl.handle.net/1887/57132>

Note: To cite this publication please use the final published version (if applicable).

Cover Page



Universiteit Leiden



The handle <http://hdl.handle.net/1887/57132> holds various files of this Leiden University dissertation

Author: Gao, Xinpei

Title: Automated planning approaches for non-invasive cardiac valve replacement procedures from CT angiography

Date: 2017-11-07

**Automated Planning Approaches for
Non-invasive Cardiac Valve Replacement
Procedures from CT Angiography**

**Xinpei Gao
2017**

Printed by: Ridderprint.nl

ISBN: 978-94-6299-722-6

@ 2017 Xinpei Gao, Leiden, the Netherlands. All rights reserved. No part of this publication may be reproduced or transmitted in any form or by any means, electronic or mechanical, including photocopying, recording or any information storage and retrieval system, without prior permission in writing from the copyright owner.

Automated Planning Approaches for Non-invasive Cardiac Valve Replacement Procedures from CT Angiography

Proefschrift

ter verkrijging van
de graad van Doctor aan de Universiteit Leiden,
op gezag van Rector Magnificus prof.mr. C.J.J.M. Stolker,
volgens besluit van het College voor Promoties
te verdedigen op dinsdag 7 november 2017
klokke 10:00 uur

door

Xinpei Gao

geboren te Jiangsu, China

in 1987

Promoters:

Prof.dr.ir. J.H.C. Reiber

Prof.dr.ir. B.P.F. Lelieveldt

Co-promotor:

Dr. ir. J. Dijkstra

Leden promotiecommissie:

Prof.dr. A. G. Webb

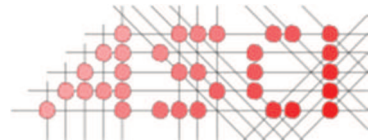
Prof.dr. T. Leiner

Utrecht University Medical Center

Dr. J.J. Wentzel

Erasmus Medical Center

This work was carried out in the ASCI graduate school.



Advanced School for Computing and Imaging

ASCI dissertation series number 379.

Financial support for the publication of this thesis was kindly provided by:

- ASCI research school,
- Bontius Stichting,
- Medis medical imaging system bv, Leiden.

Cover: Pictures from left to right, from top to bottom are all results obtained automatically by the methods in this thesis (1) segmentation of aortic root into LVOT (2) thoracic aorta quantification (3) aortic valve with segmented 2D contour (4) segmentation of aortic valve calcium (5) 3D segmentation from femoral arteries to aorta (6) aorta dilation quantification.

Cover by Xinpei Gao, layout by Hendrik Freling.

Contents

1 Introduction.....	1
2 Automatic Extraction of Arterial Centerline from Whole-body Computed Tomography Angiographic Dataset.....	17
3 Automatic Detection of Aorto-femoral Vessel Trajectory from Whole-body Computed Tomography Angiography Data Sets.....	25
4 Automatic Aortic Root Segmentation in CTA whole-body Dataset.....	43
5 Quantification of Aortic Annulus in Computed Tomography Angiography: Validation of a Fully Automatic Methodology.....	55
6 Fully automatic volume quantification of aortic valve calcium in coronary computed tomography angiography.....	73
7 Automated quantification of thoracic aorta dilatation on baseline and follow-up computed tomography angiography.....	85
8 Summary and conclusions.....	109
9 Samenvatting en conclusies.....	117
Bibliography.....	123
Acknowledgements.....	137
About the author.....	139
List of publications.....	141

1

Introduction

1.1 Cardiovascular system and diseases

Aortic root structure and disease

Structure

The heart is the engine of the circulatory system in the human body, and it pumps blood through the network of arteries, veins, and capillaries to transport oxygen and nutrients to the body and waste materials from the body (Hall 2015). The heart is constituted of the left heart (the left ventricle, the left atrium, the aortic valve and the mitral valve), and the right heart (the right ventricle, the right atrium, the tricuspid valve and the pulmonary valve)) as depicted in Figure 1.1.

The oxygen depleted blood flows from the venous system into the right atrium, descends into the right ventricle through the tricuspid valve. The tricuspid valve prevents the backflow of the blood into the right atrium. Through the contraction of the right ventricle it pushes the blood through the pulmonary valve into the pulmonary trunk, and the blood ends up in the lungs where it is recharged with oxygen. The pulmonary valve closes at the end of the contraction period of the right ventricle. Through the pulmonary veins, the oxygenated blood flows into the left atrium of the heart, and then through the mitral valve into the left ventricle. The mitral valve is closed when the left ventricle contracts. The contraction of the left ventricle pushes the blood into the arterial system through the opening of the aortic valve. As the left ventricle relaxes, the aortic valve closes due to the pressure from the aortic arch. During the cardiovascular cycle, the four valves function as one-way gates between the ventricles, the atria, the arterial system and the venous system.

The aortic root is the connecting part between the aorta and the left ventricle, defined by the sino-tubular ridge at the top and the bases of the valve leaflets at the bottom (Underwood et al. 2000). It is constituted of the following structures, which are also depicted in Figure 1.2: the sino-tubular junction is where the ascending aorta joins the Sinus of Valsalva (Ho 2009). The space between the valve leaflets and the bulb of the aortic wall is the aortic sinus, the attachment of the leaflet is the commissure, the area between the leaflets is the interleaflet triangle, and the aortic annulus is a ring constituted by three hinge points at the top of the aortic valve leaflets. Figure 1.3 shows an ex-vivo human aortic valve.

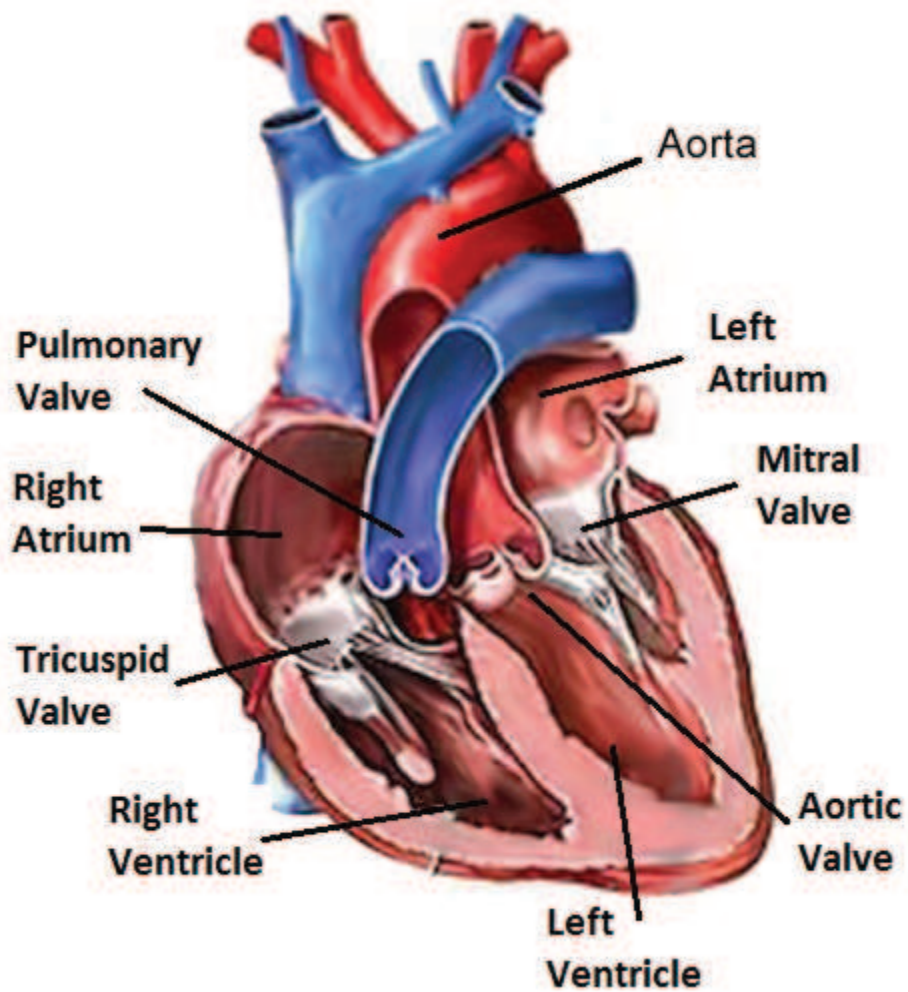


Figure 1.1 Heart anatomy (modified from source: <https://upload.wikimedia.org/wikipedia/commons/e/ee/Aorta.jpg>)

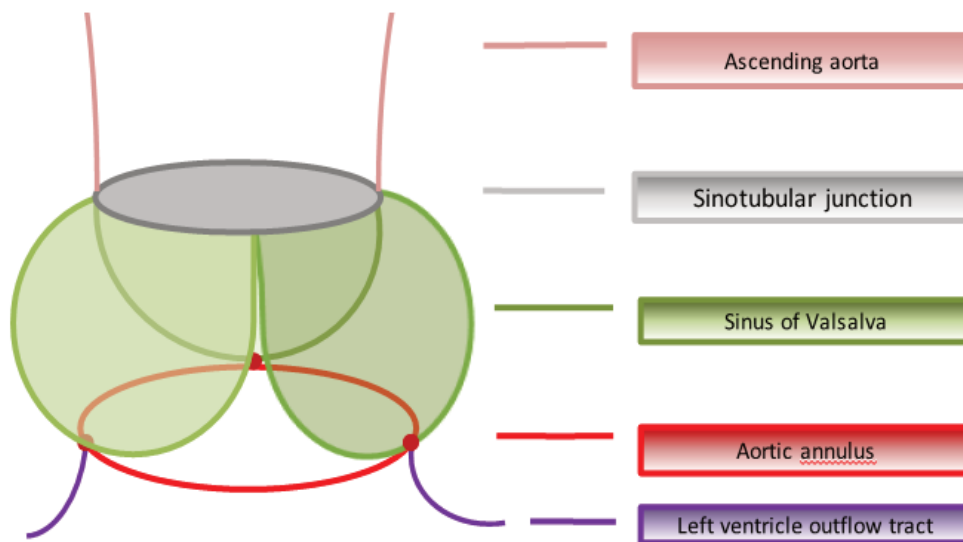


Figure 1.2. The aortic root connects the ascending aorta and the left ventricular outflow tract; the three important landmark locations of the aortic root are: the Sino tubular junction, sinus of Valsalva and the aortic annulus.



Figure 1.3 Aortic valve in human (author: CDC/Dr. Edwin P. Ewing, Jr.; source: https://commons.wikimedia.org/wiki/File:Aortic_stenosis_rheumatic,_gross_pathology_20G0014_lores.jpg?uselang=zh)

Aortic valve stenosis

The aortic valve usually constitutes of 3 leaflets, and acts as a one-way gate. During the systolic phase, the aortic valve opens, the blood is pumped from the left ventricle into the aorta thereby providing the blood supply to the whole body; during the diastolic phase, the aortic valve is closed, the left ventricle is filled again with blood from the left atrium, and the valve prevents the blood flowing back from the aorta into the left ventricle.

Over time, calcium may accumulate on the aortic valve. Subsequently, when there is heavy calcification on the aortic valve, it causes narrowing of the aortic valve, which is called aortic valve stenosis. Aortic valve stenosis results in incomplete opening and closing of the leaflets. During systole, the blood cannot be pumped out of the left ventricle easily; during diastole, the blood might leak back from the aorta into the left ventricle (Sawaya et al. 2012). This will cause a decrease in exercise capability in the patient, followed by syncope and potentially heart failure. As the third most prevalent cardiovascular disease in Europe and North America (Sawaya et al. 2012), it can cause around 50% death rate in the first two years after the onset of symptoms if left untreated (Carabello 2002).

Treatment options

Surgical aortic valve replacement (SAVR) used to be the principal therapeutic technique for aortic valve stenosis (Zajarias and Cribier 2009). Nevertheless, not all patients are suitable candidates for SAVR due to high

surgical risk and multiple co-morbidities such as renal impairment and prior stroke (Achenbach et al. 2012).

Transcatheter aortic valve replacement

TAVR (transcatheter aortic valve replacement) or TAVI (transcatheter aortic valve implantation) is a minimally invasive procedure to replace the diseased valve by a valve prosthesis delivered through a catheter. In 2002, TAVR was successfully applied for the first time in humans (Cribier 2014). The minimal invasiveness of TAVR led to a lower risk-benefit ratio in these patients, which makes TAVR a potential alternative therapy to SAVR. Until 2015, more than 200,000 procedures were carried out in more than 65 countries around the world (Vahl, Kodali, and Leon 2016). With at least similar clinical effectiveness compared to SAVR in high-risk surgical patients, TAVR has been demonstrated to be safe (Mack et al. 2015).

The first choice of implantation route is trans-femoral, i.e. through the femoral artery. It is the most minimal invasive implantation route (Mack 2012). Trans-apical, trans-subclavian and trans-aorta routes are alternatives for implantation, if the trans-femoral route is not accessible because of vascular complications. The second most frequently used access route is trans-apical which has the advantage of a short access route from the apex through left ventricle to the aortic annulus (Mack 2012); however, this approach requires surgical assistance in the catheterization lab because of the opening that has to be made in the chest wall. Trans-aortic access, as a new approach, has been proven to have a similar success rate compared to trans-apical access, posing an alternative choice for trans-apical access (Bapat et al. 2016; Lardizabal et al. 2013). Trans-subclavian access is the implantation through the left subclavian artery. However, compared to the femoral artery, the wall of the subclavian artery is more fragile. Thus trans-subclavian TAVR requires more operating skills during the procedure. As concluded by the study in (Bleiziffer et al. 2013), trans-subclavian TAVR “should be considered a valid option not only when the femoral approach is impossible but also when it is difficult, albeit feasible”.

TF-TAVR devices

There are two kinds of devices: the self-expandable and the balloon-expandable system, both of them have been demonstrated and reported to be safe and effective (Abdel-Wahab et al. 2014).

For the trans-femoral TAVR (TF-TAVR) approach the physician makes a small incision in the leg so that the catheter can be guided from the groin into the iliac-femoral artery, the descending aorta and the aortic arch (Figure 1.4) into the aortic root. The artificial valve is installed onto the remote end of the catheter which is advanced by the physician into the calcific stenotic aortic valve. The artificial valve will be anchored carefully at the exact location of the old valve by balloon expansion or self-expansion (Davidson, Welt, and Eisenhauer 2011). The old valve is pushed into the wall.

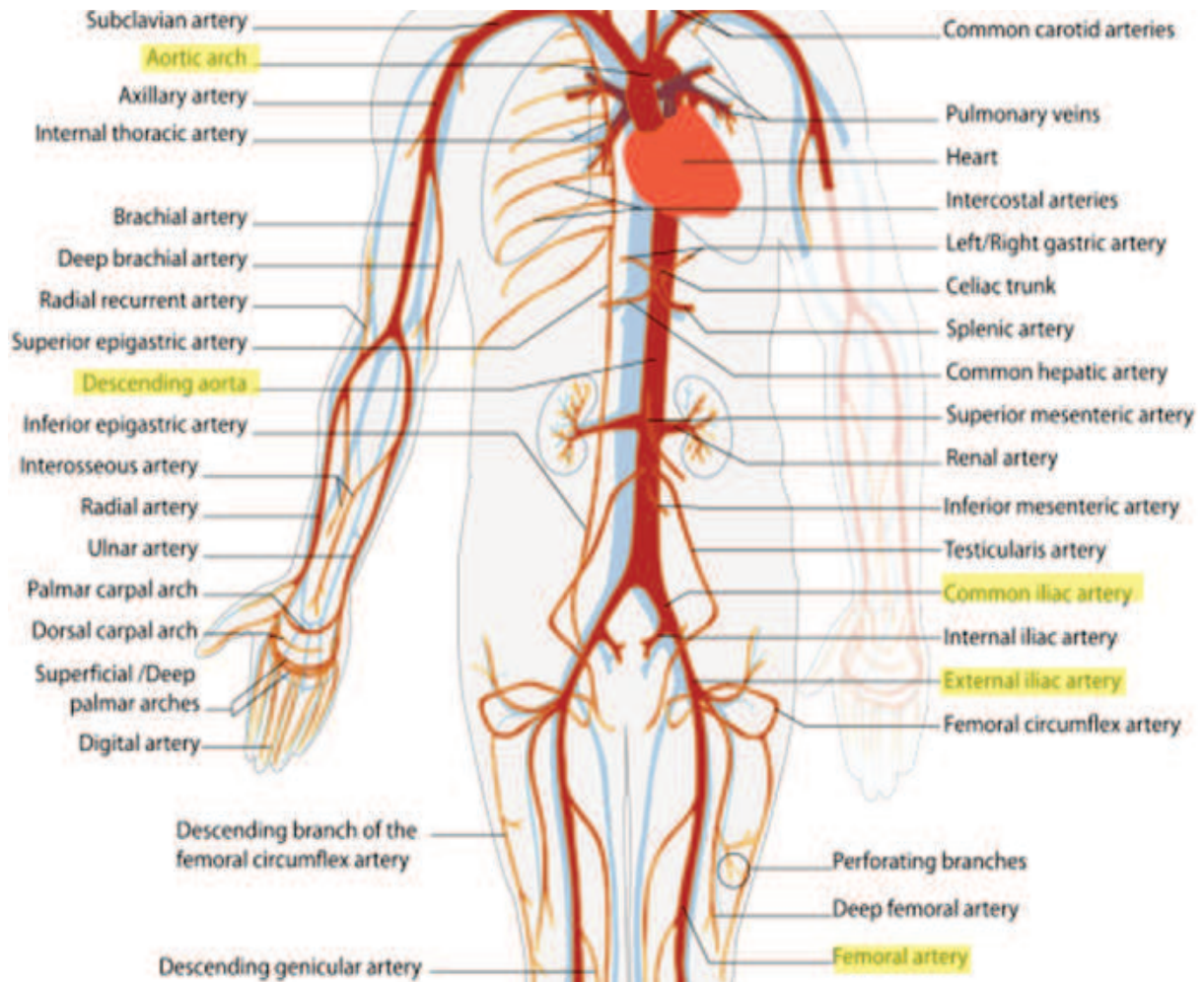


Figure 1.4 Vascular access to delivery prosthesis in TF-TAVR: femoral artery, external iliac artery, common iliac artery, descending aorta and aortic arch. (Source: https://commons.wikimedia.org/wiki/File:Arterial_System_en.svg)

Aorta structure and disease

Structure

Sofar, we have concentrated on the aortic valve stenosis. However, aortic dilatation is also a frequently occurring disease of the aorta.

The aorta is constituted of 4 parts: the ascending aorta, the aortic arch, the thoracic aorta and the abdominal aorta. The ascending aorta starts from the aortic root to the point defined by the pericardial reflection on the aorta. Next part is the aortic arch, which ends at the intervertebral disc. The thoracic aorta continues with the aortic arch and ends at the diaphragm. The aorta segment below the diaphragm is the abdominal aorta, which ends at the bifurcation to the iliac arteries. If the heart is denoted the primary pump of the circulatory system, then the aorta can be called the secondary pump because of its elasticity. It carries the blood with oxygen from the heart into the circulatory system and distributes it into all the tissues and organs of the body. Besides, in the ascending aorta and the aortic arch, there are the pressure-responsive receptors, which can help the aorta to influence the heart rate and systemic vascular resistance (Erbel et al. 2014a).

Disease

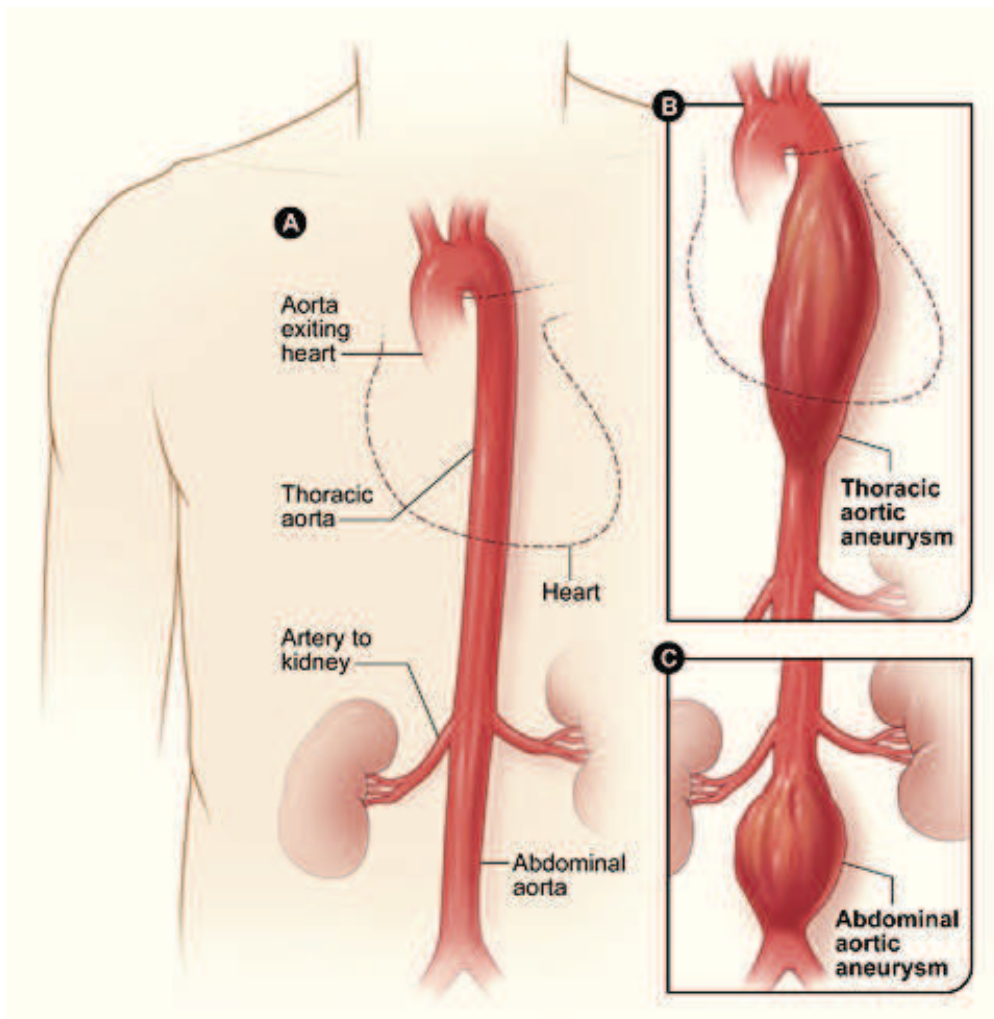


Figure 1.4 Thoracic and abdominal aorta aneurysm (author: National Institutes of Health; source: https://commons.wikimedia.org/wiki/File:Aortic_aneurysm.jpg?uselang=zh)

Aortic dilatation is a frequently occurring disease of the aorta. When the dilatation is larger than 1.5 times its normal size, it is called aortic aneurysm, which tends to further enlarge and rupture at some point in time (Mann et al. 2014). Figure 1.4 displays the thoracic and abdominal aortic aneurysms. According to the global assessment in (Sampson et al. 2014), the Global Burden of Disease 2010 study summarized that the aortic aneurysm mortality rate increased from 2.49 per 100,000 in 1990 to 2.78 per 100,000 in 2010 globally.

1.2 Challenges in TAVR procedure planning and aorta dilatation measurements

Computed tomography angiography for TAVR pre-operative planning

In contrast to SAVR, the aortic root is not visible during the TAVR procedure because of its minimal-invasiveness. To plan the access route and select the suitable prosthesis to be implanted into the aortic valve,

imaging is necessary. The size, tortuosity, and calcification burden of the access route and the size, dimension, and calcification of the aortic valve are important parameters for TAVR.

Computed tomography (CT) is a technique that produces three-dimensional images by the combinations of X-ray projections from different angles and subsequent reconstruction. Computed Tomography Angiography (CTA) is the CT scanning of the body following the injection of a contrast agent into the blood vessel. With the contrast flowing inside the vessel, the lumen border becomes visible for the physician, and the presence of an aneurysm or stenosis of the vessel will become more apparent.

Furthermore, CTA allows the evaluation of the diameter and the extent of the calcification of the ilio-femoral arteries and the thoracic aorta. In addition, it is feasible to predict the optimal projection angulation for intra-operative X-ray. Figure 1.5 shows CTA images to estimate vascular access and aortic root during the per-operative planning of TAVR.

To check whether the patient is eligible for TF-TAVR and to select the sheath with appropriate size, the minimal luminal diameter (MLD) along the ilio-femoral artery is an important indication. The “Sheath outer diameter divided by the access-side vascular diameter”, which is called Sheath-to-ilio-femoral artery ratio, is able to help to assess whether TF-TAVR is safe (Okuyama et al. 2015). Besides, the tortuosity and extent of calcification of the ilio-femoral artery access can influence the decision of the physician.

As of 2017, multiple sizes of the prosthesis are available for patients with different aortic annulus sizes: Edwards Sapien XT 23mm for 18-22 mm diameter, Edwards Sapien XT 26mm for 21-25 mm diameter, Edwards Sapien XT 29mm for 24-27 mm diameter; Medtronic CoreValve 26mm for 20-23 mm diameter, Medtronic CoreValve 29mm for 23-27 mm diameter, and the Medtronic CoreValve 31mm for 26-29 mm diameter (Ho 2009). To select the prosthesis with appropriate size and delivery into aortic valve, the size measurement and the X-ray angulation prediction of aortic root are the important steps for TAVR. The X-ray angulation in which the tops of the aortic valve leaflets are on one-and-the-same line is crucial for delivering the prosthesis properly into the native valve.

Image-based measurements for TAVR procedure

For a proper preparation of a TAVR procedure, the following measurements would be helpful:

- (1) Determine the access route by means of a definition of a centerline, the sizes of the vessels along the centerline and the tortuosity of the vessel;

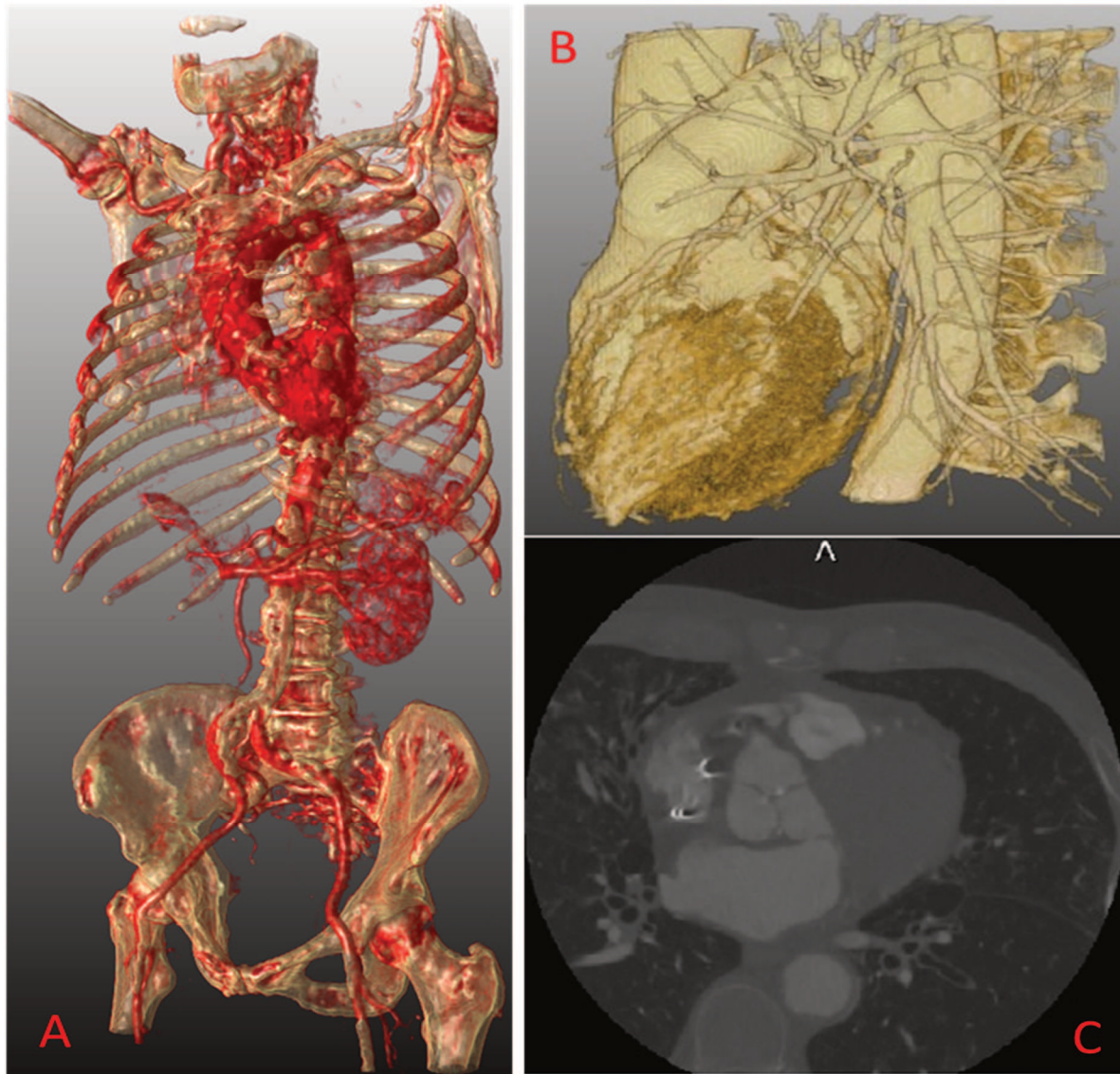


Figure 1.5 CT images for pre-operative TAVR planning: A. CTA image for vascular access, B & C. cardiac CTA image for aortic root: B. 3D view C. 2D view

- (2) Cross-sectional diameter measurements, including minimal and maximal diameters, from multi-planar images;
- (3) Calcium deposits along the aortic trajectory and the aortic root;
- (4) Determination of the proper X-ray projection for optimal view of the aortic root.

To facilitate the workflow and minimize observer variabilities, these measurements should be provided in a preferably automated manner, with minimal user interactions.

Computed tomography for assessment of aorta dilatation

Apart from treatment planning for aortic valve implantation, CT angiography is highly recommended for the assessment of aortic dilatation applications. This makes computed tomography the modality of choice during the clinical examination and treatment of aortic disease.

For instance, the maximum aneurysmal diameter, when quantified in the multi-planar reconstructed image orthogonal to the centerline along the aorta, has higher accuracy and reproducibility than the axial axis diameter measurement (Ihara et al. 2013)(Dugas et al. 2012). Axial axis measurements can overestimate an aneurysm when the aneurysmal axis is not perpendicular to the axial slice (Dugas et al. 2012). In clinical practice, diameter measurement in standardized landmark locations can support the diagnosis. In Figure 1.6, different landmarks are explained.

Challenge of manual procedure

The measurement of the aortic diameter as defined in the guidelines requires the definition of a plane perpendicular to the centerline of the aorta. Such procedure should be facilitated by the use of a workstation, which allows multi-planar reconstructions, and the proper tools to provide landmark measurements.

In clinical routine, multiple scans (baseline and subsequent follow-up scans) of a particular patient need to be interpreted over time, which requires very precise repeat measurements at corresponding positions along the aorta. To minimize variabilities, automated registration techniques should become available. As such, in line with the challenges for TAVR procedure planning and aorta dilatation measurements, we can conclude that the automatization of manual measurement procedures will surely be able to simplify and standardize the work process, reduce the effort and time of the physicians, and decrease the inter- and intra-observer variabilities.

1.3 Thesis overview

The aim of this thesis is to develop image processing solutions that enable the fully automatic pre-operative planning of aorta-related procedures. Hence, the objectives of this thesis are as follows:

1. To fully automatically quantify the aorto-iliac vascular access route, including the aortic root by image processing methods in CTA.
2. To broaden the scope of automatic methods into the detection of aorta dilatation.
3. To integrate the automatic quantification methods into applications which allow manual interactions and the calculation of clinically relevant parameters.
4. To demonstrate the accuracy and feasibility of the fully automatic planning and quantification methods in different patient cohorts.

The thesis is further structure as follows:

Chapter 2 introduces a new, fully automatic approach to extract the centerlines of aorto-femoral arteries from CTA data sets. This approach can support the planning of transfemoral aortic valve replacement. CTA images acquired in two clinical centers were used to evaluate the accuracy and robustness of the approach.

Chapter 3 describes a novel, fully automatic technique for the segmentation of the aorto-iliac arteries in CTA images by the deformable



Figure 1.6 Landmark positions along the thoracic aorta: from the aortic root to the diaphragm, line A to G represent the following landmarks in different parts of the aorta. In the aortic root: A the sinuses of Valsalva and B the sino-tubular junction; the ascending aorta: C the mid ascending aorta; the aortic arch: D the proximal aortic arch and E the mid aortic arch; the thoracic aorta: F proximal descending thoracic aorta and G the mid descending aorta (Erbel et al. 2014a).

subdivision surface model fitting method. The accuracy of the lumen border, clinical parameters including minimal luminal diameter and area were demonstrated. In our opinion, this is the first method that allows the fully automatic detection of the aortic-femoral vascular access route in CTA images.

Chapter 4 presents a novel, fully automatic segmentation framework of the aortic root in the whole-body CTA image by combining the atlas-based segmentation algorithm and deformable subdivision surface model fitting method. This framework reduces the computational cost of atlas-based segmentation algorithm and was demonstrated to be accurate by comparing the overlap of the automatic segmentation results to a reference standard by an experienced expert.

Chapter 5 evaluates a fully automatic quantification approach of aortic annulus in CTA images. The quantification approach can detect the sizing parameters of the aortic annulus, and also predicts the optimal X-ray projection curves. The automatic results were demonstrated against semi-automatic and manual results from a radiologist experienced in cardiovascular imaging.

Chapter 6 introduces a novel method for fully automatic volume quantification of aortic valve calcium in coronary CTA images. The method was evaluated in patients with calcified and non-calcified aortic valves. Aortic valve calcium volume has been proven to have a prognostic value for cardiovascular disease. The automatic method can reduce the effort of the physicians, while it increases the reproducibility of the results.

Chapter 7 presents a new automatic workflow which supports the detection of the dilatation of the aorta based on segmenting and aligning the aorta in baseline and follow-up periods. The change of the diameter along the centerline can be calculated automatically for the physicians. The workflow was demonstrated by comparing the automatic results to manual measurement generated from the experienced cardiovascular radiologist

Chapter 8 summarizes and discusses the results presented in this thesis.

2

Automatic Extraction of Arterial Centerline from Whole-body Computed Tomography Angiographic Datasets

Xinpei Gao, Shengxian Tu, Michiel A. de Graaf, Liang Xu,
Pieter H. Kitslaar, Arthur J.H.A. Scholte, Bo Xu, Johan H.C. Reiber

Abstract

The aim of this study was to develop a new, fully automated approach for the extraction of arterial centerlines from whole-body computed tomography angiographic (CTA) data sets for the planning of transcatheter aortic valve replacement (TAVR) procedures by the transfemoral approach. The method starts with an image pre-processing step to correct contrast inhomogeneities in different image slices, followed by the detection of anatomical landmarks and subsequent wave propagation, generating a cost matrix that represents the wave traveling time. Finally, the arterial centerlines are extracted from the aortic root to the femoral arteries using the conventional Dijkstra algorithm. 36 patients who underwent TAVR procedures with whole-body CTA scans were studied; 15 for training and the remaining 21 for testing. In 1 training case and 2 testing cases, user interaction was needed to correct the centerline (in the femoral artery). In the remaining 33 cases (91.7%), a fully-automated centerline was obtained with excellent results. In all cases, the average root mean square error was 2.55 ± 0.70 mm (training 2.26 ± 0.48 mm versus testing 2.77 ± 0.77 mm, $p = 0.03$) and the average mean error was 1.63 ± 0.40 mm (training 1.46 ± 0.35 mm versus testing 1.74 ± 0.39 mm, $p = 0.02$).

Computing in Cardiology 2014,
Cambridge, MA, 2014, pp. 697-700.

2.1 Introduction

Aortic valve stenosis is frequently seen in the elderly population. A severe aortic stenosis usually requires aortic valve replacement, which was the exclusive domain of open heart surgery until recent developments. The replacement is associated with a high surgical risk in elderly people, who may have various comorbidities such as porcelain aorta, pulmonary or hepatic disease, chest deformities, renal impairment, prior stroke, peripheral vascular disease, and reduced left ventricular function (Achenbach et al. 2012).

Over the past decade, Trans-catheter Aortic Valve Replacement (TAVR) has been developed as an attractive alternative for open heart surgery with likely fewer complications. One important planning step prior to TAVR is the assessment of the quality of the access pathways for the trans-catheter heart valve. This is usually done on the basis of a multi-slice computer tomography angiography (CTA) whole-body scan, including the heart and the entire femoral access route. Analytical software tools should be able to facilitate such investigations. The first step in such a tool would be to find the centerline of the entire trajectory as automatically and robustly as possible. Once an accurate centerline of the access route is available, the next step will be to calculate the cross-sections of the arteries, to determine the tortuosity, the presence and extent of calcium deposits, etc. These parameters are important indicators for assessing the risk of complications.

The goal of this study was to develop a fully automatic approach for extraction of arterial centerlines in the entire femoral access route. The approach was validated on CTA datasets that were routinely acquired prior to the TAVR procedures.

2.2 Methods

Based on our experiences, we have implemented a fully automated centerline extraction for the TAVR application. Our method extracted intensity and shape information of target arteries, and constructed a cost function representing the speed of the subsequent wave propagation. After performing the propagation implemented as a fast marching algorithm (Adalsteinsson and Sethian 1995), the Dijkstra algorithm (Dijkstra 1959) was applied to extract the centerlines of the target arteries.

Preprocessing

The CTA image was first resampled to reduce computer processing time. Next, a sigmoid filter was used to attenuate the intensity of tissues besides contrast arteries and bones. The bones near the femoral artery were removed automatically by steps including thresholding, closing, and connect component analysis. The result image was subsequently transformed into a binary image, representing the possible vascular objects. A distance transform function was constructed by applying the 3D Euclidean Distance Transform to the binary image.

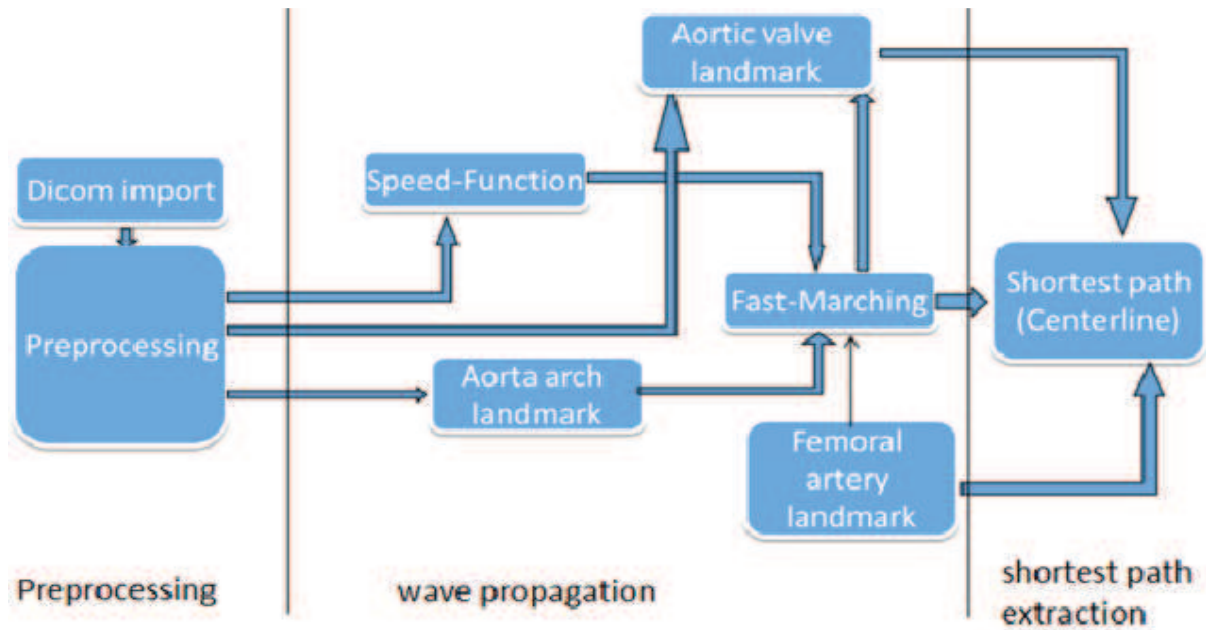


Figure 2.1. Scheme of automatic centerline extraction.

Wave propagation

Aorta arch landmark

The wave propagation requires a start point to initialize the propagation. We chose the aortic arch as the start position. Prior knowledge about the aorta diameter from literature (Mao et al. 2008) was included in the following Gaussian distribution model $S(x)$ (Metz et al. 2009).

$$S(x) = \exp\left(-\frac{(D(x) - \mu_s)^2}{2\sigma_s^2}\right)$$

Where μ_s was set to the radius of the aorta and σ_s controls the range of radii. The resulting value of $S(x)$ is a measurement of the probability of the value $D(x)$ belonging to the range of aorta diameters. With Distance Transformation result and this Gaussian Model, we can achieve the probability map. The aortic arch will be the biggest cluster constructed by high probability voxels at the top of CTA image.

Wave propagation

The cost function of the wave propagation algorithm was calculated based on a voxel's 3D Euclidean Distance value and its intensity value. The cost for the wave to travel inside the artery was lower towards the centerlines of the arteries. In our implementation, the wave initiated at the landmark inside the aortic arch, propagated into the ascending aorta, the aortic root on one side, and into the descending aorta, the abdominal aorta, the iliac arteries and the femoral arteries on the other side. A direction of 8-connectivity was applied in the wave propagation.

The wave stopped when it reached the aortic root on one side and the femoral arteries on the other side. These two landmarks were automatically detected by the following criterions:

First criterion was the femoral artery landmark: In our application, the wave propagated until it reached both the left half and the right half of the bottom slices in the CTA image. And the first point to reach in the left half bottom slice was the end point of left femoral artery, and the first point in the right half was the end point of right femoral artery.

Second criterion was the aortic root landmark: From the aortic arch landmark, the wave propagated to the other side through the ascending aorta and to the aortic root. The point that propagated the fastest in the left side of the slice is the center of the aorta. When the wave front propagated into the aortic valve, the wave front would split into 2 parts or 3 parts because the aorta valve has 2 cusps or 3 cusps. The 3D Euclidean distance value of the fastest point in aortic valve will be equal to or smaller than $\frac{1}{2}$ of the average value of the distance of former fastest points in descending aorta.

Path extraction

After the wave propagation, each voxel was assigned a value representing the cumulative time for the wave to travel from the start point to this voxel. Inside the arteries, the wave travelled fast and the associated arrival time was shorter when compared to the voxels outside the arteries.

The Dijkstra algorithm was executed twice to get the centerlines from aortic root landmark to the left and right femoral arteries, separately. From these two centerlines, the aortic bifurcation was found and the entire access path, including the aorta segment, the left femoral segment and the right femoral segment, of the TAVR procedure using the femoral artery as the site of puncture was extracted.

2.3 Validation

Study population

This study was validated on a total of 36 patient's CTA datasets that were routinely acquired prior to the TAVR procedures. 15 datasets were randomly selected and used for training of the algorithm: 11 from Leiden University Medical Center (LUMC), Leiden, the Netherlands and 4 from Fu Wai Hospital, Beijing, China. The remaining 21 datasets were used for testing: 9 from LUMC and 12 from Fu Wai Hospital.

CTA acquisition protocol

The CTA datasets from LUMC were acquired on a 320-row volumetric scanner (Aquilion ONE, Toshiba Medical System, Japan) using Helical scan protocol. A bi-phasic injection of intravenous contrast was used: 70ml contrast (5ml/sec) and 50ml saline (5ml/sec) (de Graaf, Schuijf, van Velzen, Kroft, et al. 2010). The datasets from Fuwai Hospital were acquired by SOMATOM Definition Flash (Siemens, Germany) using Helical scan protocol. A single-phasic injection of contrast was used 350mgI/ml (3-4ml/s). The image resolution of the CTA image was 512×512 . Approximately 1000 image slices were obtained per case.

Measurement of extraction error

An analyst delineated the corresponding centerlines semi-automatically in all cases and the results were reviewed by another analyst. Correction

was applied when there was disagreement until consensus was reached. The delineated centerlines were used as the reference standard; the extraction error was defined as the distance between the reference centerline point and the closest point in the automatically extracted centerline.

2.4 Results

Fig 2.2 shows an example of the extracted centerlines superimposed on the CTA image in 3D. No user interaction was needed and the approach was completely automated. The mean extraction error for this case was 2.55 ± 0.70 mm. In 1 training case and 2 testing cases, interaction was needed by the user to correct the centerline in the femoral artery. In the remaining 33 cases (91.7%), a fully automated centerline was obtained with excellent results.

Fig 2.3 shows the extraction error for each individual case. In all cases, the mean extraction error was 2.55 ± 0.70 mm (training 2.26 ± 0.48 mm versus testing 2.77 ± 0.77 mm, $p = 0.03$) and the average mean error was 1.63 ± 0.40 mm (training 1.46 ± 0.35 mm versus testing 1.74 ± 0.39 mm, $p = 0.02$).

The computational time for the algorithm to process each CTA dataset was 53 ± 11 seconds, using a work station with Intel Core2 CPU (2.4 GHz) and 6 GB RAM.

2.5 Discussions

In this paper, we developed a completely automatic method to extract the arterial centerlines from whole-body CTA images. The validation results showed that 91.7% of the extracted arterial centerlines did not need any further user correction. The CTA images that were used in the validation were acquired by different systems in two clinical centers, demonstrating the robustness of the method.

Many papers have been published on coronary centerline extraction in CTA images, among which the method based on Hessian filter such as vesselness has been widely applied. Yang et al. (Yang et al. 2012) introduced a fully automatic method to extract coronary artery based on vesselness filter. This method cannot be directly applied to whole-body CTA scans, since the size of arteries in the entire access path generally demonstrates large inhomogeneity. Other methods such as morphological operation (Schaap et al. 2009) and histogram segmentation can lead to discontinuity in the centerline extraction when significant stenosis is present.

Our future work will focus on the automatic segmentation of lumen contour of the entire access route, the aortic valve, and the implementation of various quantitative parameters that could lead towards efficient and objective TAVR planning.

2.6 Conclusions

This method is robust and effective to extract arterial centerline automatically from whole-body CTA data sets. This is a first and important step towards efficient planning of TAVR procedures.



Fig 2.2. Three-dimensional volume rendering and the extracted vascular centerline (yellow curve).

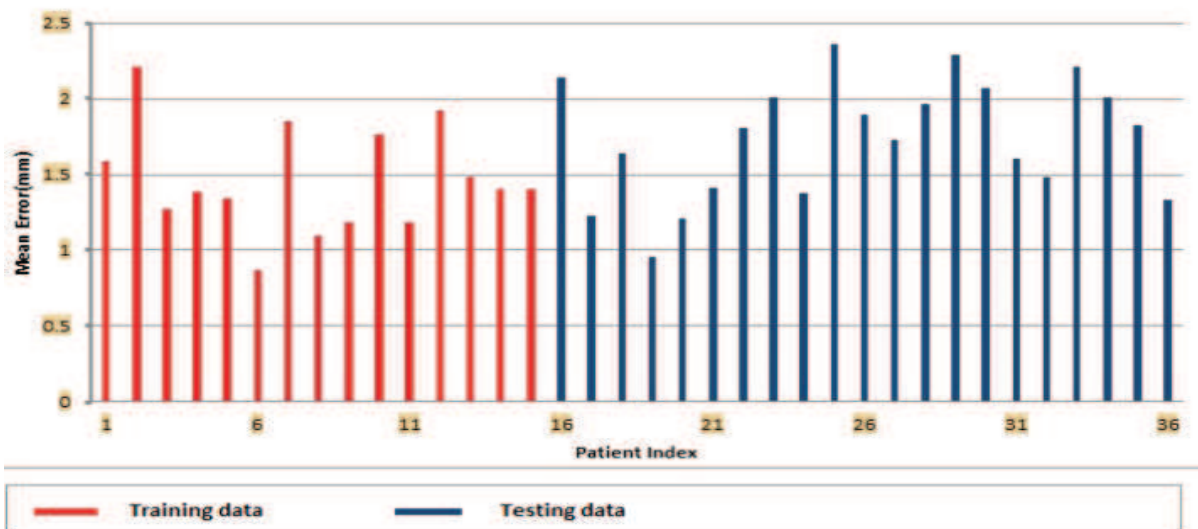


Figure 2.3. Distribution of mean extraction error.

3

**Automatic Detection of Aorto-femoral Vessel
Trajectory from Whole-body Computed Tomography
Angiography Data Sets**

Xinpei Gao, Pieter H. Kitslaar, Ricardo P. J. Budde,
Shengxian Tu, Michiel A. de Graaf, Liang Xu, Bo Xu,
Arthur J. H. A. Scholte, Jouke Dijkstra, Johan H. C. Reiber

Abstract

Purpose: Extraction of the aorto-femoral vascular trajectory is important to utilize computed tomography angiography (CTA) in an integrated workflow of the image-guided work-up prior to trans-catheter aortic valve replacement (TAVR). The aim of this study was to develop a new, fully-automated technique for the extraction of the entire arterial access route from the femoral artery to the sino-tubular junction.

Methods: An automatic vessel tracking algorithm was first used to find the centerline that connected the femoral accessing points and the aortic valve. Subsequently, a deformable 3D-model fitting method was used to delineate the lumen boundary of the vascular trajectory in the whole-body CTA dataset. A validation was carried out by comparing the automatically obtained results with semi-automatically obtained results from two experienced observers.

Results: The whole framework was validated on whole body CTA datasets of 36 patients. The average Dice similarity indexes between the segmentations of the automatic method and observer 1 for the left ilio-femoral artery, the right ilio-femoral artery and the aorta were 0.977 ± 0.030 , 0.980 ± 0.019 , 0.982 ± 0.016 ; the average Dice similarity indexes between the segmentations of the automatic method and observer 2 were 0.950 ± 0.040 , 0.954 ± 0.031 and 0.965 ± 0.019 , respectively. The inter-observer variability resulted in a Dice similarity index of 0.954 ± 0.038 , 0.952 ± 0.031 and 0.969 ± 0.018 for the left ilio-femoral artery, the right ilio-femoral artery and the aorta. The average minimal luminal diameters of the ilio-femoral artery were 6.03 ± 1.48 mm, 5.70 ± 1.43 mm and 5.52 ± 1.32 mm for the automatic method, observer 1 and observer 2 respectively. The minimal luminal diameters of the aorta were 13.43 ± 2.54 mm, 12.40 ± 2.93 mm and 12.08 ± 2.40 mm for the automatic method, observer 1 and observer 2 respectively. The automatic measurement overestimated the minimal luminal diameter slightly in the ilio-femoral artery at the average by 0.323 mm (SD= 0.49mm, $p<0.001$) compared to observer 1 and by 0.51mm (SD = 0.71mm, $p<0.001$) compared to observer 2.

Conclusion: The proposed segmentation approach can automatically provide reliable measurements of the entire arterial accessing route that can be used to support TAVR procedures. To the best of our knowledges, this approach is the first fully automatic segmentation method of the whole aorto-femoral vessel trajectory in CTA images.

International Journal of Cardiovascular Imaging.
August 2016, Volume 32, Issue 8, pp 1311–1322.

3.1 Introduction

Aortic valve stenosis is a disease particularly prevalent among senior citizens over the age of 65 years (Nkomo et al. 2006). If left untreated, it is associated with a significant mortality. Historically surgical aortic valve replacement (SAVR) was used to treat this disease. Unfortunately, not all patients are suitable for such a procedure. Especially, SAVR may be associated with a high perioperative mortality risk in elderly patients (Nkomo et al. 2006; Schoenhagen, Hausleiter, et al. 2011). Trans-catheter Aortic Valve Replacement (TAVR) / Trans-catheter Aortic Valve Implantation (TAVI) has been developed as a therapeutic option during the last decade for the inoperable or very high-risk patients (Zajarias and Cribier 2009).

To minimize the procedure-related complications, special attention should be given to the selection procedure to decide which patients are suitable TAVR candidates. Computed tomography (CT) imaging has been proven to be able to predict vascular complications among patients undergoing transfemoral transcatheter aortic valve replacement (TF-TAVR) (Krishnaswamy et al. 2014). Evaluation of the size and tortuosity of the ilio-femoral arteries is required to determine the feasibility of a transfemoral (TF) approach (Agarwal et al. 2015; Schoenhagen, Kapadia, et al. 2011). Furthermore, the size of the entire aorta is also needed for proper device selection in TAVR (Achenbach et al. 2012; Leipsic et al. 2011). To integrate such measurements seamlessly and conveniently into the TAVR clinical workflow, a fully automatic framework was developed, allowing detection of the femoral/aorta access route and the vessel sizes based on 3D contour detection approaches.

In the literature, several approaches have been described for the detection of the arterial contours in CTA data sets. David Lesage et al (Lesage et al. 2009) reviewed the state-of-the-art on vascular segmentation in multi-modality images. The model-based vascular segmentation approach is commonly used. In our study, the vessel surface was modeled by a centerline curve with a generalized cylinder. This cross-section model with prior shape information can reduce the complexity of the contour detection procedure (Kitslaar et al. 2015).

The approach that we have taken consists of 2 steps (Fig 3.1), firstly, a centerline extraction from the femoral arteries to the aortic root (Gao et al. 2014); and secondly, a 3D contour detection approach using a subdivision surface model fitting method to accurately delineate the vascular access route (Kitslaar et al. 2015). Validation of this study was realized on 36 CTA datasets which were acquired during routine clinical practice prior to the TAVR procedures.

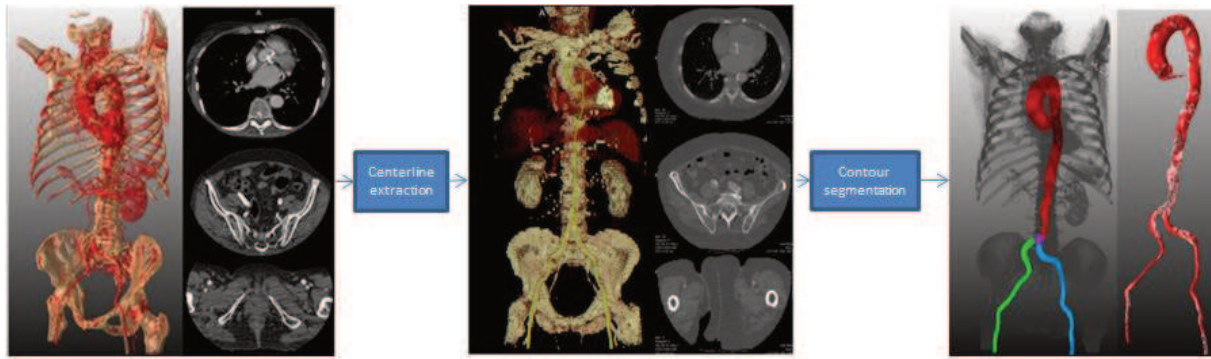


Fig 3.1. The general pipeline of trajectory contour detection, including two steps: centerline extraction and contour detection.

3.2 Methods

Centerline extraction

Since the details of the fully automatic centerline extraction algorithm were published in (Gao et al. 2014), we briefly summarize the steps below.

The CTA datasets were resampled at first to reduce the computation time. The centerline extraction step was executed on the resampled images. A wave-propagation algorithm was used, starting from the aortic arch which is detected automatically. To detect the aorta arch, prior knowledge about aorta diameter from clinical research (Mao et al. 2008) was integrated into a Gaussian probabilistic distribution model (Metz et al. 2009). After calculating the probabilistic model, a probability map was generated. From a point in the aorta arch, the algorithm propagated in two directions. One side propagated into the aortic root, and the other side propagated into the femoral arteries. After the wave propagation, the result image was used as a weight image for the Dijkstra shortest path algorithm. The Dijkstra algorithm was executed twice. First, to extract the centerline from the left femoral artery end to the aortic root. Second, to extract the centerline from the right femoral artery end to the aortic root. After these two centerlines were found, the bifurcation point of the two centerlines was detected. Finally, the centerlines were split into 3 parts: the centerline in the aorta, in the left ilio-femoral artery and in the right ilio-femoral artery.

Next, the centerlines in the femoral arteries were improved by a centerline refinement step. For this, a multi-scale medialness response based wave-propagation scheme (Gülsün and Tek 2008) was used. First, multi planar reconstruction (MPR) transversal image slice stacks were generated according to the initial centerline along the femoral artery. Next, the medialness response was computed from a circle centered at the initial centerline point, with multi-scale radius. This response was constructed as to give high values inside the center of the lumen and lower values inside calcifications. The response was used as the speed function for the wave propagation and back tracking method to generate the final refined centerline. Fig 3.2 shows an example of the comparison of the automatic extracted centerline and the refined centerline.

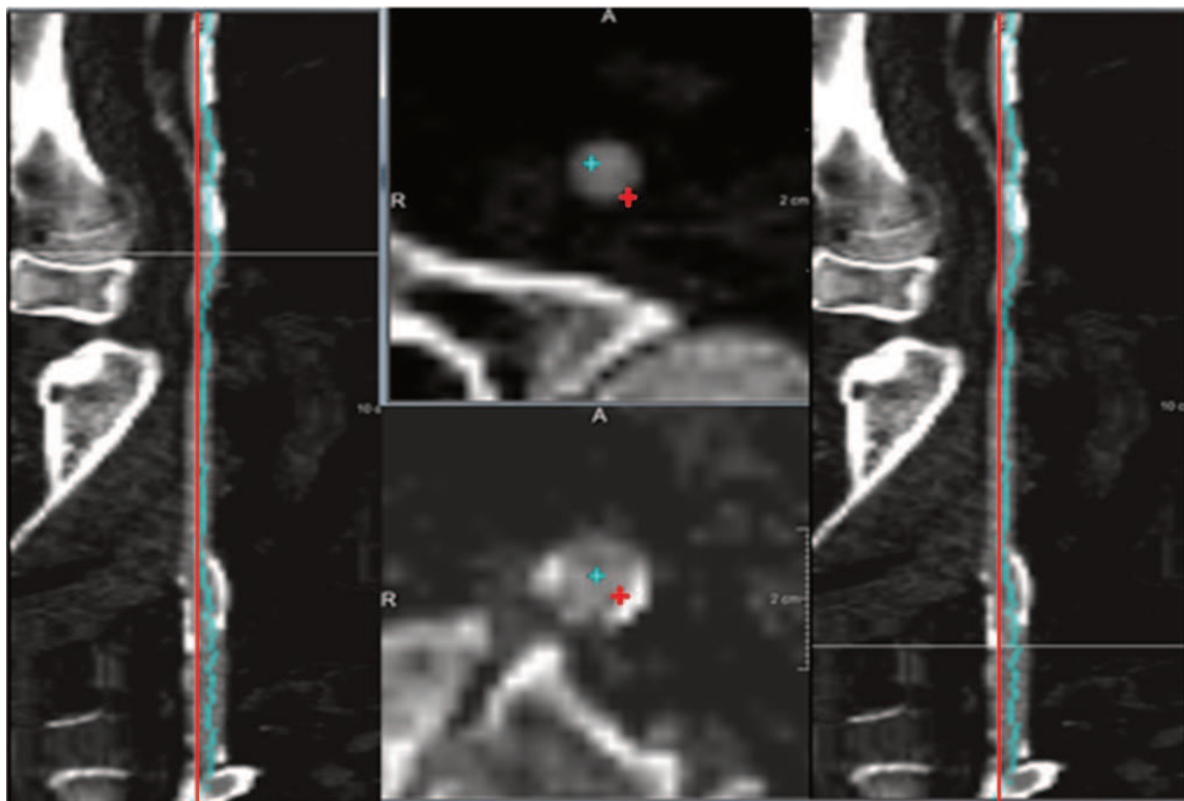


Fig 3.2. Result of centerline refinement step. The red crosses are the original centerline points; the blue crosses are the refined centerline points. The blue points avoid the calcium, and are better located in the middle of the cross-section of the artery lumen compared to the red points.

Contour detection

The vascular trajectory was segmented by a deformable model fitting method (Kitslaar et al. 2015). The deformable model was constructed from a coarse surface mesh representation created from the obtained centerlines. From this coarse mesh a smooth higher resolution surface mesh was created using a standard subdivision refinement scheme. This higher resolution subdivision surface was next deformed by iteratively updating the coarse mesh description by fitting to the lumen edge information in the CT scans. In (Kitslaar et al. 2015), this model was applied in CTA images of the carotid artery including bifurcations, and provided good results. A big advantage of the subdivision surface approach is that it is able to model the bifurcation of the iliac arteries.

Pre-processing

In our study, whole-body CTA datasets were used. In these images different kinds of anatomic tissues can be distinguished. The surrounding background of the contrast-filled vessels is quite complex and may confuse the subdivision surface fitting. For our purposes, we distinguished two background categories: high intensity tissue (calcifications, bones, and metal artifacts), and low intensity tissue (muscles, fat, liver etc.). We masked out the surrounding background by an adaptive threshold method similar to Shahzad et al (Shahzad et al. 2013).

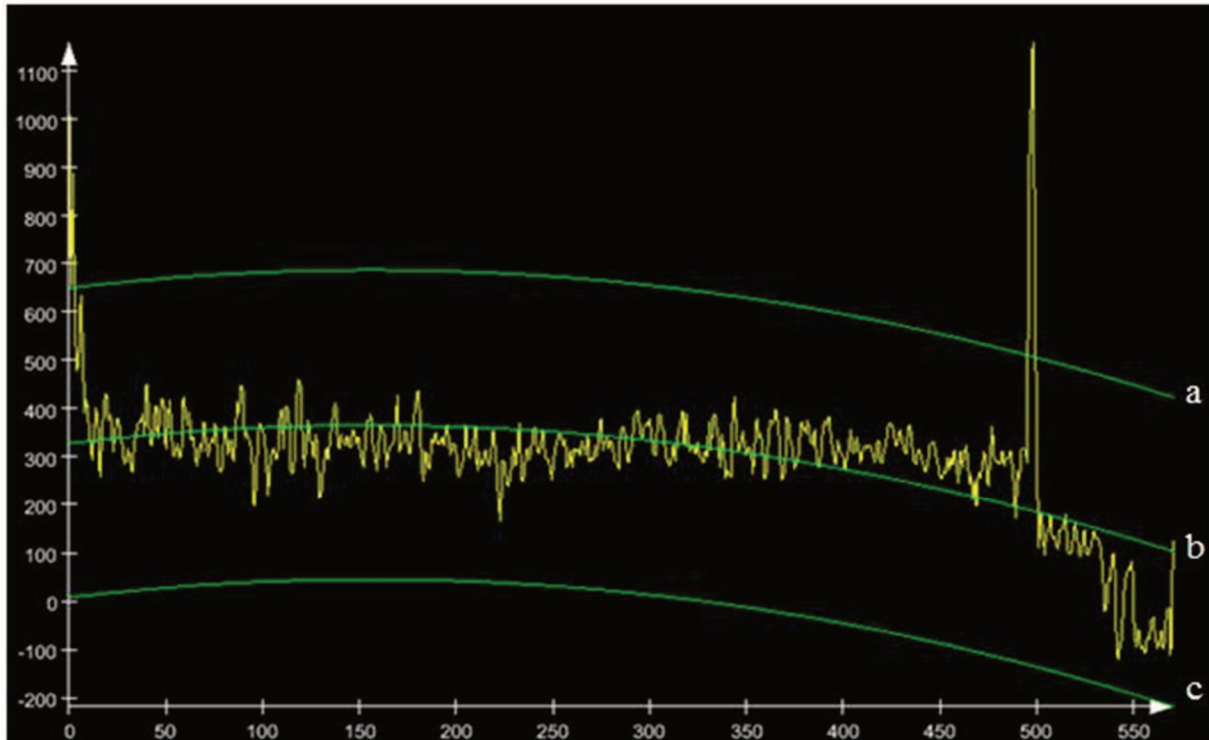


Fig 3.3. Intensity profile along the centerline (yellow curve), polynomial curves (green). Yellow curve: intensity values in HU of the voxels along the centerline (in mm). Green curves: 2nd order polynomial fit (b) of the intensity values with standard deviation margin above (a) and below (c).

This method is based on the assumption that the HU value (intensity) along the artery should be a smooth gradual decreasing curve when this artery is without the presence of calcium (Steigner et al. 2010).

Based on this, an intensity profile of the voxels along our initially extracted centerline was extracted (Fig 3.3). Next, a 2nd order polynomial curve was fitted through the intensity profile data; this curve simulated the ideal case without calcium. Curve "b" in Fig3. shows this polynomial fit curve. Also shown is curve "a" which is an upward shifted version of curve "b" obtained by adding a constant value proportional to the standard deviation of the intensities in the profile. The values on curve "a" were used as the intensity threshold values for the high intensity structures (e.g calcium) on the corresponding image slices along the vessel centerline. A similar method was used to find the tissue with lower intensity than the contrast-filled lumen using curve "c" which is a downward shifted version of curve "b". Fig 3.4 shows examples of the original and mask slices in the CTA data using this method.

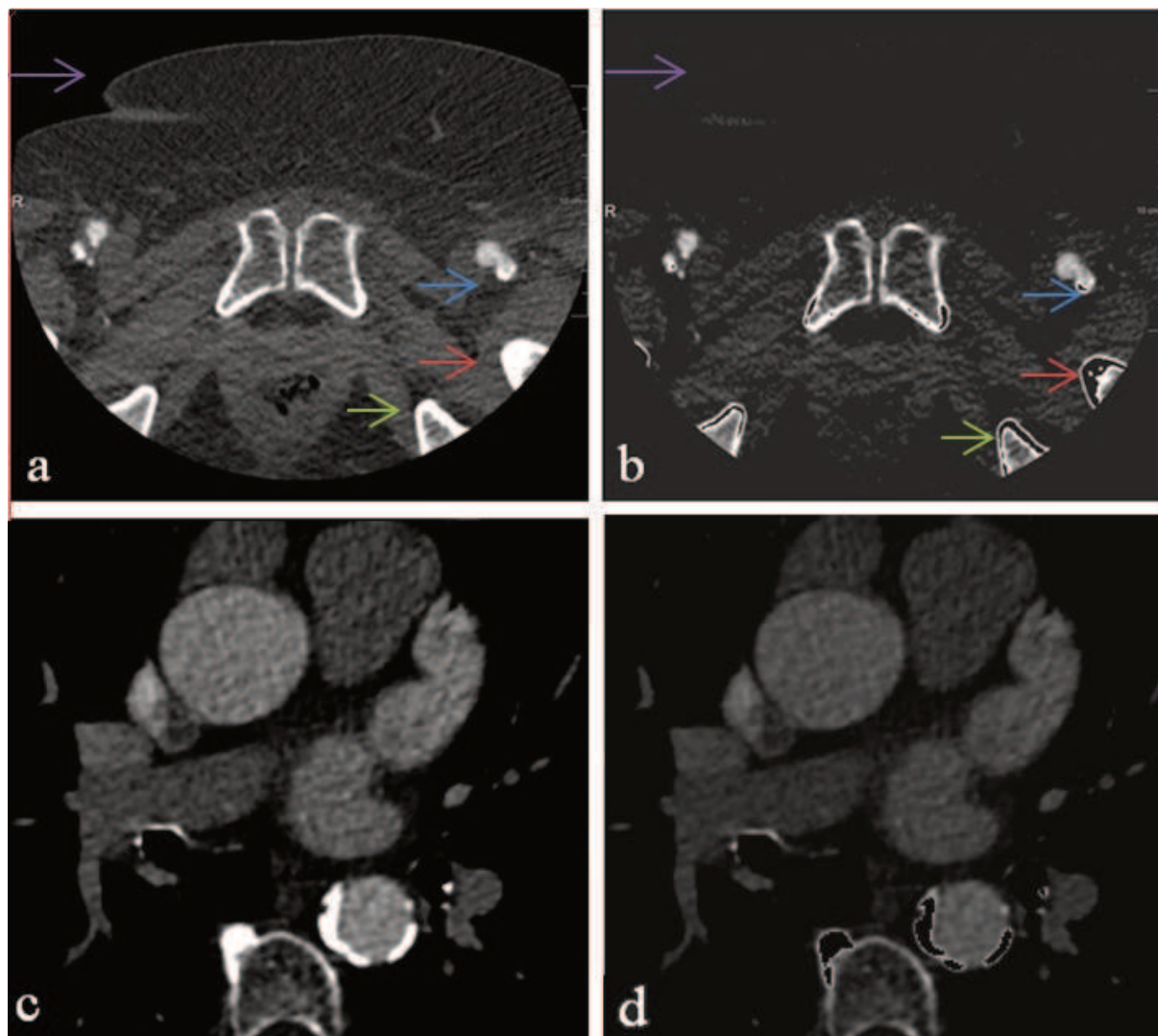


Fig 3.4. Examples of pre-processed slices. (a). original femoral artery image (b) processed femoral artery image (c) original aorta image (d) processed aorta image. The purple arrows in (a) and (b) indicate low intensity tissue that has been removed in processed image, other arrows indicate the processed high intensity tissue.

Model fitting

The deformable model was initialized from the centerline curves as a generalized cylinder with local diameter information obtained during the centerline extraction step (Gao et al. 2014). At the bifurcation a dedicated model was used to best describe the current bifurcation configuration. After initialization, the complete surface model was subdivided using the Loop subdivision scheme to generate a smoother surface model (Loop 1987). The subdivision surface model fitting was next performed on the processed intensity image. The fitting of the surface was based on the iterative movement of the control points according to the computed image forces.

During the deformation iterations, a re-initialization step was used (Kitslaar et al. 2015). During this re-initialization, a new subdivision surface model is generated based on the current fitted surface. For this, new centerline and diameter information was extracted from the current deformed subdivision surface and used to initialize the new surface model.

The re-initialization allows adapting the surface mesh model to various vessel radii in the vessel trajectory.

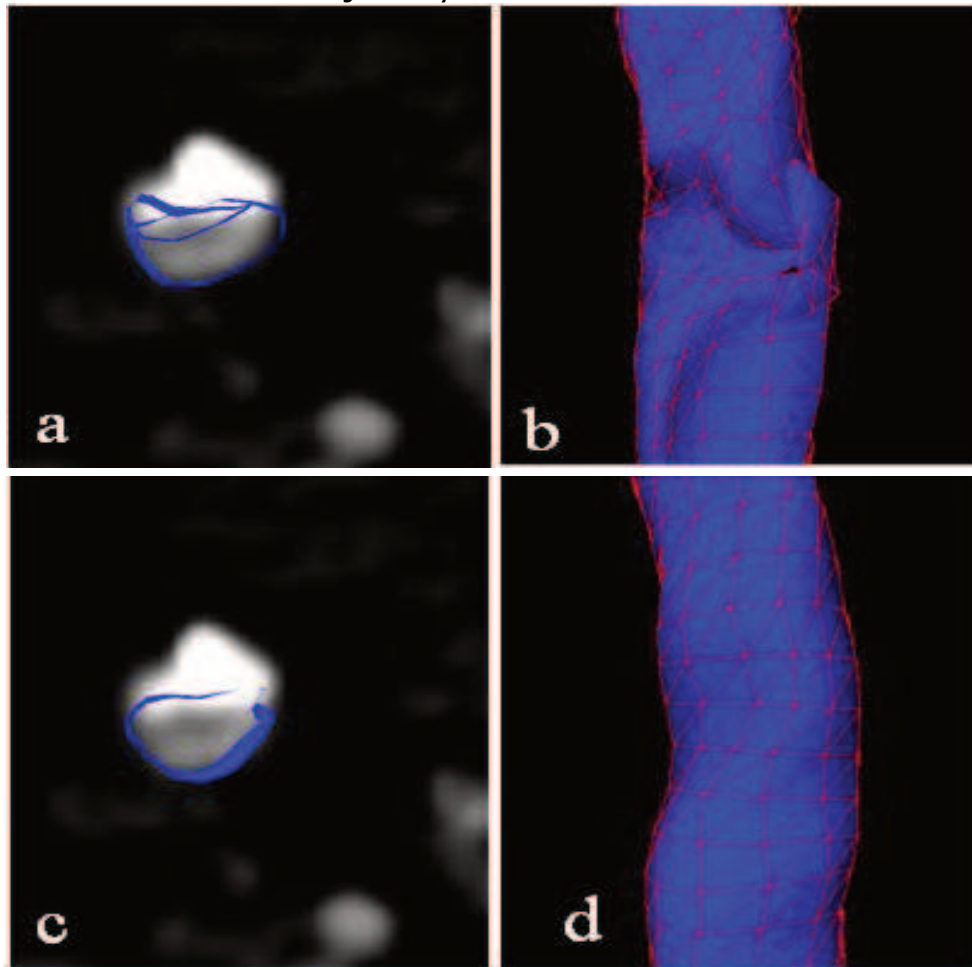


Fig 3.5. a, self-intersection in 2d cross-section contour b. 3D surface with self-intersection c.d. 2D cross section contour and 3D surface with no self- intersection when using a non-self-intersection force.

To prevent unwanted deformations during the fitting, a non-self-intersection force was used, similar to the method in (Park et al. 2001) (see Fig 3.5).

The whole algorithm pipeline was implemented in C++ and Python using the MeVisLab environment (version 2.7, Bremen, Germany).

VALIDATIONS

Segmentation evaluation

To evaluate the automatic segmentation method two experienced observers independently corrected the automatic segmentation result. This was done using a dedicated editing tool in which the automatically obtained surface model could interactively be deformed.

To compare the different segmentation results to obtained 3D surface models were resliced along the centerlines to obtain planar 2D contours. From these contours the cross sectional area and the minimal diameter were calculated as clinical parameters and compared between the different segmentation results. Also the Dice similarity index (or coefficient) was calculated between the contours from the different segmentation results.

To investigate the influence of image quality, also the mean and standard deviation of the HU values in the descending aorta were measured for each subject.

Statistical analysis

The results of the clinical parameters from the automatic segmentations were compared with the results from the semi-automatic segmentations of the observers by the paired t-test. The Bland-Altman plots were calculated to quantify the mean error and the standard deviation (SD). The correlations were estimated by Pearson's correlation coefficient.

The statistical analyses were conducted with SPSS (version 20.0, SPSS Inc, Chicago, IL, USA) and MedCalc (version 15.6, Ostend, Belgium).

3.3 Results

Data acquisition protocols

This is a retrospective study; the datasets were acquired before this research project started as part of routine clinical care protocols. Only anonymous routine clinical datasets were used.

A total of 38 patients underwent pre-operative CTA scanning for TAVR. The baseline characteristics of these patients are listed in Table 3.1. Two patients were excluded for the following reasons: one patient did not have a whole-body CTA dataset, whereas in the other patient the contrast in the aorto-femoral vessel trajectory was very low.

The datasets were acquired in two hospitals: Leiden University Medical Center (LUMC) in Leiden, the Netherlands, and Fuwai Hospital in Beijing, China. The CTA datasets from LUMC were collected on a 320-row CT scanner (Aquilion ONE, Toshiba Medical System, Japan) by using a helical scan protocol. A bi-phasic injection protocol with intravenous contrast was used: 70ml contrast (5ml/sec) and 50ml saline (5ml/sec) (de Graaf, Schuijff, van Velzen, Boogers, et al. 2010). The datasets from Fuwai Hospital were acquired on a dual source CT scanner (SOMATOM Definition FLASH, Siemens, Germany) by using a helical scan protocol. A single-phasic injection protocol was used: 350mgI/ml (3-4ml/s). The axial image size of the whole-body CTA image was 512×512. In each patient, there were approximately 1000 image slices in the z axis.

Centerline evaluation

As was described in (Gao et al. 2014), in all the 36 patients (100%) the centerlines were extracted successfully from the common femoral arteries to the sino-tubular junction, inside the lumen of the vessel. The average root mean square error between the automatic and manual corrected centerlines was 2.55 ± 0.70 mm and the average mean error was 1.63 ± 0.40 mm.

Contour evaluation

	Total (38)
Age (years)	77±13
Gender (% male)	21 (55)
Diabetes	7 (18)
Hypertension ^a	23 (61)
Hypercholesterolemia ^b	21 (55)
Family history of CAD ^c	8 (21)
Smoking	10 (26)
Obesity	4 (11)
Previous PCI	12 (32)
Previous CABG	10 (26)
Previous MI	6 (16)

Data are represented as mean±SD, median (interquartile range) or as number and percentages of patients

CABG coronary artery bypass graft, *CAD* coronary artery disease, *MI* myocardial infarction, *PCI* percutaneous coronary intervention

^a Defined as systolic blood pressure ≥ 140 mmHg and/or diastolic blood pressure ≥ 90 mmHg or the use of antihypertensive medication

^b Defined as serum total cholesterol ≥ 230 mg/dl or serum triglycerides ≥ 200 mg/dl or treatment with lipid lowering medication

^c Defined as the presence of coronary artery disease in first-degree family members at age <55 years in men and age <65 years in women

Table 3.1 Baseline characteristics

Table 3.2 shows the Dice similarity results comparisons between the automatic and the observer corrected segmentations for the different parts of the segmented trajectory.

The average Dice similarity indexes between the automatic method and the first observer were 0.977 ± 0.030 , 0.980 ± 0.019 , 0.982 ± 0.016 for the left ilio-femoral artery, the right ilio-femoral artery and the aorta, respectively; the average Dice similarity indexes between the automatic method and the second observer were 0.950 ± 0.040 , 0.954 ± 0.031 and 0.965 ± 0.019 , for the left ilio-femoral artery, the right ilio-femoral artery and the aorta, respectively. The inter-observer variability resulted in a Dice similarity index of 0.954 ± 0.038 , 0.952 ± 0.031 and 0.969 ± 0.018 for the left ilio-femoral artery, the right ilio-femoral artery and the aorta, respectively (Table 3.2).

Dice similarity index (mean±SD)	Automatic vs observer 1	Automatic vs observer 2	Observer 1 vs observer 2
Left ilio-femoral artery	0.977±0.030	0.950±0.040	0.954±0.038
Right ilio-femoral artery	0.980±0.019	0.954±0.031	0.952±0.031
Aorta	0.982±0.016	0.965±0.019	0.969±0.018

Table 3.2 Performance of automatic segmentation comparing to each of the observers and the observers to each other.

To find if there is any correlation between the contour detection and the quality of the datasets, the mean and standard deviation of the HU value within the descending aorta of each patient were measured and plotted together with the Dice similarity index of the aorta between the automatic system and observer 1 (Fig 3.6).

Clinical evaluation

The most important clinical parameter for the vascular access route is the minimal luminal diameter (MLD). In this study we separated the vascular access route into 3 segments: the two ilio-femoral arteries and the aorta. The cross-sectional diameter was calculated at every point along each centerline segment to build a diameter curve.

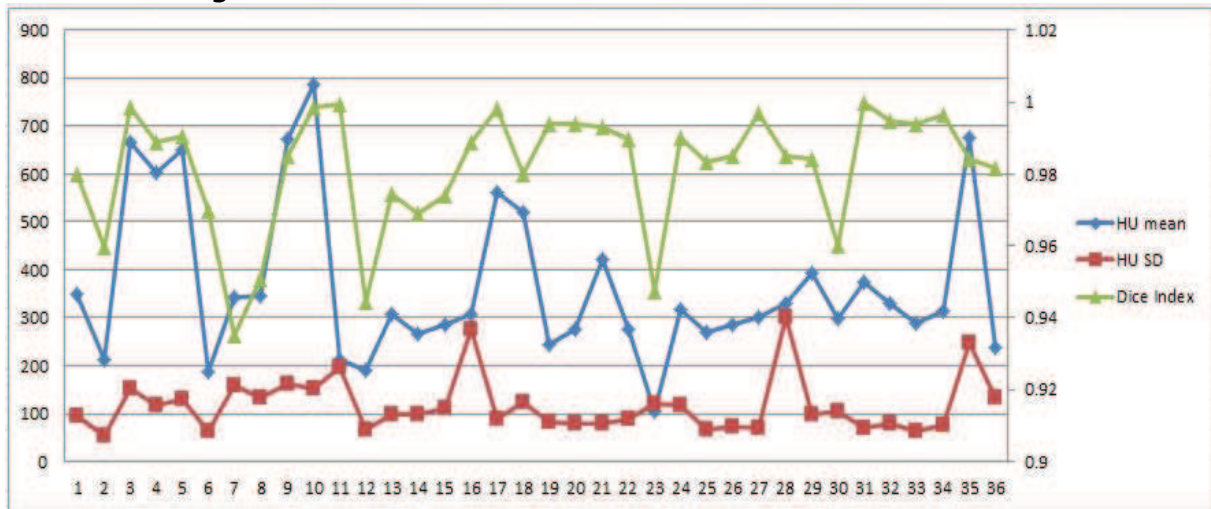


Fig 3.6. The image qualities and the contour detection evaluation of the datasets: the blue line is the mean of HU value of the descending aorta, the red is the standard deviation (left vertical axis) and the green is the Dice index (right vertical axis).

For the ilio-femoral access, the diameter and area measurements were taken along the centerline bilaterally with the minimum luminal measurement in both left and right side, including common iliac artery(CIA), external iliac artery(EIA), and common femoral artery(CFA) (Krishnaswamy et al. 2014; Kurra et al. 2009; Leipsic et al. 2011; Okuyama et al. 2014) . For the aorta, the diameter measurements were taken along the centerline from the abdominal aorta until the sino-tubular junction,

including abdominal aorta, descending aorta and ascending aorta (Achenbach et al. 2012).

The mean value, standard deviation and 95% confidence interval of the parameters are shown in Table 3.3. The correlation and Bland-Altman bias are shown in Table 4. The correlations between automatic group and observer groups were 0.81- 0.94, with p-values smaller than 0.001. With the commonly used significance level value 0.05, the correlations can be called statistically significant.

	Automatic measurement			Observer 1 measurement			Observer 2 measurement		
	Mean	SD	95% CI	Mean	SD	95% CI	Mean	SD	95% CI
Ilio-femoral									
Minimal luminal diameter (mm)	6.03	1.48	5.53–6.53	5.70	1.43	5.22–6.19	5.52	1.32	5.07–5.97
Minimal luminal area (mm ²)	38.43	12.95	34.04–42.81	35.90	12.28	31.74–40.05	32.24	11.14	28.47–36.01
Aorta									
Minimal luminal diameter (mm)	13.43	2.54	12.57–14.29	12.40	2.93	11.41–13.39	12.08	2.40	11.27–12.89

Table 3.3. Results of minimal luminal diameter and area measurements from automatic, the observer 1 and the observer 2 measurement.

	Observer 1 vs automatic	Observer 2 vs automatic	Observer 1 vs observer 2
Ilio-femoral			
<i>Diameter</i>			
Correlation	0.94	0.88	0.87
Bias (95% CI)	–0.32 (0.64 to –1.28)	–0.51 (0.89 to –1.90)	0.18 (1.57 to –1.20)
p value	<0.001	<0.001	<0.001
<i>Area</i>			
Correlation	0.92	0.81	0.83
Bias (95% CI)	–2.5 (7.7 to –12.8)	–6.2 (8.7 to –21.1)	3.7 (17.2 to –9.9)
p value	<0.001	<0.001	<0.001
Aorta			
<i>Diameter</i>			
Correlation	0.88	0.92	0.90
Bias (95% CI)	–1.0 (1.7 to –3.8)	–1.3 (0.6 to –3.3)	0.3 (2.8 to –2.2)
p value	<0.001	<0.001	<0.001

Table 3.4. Results of minimal luminal diameter and area measurements: comparing the automatic to observer 1 and observer 2, and the observers to each other.

The Bland-Altman plots of the minimal ilio-femoral luminal lumen diameter and area are shown in Fig 3.7. The mean and SD of the difference between the minimal luminal diameters (MLD) of the automatic segmentation and the observer1 segmentation were 0.32mm and 0.49mm, respectively, and for the minimal luminal area (MLA) 2.53mm² and 5.23mm². The mean and SD of the difference between the MLD of automatic segmentation and the observer2 segmentation were 0.51mm and 0.71mm,

respectively, and for the MLA 6.19mm^2 and 7.58mm^2 . The mean and SD of the difference between the MLD of the observer1 segmentation and the observer2 segmentation were 0.18mm and 0.71mm , respectively, and for the MLA 3.66mm^2 and 6.89mm^2 .

The Bland-Altman plots of the aorta minimal luminal diameter are shown in Fig 3.8. The mean and stand deviation of the difference between the MLD of the automatic segmentation and the observer1 segmentation were 1.03mm and 1.41mm . The mean and stand deviation of the difference between the MLD of the automatic segmentation and the observer2 segmentation were 1.35mm and 1.00mm . The mean and stand deviation of the difference between the MLD of the observer1 and the observer2 segmentation were 0.32mm and 1.28mm .

3.4 Discussion

Over the past few years, the development of TAVR pre-operative planning applications has been driven by the increasing need for proper access route selections and prosthesis size selection during TAVR, and prediction of post-TAVR vascular complications. Computed tomography has received a lot of interest because of its 3D imaging specifications as compared to 2D angiography's limited information (Okuyama et al. 2014). With multiplanar reformatting (MPR) images, the arterial lumen can be measured accurately in each cross-section, appreciating the elliptical nature of the artery (Delgado et al. 2010; Goenka et al. 2014; Krishnaswamy et al. 2014). However, such a manual detection procedure will require too much time and will introduce variabilities. An automatic procedure will be able to reduce the effort and support both inexperienced and experienced observers.

In this paper, a 3D method was introduced for the automatic segmentation of the vessel trajectory for TAVR pre-operative planning in whole-body CTA images. To our knowledge, this is the first solution which can automatically segment the whole vessel trajectory from femoral artery, iliac artery, abdominal aorta, descending aorta up to the ascending aorta in a whole-body CTA image data set published in articles.

The whole procedure only requires about 90 seconds on a computer with Core i7 3770 and 8GB RAM with 4 CPU threads, and can be further optimized. In our procedure, the quantification of the entire aorta-femoral trajectory is implemented, including the ilio-femoral arteries, the thoracic and abdominal aorta. In previous studies on aortic aneurysms, aortic measurement have also been implemented. In the work by Müller-Eschner et al it took 2.5-5.7 minutes with purely manually measurement on axial slices, and 4.6- 9.3 minutes on MPR images on the thoracic aorta; with a semi-automatic centerline extraction method, the analysis time was 3.5-9.3 minutes (Müller-Eschner et al. 2013). In the study by Kaufmann et al, the mean time to only detect the maximal diameter of the abdominal aorta aneurysm manually was 104.7 ± 24.9 s with double-oblique images and 175.2 ± 100.9 s to segment semi-automatically the abdominal aorta aneurysm to achieve maximal diameter (Kauffmann et al. 2011).

In our fully automatic segmentation procedure, a deformable subdivision surface model fitting was used. The deformable subdivision surface model is a new 3D model which processes the entire 3D data set instead of detecting the 2D transversal contour separately in each 2D image slice or detecting the 2D longitudinal contour on stretched MPR image. The control points on the subdivision surface are always searching in 3D space for the target boundary of artery. Another method which is similar to our method is the 3D deformable cylindrical Non-Uniform Rational B-Spline (NURBS) model fitting (van't Klooster et al. 2012). However, the advantages of deformable subdivision surface model fitting are that it is able to deal with objects with complex topology such as artery bifurcations and it is flexible to deal with complex shapes in the ilio-femoral luminal areas. However, when the model is too flexible, there might be self-intersection of surface. In this study, therefore, a non-self-intersection force was added to overcome this problem. In the future, we believe that the deformable subdivision surface model can also be used to segment other complex anatomical structures, such as the aortic root.

The ability to detect the minimal luminal diameter and area of the ilio-femoral arteries in each patient is another important feature of this application. For the pre-operative planning of TF-TAVR, the minimal ilio-femoral artery diameter decides the external sheath size. Post-operatively, vascular access site issues in TF-TAVR procedure are the most common companion disease (Toggweiler et al. 2013). It is the main complication in more than 15% of the patients undergoing TF-TAVR in (Krishnaswamy et al. 2014). Sheath-to-ilio-femoral artery ratio (SIFAR), defined as "sheath outer diameter divided by access-side vascular diameter" is known to be predictive of major vascular complications which have high correlation with higher mortality. Whether the TF-TAVR is acceptable will depend on the value of SIFAR (Okuyama et al. 2014). In (Krishnaswamy et al. 2014), the sheath to artery ratio was calculated by diameter and area, and the area's result seems more reliable. In this study, both diameter and area of the ilio-femoral arteries were calculated, making the patient selection procedure in TAVR pre-operative planning reliable.

Quantitative evaluations were performed in two stages. The first stage was a comparison of the automatic contours with the manually corrected contours. The dice similarity index in our study was found to be at least 0.95.

In Fig 6, the measurement of the Hounsfield units of the contrast in the descending aorta was shown. This provides the indication on the quality of the datasets, which are the amount and the standard deviation of contrast in the aorta. It is apparent that if there is less contrast in the aorta and the contrast is inhomogeneous, the extraction of the aorta will be more difficult. But however, in our procedure, the automatic segmentation results of different datasets were always good according to dice similarity index. This proves the robustness of our method.

The second stage was the comparison of clinical parameters from automatic and manually-corrected segmentation. The correlation between the automatic method and the first observer was much higher than the

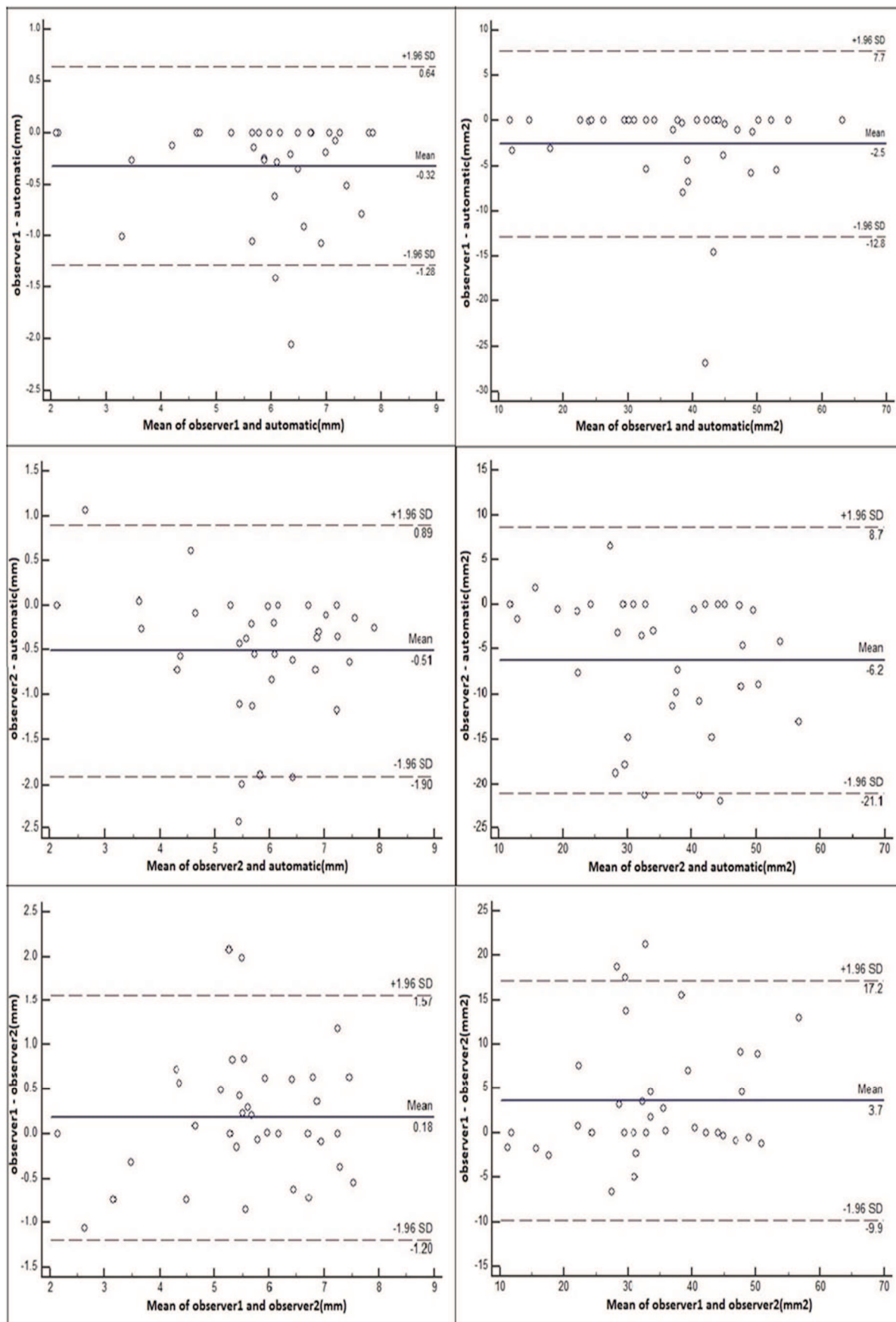
inter-observer variability, and the correlation between the automatic method and the second observer was similar to the inter-observer variability. The result indicates that the automatic method is trustful compared to the manual corrected method. The automatic method overestimated the lumen area and diameter in the ilio-femoral arteries comparing to the results from both observers slightly by around 1 pixel. The variabilities between the observers of clinical parameters are much higher than the variabilities between automatic measurement and observer 1; the variabilities between the observers of clinical parameters are similar to the variabilities between automatic measurement and observer 2. This means that our technique is more reproducible than between the observers.

In research, CTA-based semi-automatic segmentation software was used to measure minimal luminal diameter for TF-TAVR. The result was evaluated by manual results on projection angiography (XA). The difference in minimal luminal diameter between the software and the ground truth was higher than 1.2 mm in the ilio-femoral artery segments. In our study, the automatic measurement overestimated the MLA only by 0.323 mm compared to observer1, and by 0.51mm compared to observer2, similar to the size of one pixel in the images we used.

In three cases the automatic procedure showed segmentation issue, this can be explained as follows. During the subdivision surface model fitting step, the strongest edge in the intensity image was searched for within certain distance range. This search range was the same for both tiny vessel (such as femoral artery) and larger vessel such as the aorta. Making the search ranges variable for the different vessel sizes should improve the framework and prevent these issues in the future.

3.5 Conclusions

In conclusion, this automatic TAVR pre-operative application has demonstrated to be able to accurately segment the whole vascular access and measure minimal lumen of the vascular access for TAVR planning in CTA data set.



(a) Diameter

(b) Area

Fig 3.7. Bland-Altman plot of minimal ilio-femoral luminal lumen comparing automatic measurement, the observer1 and the observer2

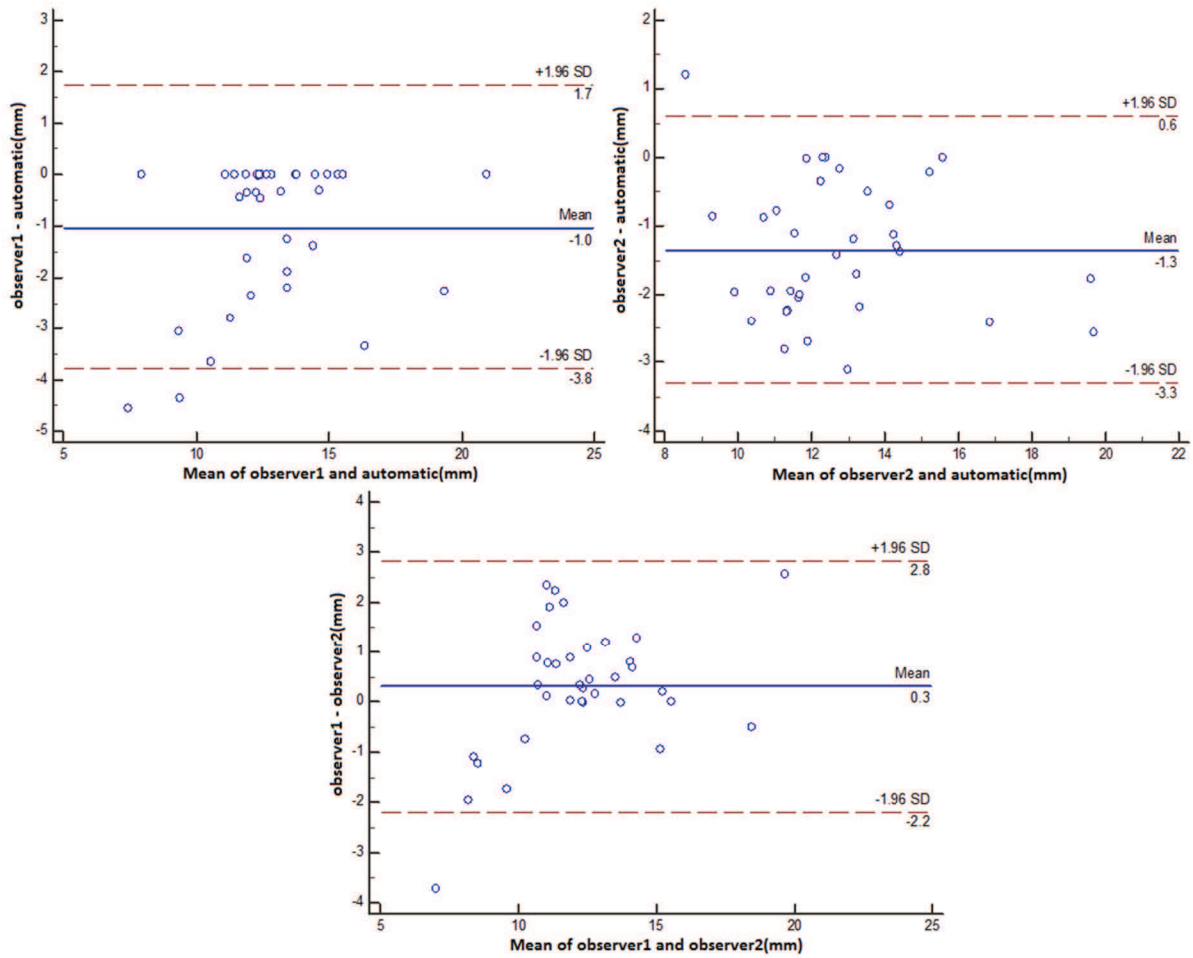


Fig 3.8 Bland-Altman plots comparing minimal aorta luminal diameter measurements between automatic, observer 1 and observer 2.

4

Automatic Aortic Root Segmentation in CTA whole-body Dataset

Xinpei Gao, Pieter H. Kitslaar, Arthur J.H.A. Scholte,
Boudewijn P. F. Lelieveldt, Jouke Dijkstra, Johan H.C. Reiber

Abstract

TAVR is an evolving technique for patients with serious aortic stenosis disease. Typically, in this application a CTA data set is obtained of the patient's arterial system from the subclavian artery to the femoral arteries, to evaluate the quality of the vascular access route and analyze the aortic root to determine if and which prosthesis should be used. In this paper, we concentrate on the automated segmentation of the aortic root. The purpose of this study was to automatically segment the aortic root in computed tomography angiography (CTA) datasets to support trans-catheter aortic valve replacement (TAVR) procedures.

In general terms, the method in this study included 4 major steps. First, the patient's cardiac CTA image was resampled to reduce the computation time. Next, the cardiac CTA image was segmented using an atlas-based approach. The most similar atlas was selected from a total of 8 atlases based on its image similarity to the input CTA image. Third, the aortic root segmentation from the previous step was transferred to the patient's whole-body CTA image by affine registration and refined in the fourth step using a deformable subdivision surface model fitting procedure based on image intensity.

The pipeline was applied to 20 patients. The ground truth was created by an analyst who semi-automatically corrected the contours of the automatic method, where necessary. The average Dice similarity index between the segmentations of the automatic method and the ground truth was found to be 0.965 ± 0.024 . In conclusion, the current results are very promising.

SPIE Medical Imaging.
International Society for Optics and Photonics,
2016: 97850F-97850F-7.

4.1 Introduction

Aortic valve stenosis is one of the most common and most serious valve diseases, which indicates the narrowing of the valve (Nishimura 2002). If left untreated, it may cause severe problems like heart failure. Previously, surgical aortic valve replacement (SAVR) was used to deal with this disease. However, not all the patients can go through this procedure. Especially, SAVR may be related with high perioperative mortality for elderly patients. Trans-catheter aortic valve replacement (TAVR) or trans-catheter aortic valve implantation (TAVI) has been introduced into clinical trial over the past years as an acceptable approach for surgically inoperable patients with severe aortic stenosis. It is a minimally invasive catheter-based implantation of a bio prosthetic aortic valve. The prostheses are set in the aortic annulus and supplant the native aortic valve leaflets (Bax et al. 2014). Until now, over 100 000 procedures have been performed across the world by the cardiologists (Wendler and Dworakowski 2014).

In contrast to SAVR, it is impossible to see the valve and annulus during the TAVR procedure. Therefore, imaging is required to help the surgery (Bax et al. 2014). With the high-resolution display of the anatomy, meanwhile with the advantage of being non-invasive, multi-slice computed tomography (MDCT) imaging has become an important pre-operative planning tool. Comparing with other image modalities such as fluoroscopy and ultrasound, CT images allow an in-depth assessment of the sophisticated 3-dimensional geometrical structure of the aortic root for prosthesis selection (Bax et al. 2014). However, manual measurements are complex with multiple operation steps, time consuming and easy to lead to variations between observers. Fully or minimally semi-automatic methods have the potential to generate faster, more reproducible analyses (Lou et al. 2015).

To support the TAVI procedures in routine clinical practice, a fully automatic measurement framework based on MDCT imaging should be strived for. So far only few papers have appeared in the literatures about segmenting the aortic root in MDCT. The work by Zheng et al (Zheng et al. 2012) describes automatic aortic root segmentation procedure in C-Arm CT images without contrast agent in left ventricle outflow tract (LVOT). This special image protocol, however, is not used in all the medical institutions. Ecabert et al (Ecabert et al. 2011) acquired the structures and big vessels in the heart ground on model-based segmentation. This workflow didn't take care of the detail of aortic root since this is not their main focus. Elattar et al (M a Elattar et al. 2014) presented a procedure to segment the aortic root in CT images fully automatically consisted by centerline extraction in ascending aorta, centerline extension into Left Ventricle Outflow Tract(LVOT) by cubic-spline extrapolation and aortic root segmentation by 3D normalized cuts. The centerline in the aortic root is achieved following the trend of the centerline in ascending aorta, which means that if the aortic root has greater curvature than ascending aorta, the centerline will have great possibility to deviate.

Atlas based segmentation is an algorithm that can integrate spatial prior knowledge from manual expert annotations into the segmentation procedure. Atlas based segmentation has the capability to capture anatomical variation more nicely and acquire better segmentation accuracy than model based approaches (Iglesias and Sabuncu 2015). However the shortcoming of atlas-based segmentation is high computational cost.

Deformable subdivision-surface model fitting is a method which segment image by deforming a triangle-based mesh surface. During the deformation step, only the neighborhood local region of the surface will be detected in the image. This makes the computational cost lower than other segmentation methods which need to capture the information of the whole images. The short-coming of the deformable subdivision-surface model fitting is that the initial model has great impact on the final result.

In this paper, a fully automatic algorithm framework for aortic root segmentation is described. This framework was composed by atlas-based segmentation as initialization and deformable subdivision-surface model fitting as refinement. The two segmentation methods can complement each other. The framework has been validated on 20 patients' CTA datasets. The accuracy of the results was evaluated by calculating the Dice similarity index of the automatic contours to the analyst corrected contours.

4.2 Materials and methods

A total of 20 patients' CTA datasets were acquired for pre-operative planning of TAVR procedures. The datasets were acquired at Leiden University Medical Center (LUMC, Leiden, the Netherlands) using standard clinical protocols. For each patient, whole-body CTA dataset and Cardiac CTA dataset were acquired. The datasets were collected using a 320-row volumetric Aquilion ONE CT scanner (Toshiba Medical System, Japan). The whole-body CTA datasets were generated by using a helical scan protocol. The cardiac CTA datasets were all R-R full dose, most cases had no ECG modulation. The voltage was 100 kV, 120 kV or 135 kV, the maximal tube current was 400–580 mA. The bi-phasic injection protocol with intravenous contrast was used: 70ml contrast (5ml/sec) and 50ml saline (5ml/sec). An example of the whole-body CTA dataset and the cardiac CTA dataset from the same patient can be seen in Figure 4.1.

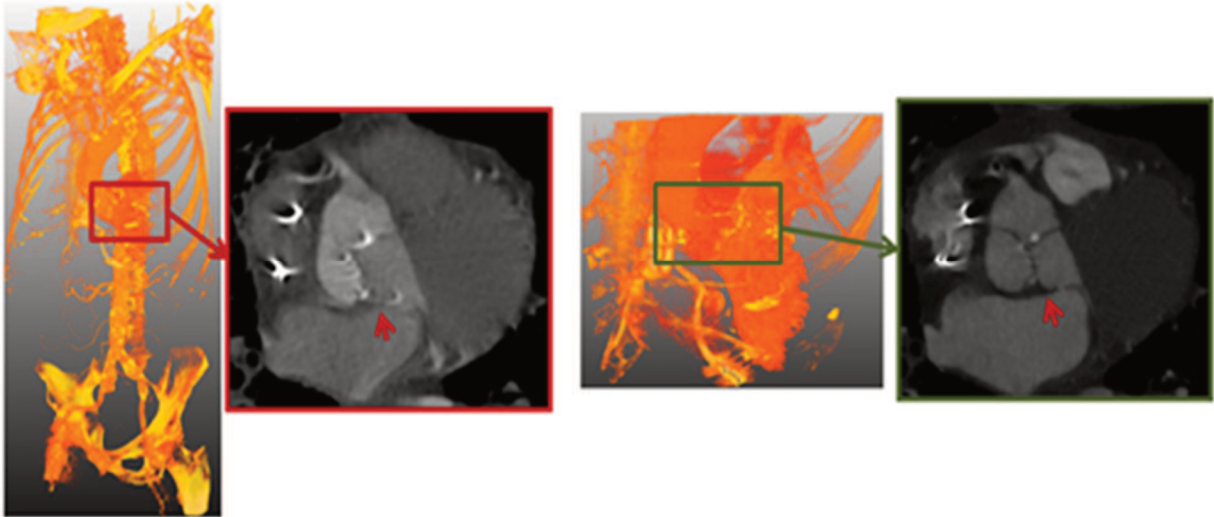


Figure 4.1. The first image is the whole-body CTA dataset, the third image is the cardiac CTA dataset. The two images are both shown by volume rendering technique. The whole-body CTA image protocol scans the patient from the femoral arteries to the subclavian arteries; the cardiac CTA image only includes the heart region and part of the aorta. The cardiac CTA images have higher quality in the heart region than the whole-body CTA images, which we can see in the second and the fourth image. The fourth image has a much clearer border of the aortic root than the second image in the area pointed by the two red arrows.

Method scheme

In this study, a fully automatic aortic root segmentation detection procedure in the whole-body CTA dataset was implemented. Figure 4.2 shows a schematic overview of the procedure, which will be described in more detail in the following paragraphs.

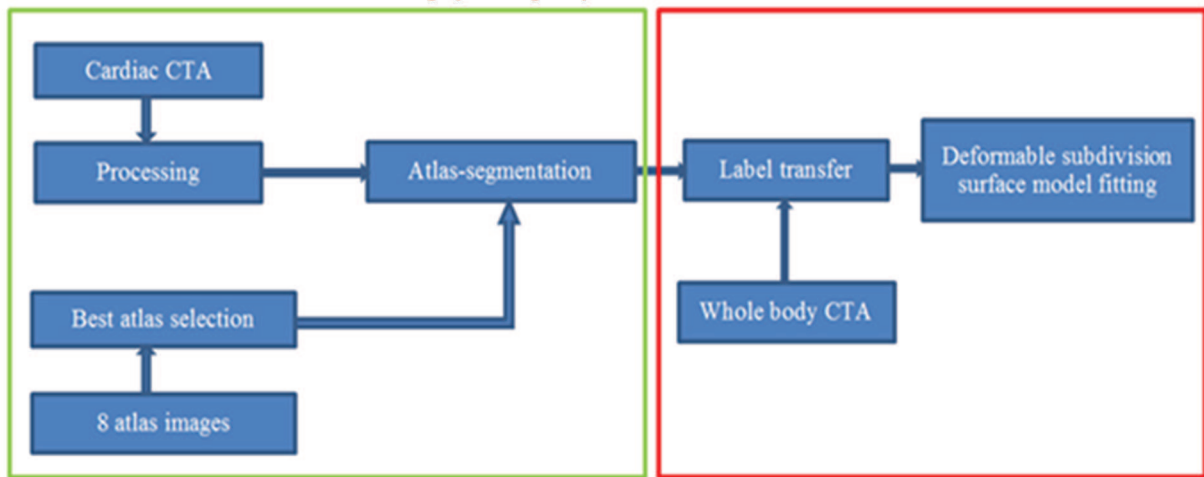


Figure 4.2. Scheme of automatic aorta valve segmentation in the whole body CTA dataset.

Preprocessing

First of all, the cardiac CTA images were down-sampled to an isotropic image for the computation time reduction. In a second step, a binary mask was generated automatically by deformable subdivision surface fitting (Kitslaar et al. 2015) to detect the edge of the lung, in this way to reduce

the background noise for registration. With the resulted subdivision surface, a binary mask image can be generated by searching for the voxels that are inside subdivision surface. This mask was used in the atlas-based segmentation step.

Atlas-based segmentation

In this paper, the image with manual segmentation by expert will be alluded to as the atlas image and the image to be segmented as the raw image. An atlas image is consisted of an intensity image and a label image, where the label image denotes the segmented area. A total of 8 atlas images were used in this study. The 8 atlas images were all from the H3D - CTA Cardiac segmentation open source package (Kirişli et al. 2010).

The atlas-based segmentation is based on the registration of the atlas image with the raw image. The whole registration procedure was realized using the Elastix toolbox, an open source software package (<http://elastix.isi.uu.nl>).

At first, the atlas images were aligned at the global level to the raw image by the affine transformation in 3D coordinates. Since the anatomical morphology of the aortic valves can vary between different patients, a local alignment of the atlas images and the raw image becomes inevitable. Therefore, as a next step a non-rigid transformation was performed to match the most similar atlas image and the raw image on a regional basis. The non-rigid transformation was brought out by B-spline parameterization (Rueckert et al. 1999).

There are different kinds of strategies in atlas-based segmentation. Most common strategy is Multi-Atlas segmentation. However the computational cost will be expensive because of multiple times of registration of atlas image and raw image. To reduce the cost, we do atlas selection after the affine transformation procedure.

The Mutual Information (MI) (Thévenaz and Unser 2000) was chosen to measure the image similarity for the registration and the atlas image selection. It reflects the relation between the probability distributions of the intensities. Because of the variation of contrast agent inside the aortic root between different patients, the intensity values of the CTA images of different patients might be nonlinear. Comparing to Correlation Coefficient, MI is more reliable and can produce better result.

The transformation parameters from the affine transformation and non-rigid transformation were applied to the related label image of the selected atlas image to produce the segmentation for the raw image. The mask from previous step was used as fixed image mask in the affine transformation and B-spline transformation step.

Label transfer

The first segmentation step was carried out on the cardiac CTA image for reasons of high image quality and more contrast agent in the aortic root; next, the segmentation result is transferred to the whole-body CTA image for doctor's convenience.

Since heart motion may have occurred between the two images, an affine registration is needed to align the two images, and to transform the

segmentation of the cardiac CTA image to the whole-body CTA image using the Elastix toolbox (Klein et al. 2010). With the centerline extracted automatically in whole-body CTA image in our previous research (Gao et al. 2014), the location of aortic root was detected. With this location as the center, the region of interest (ROI) with the same size of the cardiac CTA image in world 3D coordinate was defined in whole-body CTA image. Affine registration between the ROI image from the whole-body CTA image and the cardiac CTA image was executed. Then the transformation parameters were applied to the segmentation in cardiac CTA image. In this way, the initial segmentation of whole-body CTA image was generated (Figure 4.3).

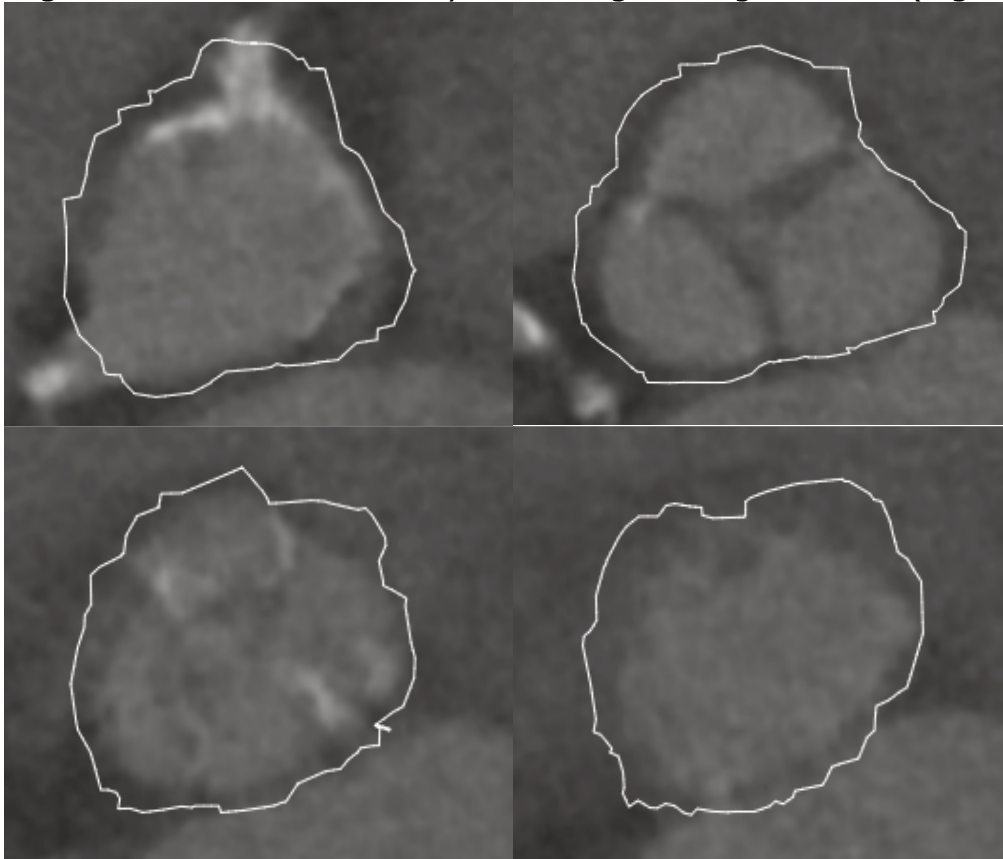


Figure 4.3. The initial result shown in MPR images with 2D contours.

Deformable subdivision surface model fitting

After the previous steps, the coarse boundary of the aortic root can be initialized in whole-body CTA image. To refine the boundary of the aortic root, a deformable subdivision surface model fitting was used as follows:

The aortic root was constructed by constant value based iso-surface. The 3D iso-surface was generated from binary image result of atlas-based segmentation by a method similar to Marching Cubes algorithm (Lorensen and Cline 1987). The image volume was discretized in cells constituted by voxels. According to the intensity value of the voxel, the triangles in the cells can be generated to conform a closed surface. In the Marching Cubes algorithm, there can be ambiguities. But here, the ambiguities would be constrained. After the iso-surface was extracted, Laplacian smoothing is

executed to reduce noise and avoid intersection of subdivision surface in the next step. To increase the control points of this mesh model to capture more details in deformable subdivision surface model fitting step, a loop subdivision scheme was used in this study (Kitslaar et al. 2015). After the initial subdivision surface was generated, the surface was refined detecting the strongest edge in CT image based on moving the control points.

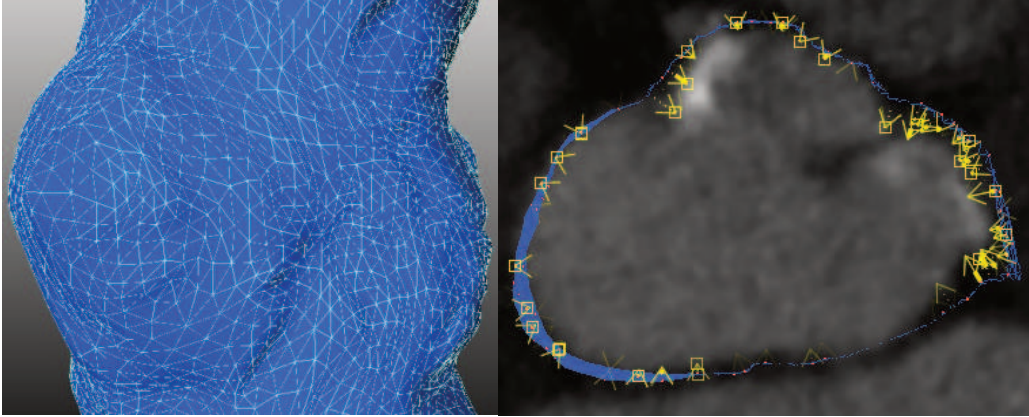


Figure 4.4. The deformable subdivision surface: left is the 3D view of the surface, right is the 2D view of the surface. In the right picture, the yellow arrow show the direction and distance the surface is going to be deformed.

4.3 Experiments and results

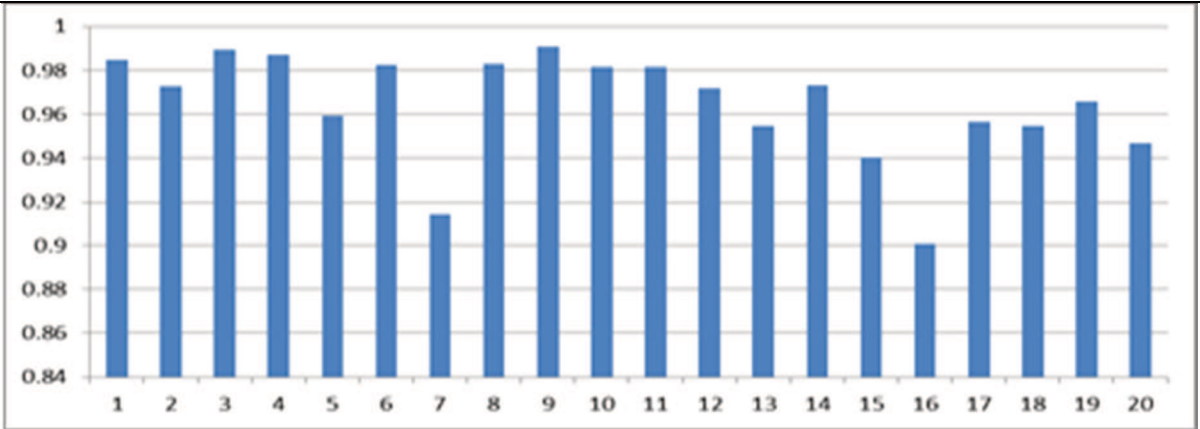


Figure 4.5. The dice similarity indexes of all the patients

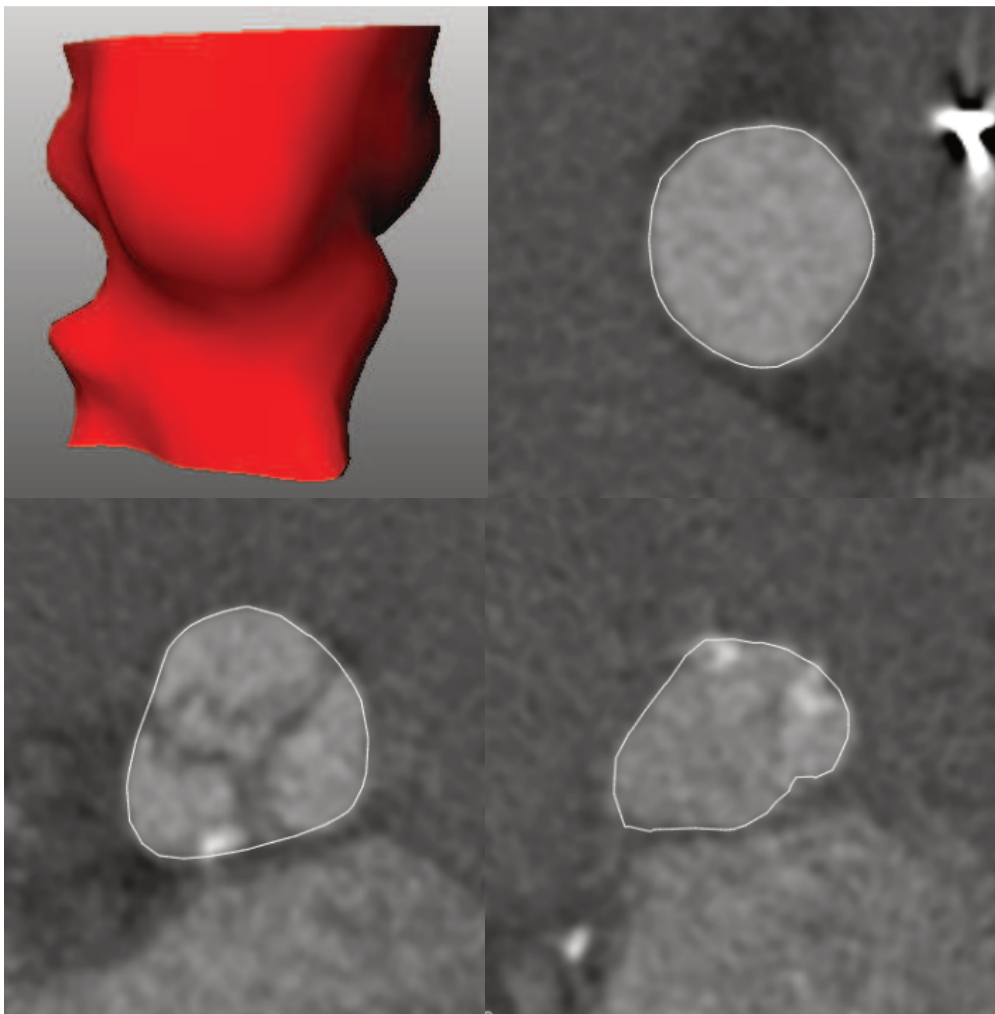


Figure 4.6. The final result. The left top is the 3D mesh surface of the segmentation; the other three images show the results of the multi-planar reconstruction images along the long axis of the aortic root.

The segmentation includes the part of the aortic root from the sinotubular junction level to the aortic annulus level. The ground truth of the 20 datasets was generated by an analyst manually correcting the automatic contours in the transversal and longitudinal planes along the long axis of the aortic root by a dedicated tool developed in MevisLab. After correcting, the 3D contour surface was resliced into 2D transversal contours to calculate the Dice similarity indexes. The average Dice similarity index between the segmentations of the automatic method and the ground truth is 0.965 ± 0.024 ; the individual results of the 20 patients are presented in Figure 4.5. In Figure 4.6, we show some automatic segmentation result by the 3D mesh surface and 2D contours in the multi-planar reconstruction images along the long axis of the aortic root.

4.4 Discussion and conclusion

In this paper, we developed a fully automatic method to segment the aortic root from the cardiac CTA datasets and whole-body CTA datasets. The validation results demonstrate high Dice similarity indexes between the fully-automated and the semi-automatic segmentation results. The whole procedure for each patient only requires about 60 seconds on a computer with Core i7 3770 and 8GB RAM with 4 CPU threads, and is able to be further optimized.

Several papers have been published on aortic root segmentation (Ecabert et al. 2011; M a Elattar et al. 2014; Grbic et al. 2012; Zheng et al. 2012). Elattar et al (M a Elattar et al. 2014) proposed an aortic root segmentation scheme, and the validation was done on 2D contours in only 3 image slices in each patient and the average dice similarity index between the automatic contour and the expert result was 0.95 ± 0.03 . In the paper, it was also showed that his result is better than those of Zheng et al (Zheng et al. 2012) and Grbic et al (Grbic et al. 2012). Our method has provided a higher average dice similarity index than 0.95 on our data set.

In some methods like graph-based segmentation algorithm, it can be a problem to segment the detail structure of aortic valve out. Some graph-based algorithms are based on the intensity similarity within the same tissue and dissimilarity between different kinds of tissues. However, there is contrast agent in both aortic valve and LVOT in CTA image. It could be difficult to differentiate aortic valve and the LVOT by these kinds of methods with similarity of intensities.

However, in this paper, the procedure we proposed has the potential to segment the detailed structure of aortic root out. The alignment of patient's image and atlas image is done globally and locally by spatial intensity distribution. After the alignment of the images, the label in the atlas image will be transferred into the patient image. If the alignment by registration is accurate enough, even if the structure is sophisticated, the segmentation can be fulfilled.

The segmentation result of aortic valve will be included in our future paper. Some initial result of segmentation the aortic valve can be shown (Figure 4.7).

From the above, we may conclude that we have developed an efficient and fully automatic aortic root segmentation algorithm with big potential. We hope that our approach will be used in the future as a support tool in the pre-procedure planning of TAVR procedures.

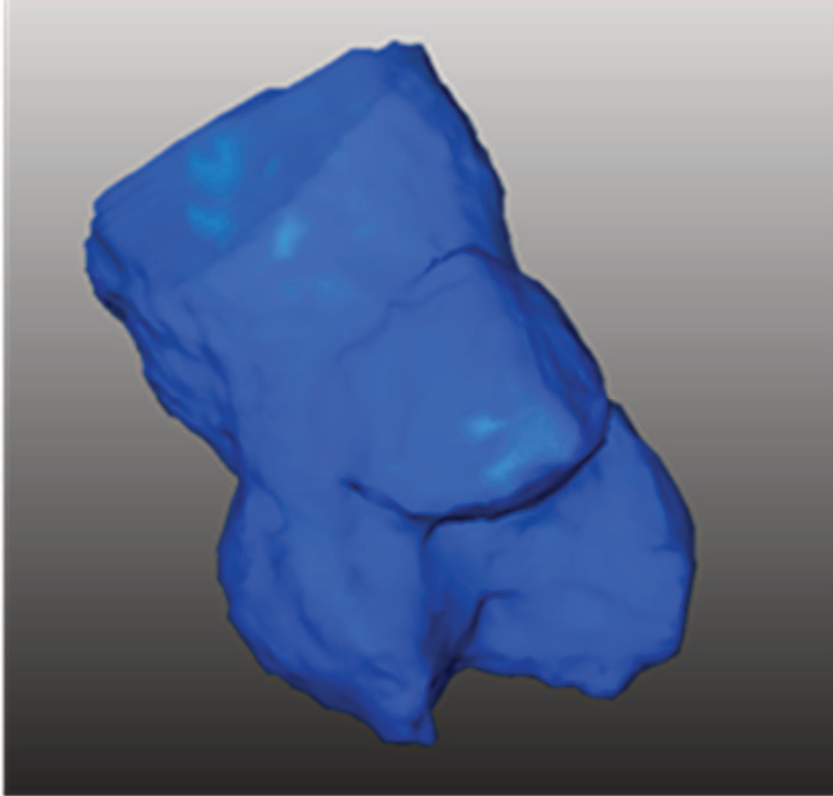


Figure 4.7. The initial result of segmentation of the aortic valve shown in 3D subdivision surface

5

Quantification of Aortic Annulus in Computed Tomography Angiography: Validation of a Fully Automatic Methodology

Xinpei Gao, Sara Bocalini, Pieter H. Kitslaar, Ricardo P.J. Budde, Mohamed Attrach, Shengxian Tu, Michiel A. de Graaf, Tomas Ondrus, Martin Penicka, Arthur J.H.A. Scholte, Boudewijn P.F. Lelieveldt, Jouke Dijkstra, Johan H.C. Reiber

Abstract

Background: Automatic accurate measuring of the aortic annulus and precise determination of the optimal angulation of X-ray projection are important for the trans-catheter aortic valve replacement (TAVR) procedure. The objective of this paper was to present a novel fully automatic methodology for the quantification of the aortic annulus in computed tomography angiography (CTA) images.

Methods: CTA datasets of 26 patients were analyzed retrospectively with the proposed methodology, which consists of a knowledge-based segmentation of the aortic root and detection of the orientation and size of the aortic annulus. The accuracy of the methodology was determined by comparing the automatically derived results with the reference standard obtained by semi-automatic delineation of the aortic root border and manual definition of the annulus plane.

Results: The difference between the automatic annulus diameter and the reference standard by observer 1 was 0.2 ± 1.0 mm, with an inter-observer variability of 1.2 ± 0.6 mm. The Pearson correlation coefficient for the diameter was good (0.92 for observer 1). For the first time, a fully automatic tool to assess the optimal projection curves was presented and validated. The mean difference between the optimal projection curves calculated based on the automatically defined annulus plane and the reference standard was 6.4° in the cranial/caudal (CRA/CAU) direction. The mean computation time was short with around 60 seconds per dataset.

Conclusion: The new fully automatic and fast methodology described in this manuscript not only provided reliable measurements about the aortic annulus size with results comparable to experienced observers, but also predicted optimal X-ray projection curves from CTA images.

European Journal of Radiology, August 2017, Volume 93, Pages 1–8, 2017. DOI:
<http://dx.doi.org/10.1016/j.ejrad.2017.04.020>

5.1 Introduction

During TAVR procedure, the aortic root is not directly visible for physicians, thus pre-operative imaging is principal to determine the size and orientation of the aortic annulus. These measurements are essential to select and deliver the appropriate prosthesis in the aortic valve. Bias in the selection and placement of the prosthesis, may result in complications e.g. aortic annulus rupture, prosthesis shift or paravalvular regurgitation.

As a noninvasive, high-resolution 3D imaging modality, computed tomography (CT) enables the accurate imaging of the anatomical structures of the aortic root (Achenbach et al. 2012). The orientation of the aortic root can be determined manually from the CTA dataset in order to predict the optimal X-ray projection angle during prosthesis implantation in the Cath lab. An optimal X-ray projection curve with multiple available angles can be useful for physicians to choose their familiar angles (Gurvitch et al. 2010).

This reduces procedure time, the volume of contrast material used and radiation dose. However, in order to avoid the potential reproducibility issues of a manual measurement and to achieve faster reporting time, a fully automatic aortic root analysis methodology based on CTA images would be promising.

In this paper, we put forward a novel fully automatic methodology which is able to size the aortic annulus, and predict the optimal projection curve based on CTA image. The results were validated in datasets from two clinical centers to investigate its accuracy and robustness.

5.2 Materials and methods

Study population and CT protocol

26 patients from two hospitals were candidates for TAVR and underwent an ECG-gated CTA scan as the routine clinical investigation. The patients' identifiable information was completely anonymized before this study started. Table 5.1 describes the scan protocols for the CTA scans used in this study. Diastolic phases from the reconstructed images were used.

	Hospital A	Hospital B
Number of patients	19	7
CT scanner	320-row detector	128 x2 detector
	Single source	Dual source
	Aquilion ONE	Somatom Definition Flash

	Toshiba Medical System, Otowara, Japan	Siemens Healthcare, Forchheim, Germany
Acquisition	R-R full dose, in most cases no ECG modulation.	Prospective ECG-gating
Scan parameter [‡]	100, 120kV or 135kV, 400-580mA	100,120kV, 350-400mA
Injection protocol	bi-phasic injection	bi-phasic injection
	Intravenous in ante-cubital vein	Intravenous in ante-cubital vein
	70ml contrast (5ml/sec) and 50ml saline (5ml/sec)	90ml contrast(4ml/sec) and 100ml saline (4ml/sec)
Reconstruction parameter	slice thickness 0.5mm, interval 0.25mm	slice thickness 0.75mm, with 0.4mm increment

‡ Tube voltage and current were adapted for each patient on the basis of body mass index (BMI) and thoracic anatomy.

Table 5.1 CTA protocols of the two clinical centers

Fully automatic aortic annulus detection framework

In a previously published study (Gao, Kitslaar, Scholte, et al. 2016), we described a fully automatic segmentation method for pre-TAVR whole-body CTA datasets with a high mean dice similarity coefficient (0.965 ± 0.024) of the contours of the automatic methodology and the reference. In this study, an adapted framework based on the previous method was used for segmentation of the aortic root in the cardiac CTA images.

The procedure for automatic annulus detection works as follows: first, the data sets were resampled and the heart region was masked out automatically by a deformable subdivision surface fitting algorithm (Gao, Kitslaar, Scholte, et al. 2016). Then, the three-dimensional contours of the aortic root, as well as left ventricle outflow tract (LVOT) were detected with an atlas-based segmentation algorithm. Eight cardiac CTA images with manual annotations were used as the atlas images. Each patient's image was registered to the atlas images by an affine registration algorithm. The most similar atlas image was selected based on the similarity measure (Mutual information) of the atlas image and the patient image for a subsequent B-Spline deformation registration algorithm (Klein et al. 2010). After registration, the manual segmentation of the selected atlas image was

deformed by the transformation parameters from previous steps, therewith the patient's image was initially segmented. Finally, we refined the segmentation by an adaptive subdivision surface model fitting method based on gradient information (Kitslaar et al. 2015).

The automatic extraction of the aortic annulus depend on the anatomy of the aortic root. The aortic root is a complex 3-dimensional structure that starts at the left ventricle outflow tract (LVOT). It consists of the sinotubular junction, aortic sinuses of Valsalva, as well as valve leaflets (Underwood et al. 2000). The aortic annulus plane is a suppositional plane composed by the hinge points of the leaflets beyond the LVOT. It can also be called 'basal ring' (Schoenhagen, Hausleiter, et al. 2011). The prosthesis is settled on the location of the aortic annulus during the TAVR procedure.

After the extraction of the aortic root and the LVOT by the atlas-based segmentation, we calculated the connecting region between the aortic root and the LVOT. By applying the principal component analysis (Shlens 2014), the orientation of the connecting region between the aortic root and the LVOT can be found, which defines the orientation of the annulus plane.

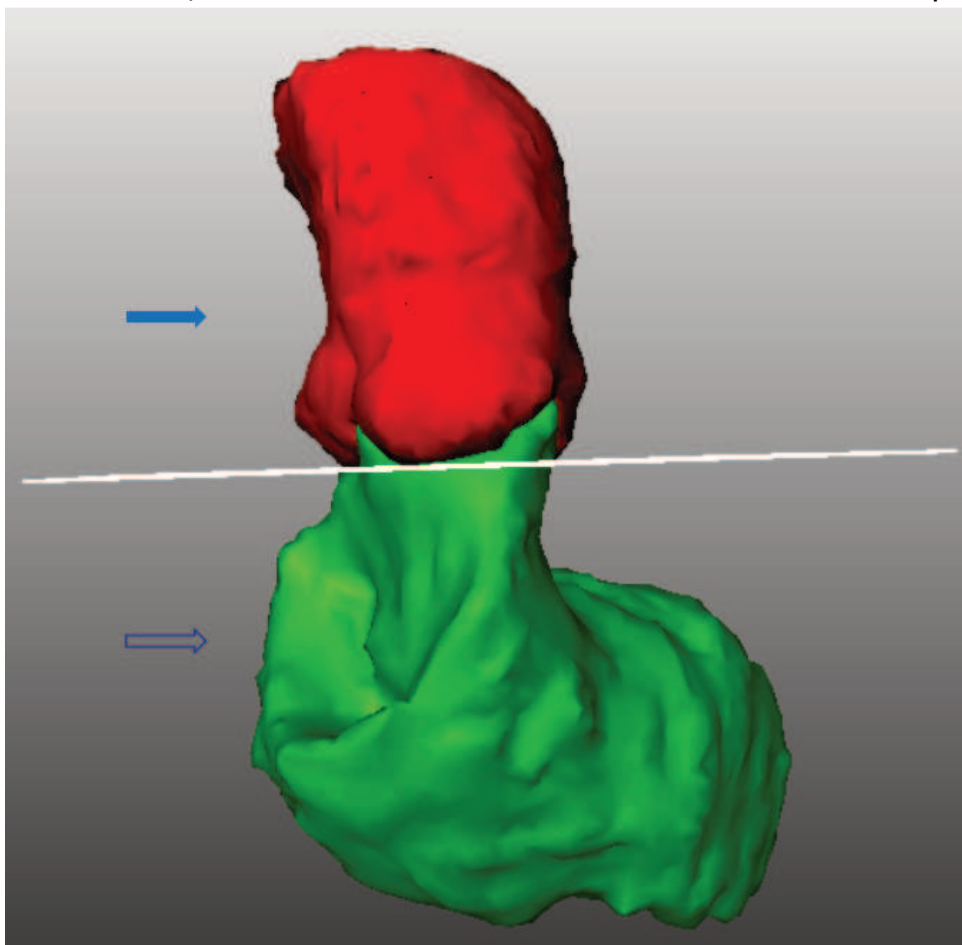


Figure 5.1 - Annular plane detection: the red top part represents the segmentations of the aortic root (solid arrow) and green low part LVOT (hollow arrow), the white plane corresponds to the plane of the aortic annulus.

Prediction of optimal projection curve for X-ray

The identification of X-ray projections orthogonal to the aortic annular plane is important for the correct valve deployment during the TAVR procedure. With the orientation of the aortic annulus plane computed in the previous step, an infinite number of projections can be calculated which allows the 3 hinge points of the valves to appear on the same line in the X-ray projection view (Kurra et al. 2010). An optimal projection curve with left/right anterior oblique (LAO/RAO) angles as the x-axis, and cranial/caudal (CRA/CAU) angles as the y-axis, was calculated. Following the diagram style employed in the study by Binder et al (Binder et al. 2012), LAO/RAO angles ranging from 45° RAO to 45° LAO were represented with 5° steps. Based on these LAO/RAO angles, each patient's CRA/CAU angles were computed (Figure 5.2).

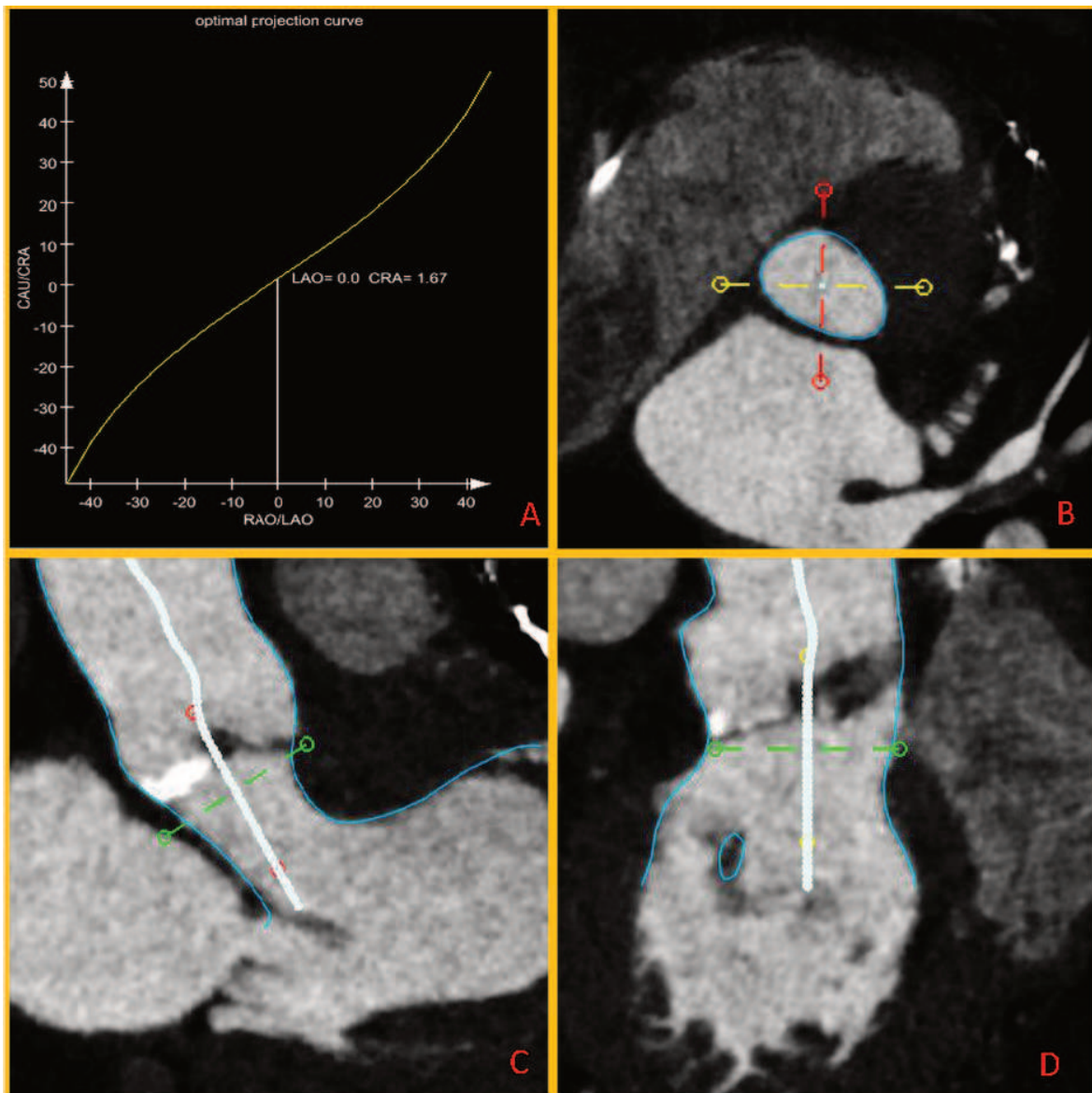


Figure 5.2 - The optimal projection curve and related images: A - the optimal projection curve; B – multi-planar image of the annulus plane; C – oblique image

corresponding to the optimal X-ray projection D – oblique image perpendicular to image B & C.

Evaluation of aortic annulus detection

The automatic methodology was integrated into a dedicated in-house tool (AortaValveViewer 1.2, LKEB, Leiden, Netherlands), with functions for manual interactions. The tool was implemented in the MeVisLab environment (version 2.7.1, MeVis Medical Solutions AG, Bremen, Germany) with C++ and Python code.

Two observers performed the measurements for the evaluation of the performance of our automatic methodology (both of them have at least 4 years' experience working in cardiovascular imaging and 100 annulus diameters assessments). The two observers used the in-house tool independently to create reference standards for statistical analysis. The observer adjusted double oblique multiplanar reconstruction (MPR) images manually to find the plane in which the three aortic valve hinge points appear in the same slice. Three landmarks were annotated manually on the hinge points, which defined the annulus plane. Then the observer corrected the automatically segmented surface from the sinotubular junction to the LVOT (5mm under the aortic annulus) by drawing contours in cross-sectional and oblique view images (Figure 5.2 B, C & D).

The annular cross-sectional contour was extracted from the aortic root segmentation where it intersected with the annulus plane. The size of the aortic annulus was surveyed using the area, radius, diameter, long-axis diameter (LAD), as well as short-axis diameter (SAD) and perimeter. The radius (R) of the aortic annulus was calculated based on the area (A): $R = \sqrt{A/\pi}$; the diameter was obtained based on the radius (D): $D = 2R$.

The center of the annulus was defined as the center of its contour and automatically calculated. Next, the angle between automatic and manual plane orientations, the 3D Euclidean distance between the centers of the annulus contours obtained from the automatic and manual planes were measured (Deza and Deza 2009). In addition, the optimal X-ray projection curve was calculated for each patient from the automatic and manual plane orientations by observer 1. The mean optimal X-ray projection curve of all the patients was obtained. Automatic and manual curves were compared with each other in the CRA/CAU axis.

A four points scale quality score (4 = perfect, 3 = good, 2 = reasonable, 1 = poor) based on motion artifacts and contrast in the aortic root was used to evaluate the image quality by observer 1. The extent of the calcification in the aortic root at the level of the annulus or immediately nearby (caudal part of the cusps and cranial LVOT) was graded into 4 levels: 1 = none, 2 = light, 3 = medium, 4 = heavy.

Evaluation of prosthesis size selection

The sizes of the prosthesis which had been implanted during the TAVR procedure into the patients from hospital A were retrieved. The selection of the prosthesis performed in clinical practice was retrospectively compared with a theoretical choice of the valve based on the automatic and semi-automatic annulus measurements of our tool. The annulus area measurements of the in-house tool were categorized based on the commercially available valve sizes: 23, 26, 29 mm for the Edwards SAPIEN XT valves and 23, 26, 29, 31 mm for the CoreValve (Kasel et al. 2013; Lou et al. 2015). Prosthesis selection based on area measurements is summarized in Table 5.5 and 5.6. If the measurement fell into the gray zone, both prostheses with smaller or bigger size were considered as suitable.

Edwards SAPIEN Valve (mm)	23	gray zone	26	gray zone	29
Area (mm ²)	300 - 380	380 - 415	415 - 490	490 - 530	530 - 620

Table 5.5 Selection table for Edwards SAPIEN XT valve

Core Valve (mm)	23	26	29	31
Area (mm ²)	254.5 - 314.2	314.2 - 415.5	415.5 - 572.6	530.9 - 660.5

Table 5.6 Selection table for Core valve

Statistical analysis

In this study, SPSS (version 20.0, SPSS Inc., Chicago, IL) were used for the statistical analyses, along with MedCalc (version 15.6, Ostend, Belgium). The variables were analyzed by the mean, standard deviation (SD), and the Pearson correlation coefficient if normally distributed and continuous. The normality was evaluated by the Shapiro-Wilk test (Shapiro and Wilk 1965). Bland-Altman plots were drawn to visualize the bias. P value < 0.05 indicated significant result.

5.3 Results

This study population consists of 26 patients, and the baseline characteristics are described in Table 5.2. The patients differ in age, gender, as well as the existence of previous percutaneous coronary intervention (PCI), previous myocardial infarction (MI) and previous coronary artery bypass grafting (CABG), in other words, a population with pathological diversity.

Patient number	Total (26)
Age (years)	79 ± 13
Gender (% male)	15 (58%)
Diabetes	4 (15%)
Hypertension	17 (65%)
Hypercholesterolemia	16 (62%)
Family history of CAD	3 (12%)
Smoking	2 (8%)
Obesity	5 (19%)
Previous PCI	13 (50%)
Previous CABG	12 (46%)
Previous MI	5 (19%)

In the data, age is described by mean ± SD, other items are outlined by percentages of the population.

Table 5.2 Baseline Characteristics of the patients in the study

Image quality score and calcification level

The average image quality score was 2.4. The percentage of scans with poor image quality was 15%, reasonable 42%, good 31%, and perfect 12%. The average score of images from hospital A was 2.6, the mean score of hospital B was 1.9. Only 1 patient had no calcification (4%). The amount of calcification in the remaining patients was light in 12 cases (46%), medium in 10 cases (39%) and heavy in 3 patients (12%). The mean calcification amount of all the patients was light to medium (2.6) with a lower average value for patients scanned at hospital A (2.4) compared to hospital B (3.1).

Accuracy of the orientation of the aortic annulus

The difference between the annulus plane orientations was 9.4 ± 4.6 degrees for observer 1, and 7.6 ± 3.7 degrees for observer 2, with 4.2 ± 3.3 degrees for the inter-observer variability. The average and standard deviation of the distance between the automatic and manual annulus center locations was found to be 1.7 ± 1.0 mm for observer 1, 1.6 ± 1.0 mm for observer 2, and the inter-observer variability was 1.2 ± 0.7 mm. The individual errors are presented in Figure 3, where the patients are represented by numbers. For patients 13 and 19 with an associated error higher than 15 mm, the image quality was poor. For patients 10 and 26, who presented an error for the location of the center higher than 3mm, the image quality was reasonable.

For the patients from hospital A, the average error of the plane orientation was 9.0 degrees for observer 1 and 7.2 degrees for observer 2; for patients from hospital B, the mean error of the orientation was 10.4 degrees for observer 1 and 8.2 degrees for observer 2.

Assessment of the optimal projection curve

In Figure 5.4, the mean optimal projection curves of the patients from the automatic methodology and observer 1 are presented together with their standard deviations. The mean difference in CAU/CRA for all the patients was 6.4 degree. The standard deviations of the two curves were similar to each other, representing the range of the CAU/CRA angle in all the patients.

Evaluation of the size of the aortic annulus

Area, radius, diameter, LAD, SAD, and perimeter were calculated for the evaluation of the aortic annulus size measurement. Table 5.3 shows the mean, standard deviation and 95% CI of these parameters of the automatic measurement and the two observers. Table 5.4 shows the Pearson correlation coefficient and difference (mean \pm SD) of the parameters between the automatic measurement and the reference standards. Figure 5.5 shows the Bland-Altman plots for all the annulus size measurements (automatic VS observer 1).

Evaluation of prosthesis size selection

Based on our fully-automatic measurement, in 78.9% (15 out of 19) of cases the selection of the prosthesis size would have been the same as in clinical practice. When observer 1 applied corrections to the fully-automatic measurement, the agreement rate increased to 89.5% (17 out of 19).

Computation time of the method

Our automatic methodology takes around 60 seconds to detect the contour of the aortic root and measure the aortic annulus in one dataset on

a workstation. Observers needed on average 12 minutes to generate the reference standard.

5.4 Discussion

In recent years, many studies have been published on aortic annulus size quantification based on CTA images, for the evaluation and validation of both semi-automatic (Delgado et al. 2011; Foldyna et al. 2015; Stortecky et al. 2014; Watanabe et al. 2013) and fully-automatic (Mustafa Elattar et al. 2016; El Faquir et al. 2016; Ionasec et al. 2010; Lou et al. 2015; Wächter et al. 2010) tools. Fully automatic tools require less user interaction for the physicians. In our study, the main goal was to evaluate our tool for fully automatic annulus size quantification. Ionasec et al. (Ionasec et al. 2010) developed a system to model and quantify the left heart valves. In their study the precision of the annular circumference was 8.46 ± 3.0 mm. Elattar et al. (Mustafa Elattar et al. 2016) introduced an automated detection method which enabled automated sizing based on Normalized cut, and Gaussian curvature map. The automatically generated aortic annulus radius' average difference was 0.2 ± 0.7 mm with observer 1, and 0.4 ± 0.8 mm with observer 2. Lou et al. (Lou et al. 2015) evaluated the results of fully automatic aortic annulus sizing from a commercial tool, and reported an area measurement calculated by observer 1 with the automated method without manual correction of 5.4 ± 0.96 cm², and of 4.8 ± 0.87 cm² with manual correction; with the same methods, observer 2 obtained area values of 5.4 ± 0.95 cm² versus 5.0 ± 0.91 cm². Wachter et al. (Wächter et al. 2010) used a model-based algorithm to detect the aortic valve anatomy, obtaining errors for the short and long diameters of the annulus of 0.8 and 1.0 mm, respectively. In Queirós et al.'s study (Queirós et al. 2016), the area-derived diameter calculated by the automatic aortic root algorithm was compared with manual results from two observers, the difference was 0.08 mm for the observer 1 and 0.25 mm for the observer 2. Our framework can detect the aortic root in all the patients, the correlation of the diameter was good, and the errors of the aortic annulus size parameters were small, comparable with previous studies (Mustafa Elattar et al. 2016; Ionasec et al. 2010; Lou et al. 2015; Wächter et al. 2010) and comparable to the human observer difference (Table 4).

Just a few studies about optimal X-ray projection curve prediction were published (El Faquir et al. 2016; Samim et al. 2013). In Faquir et al.'s study (El Faquir et al. 2016), the optimal projection curves of the automated software were calculated based on the aortogram, not on CTA images. The median difference between the optimal projection curves of the automated software calculated based on the aortogram and manual ground-truth was

8.8 and 14.6 degrees in two different cohorts. In Samim et al.'s study (Samim et al. 2013), the calculation was based on CTA images, however, the prediction of optimal projection curves was not performed fully automatically. The novelty of the present study consists in the fact that for the first time a fully automatic tool is presented which can perform the optimal projection curve prediction on CTA images.

In the study by Lou et al. (Lou et al. 2015), the influence of the measurement on the prosthesis size selection was also evaluated. For the first observer, the fully automated and the manual measurements agreed on the prosthesis selection in 51.8% of the patients, while the agreement of the semi-automated and the manual measurements was 87.6%. For the second observer, the fully-automated and the manual measurement agreed in 52.8% of the cases, while the agreement of the semi-automated and the manual measurement was 82.4%. In our study, the agreement rate between our fully automatic measurement and clinical practice was 78.9%, and between our semi-automatic measurement and clinical practice 89.5%.

Due to the broader employment of the TAVR procedure and the subsequent increase in the number of pre-procedural CT scans, the images processing time is becoming crucial. According to Elattar et al.'s description (M a Elattar et al. 2014), their automatic contour detection of the aortic root took 90 seconds without the detection of the aortic annulus and the calculation of the clinical parameters in the aortic root. In our study, the average computation time including aortic root segmentation, automatic detection, and calculation of the clinical parameters of the aortic annulus was shorter (around 60 seconds) and can be further improved.

Only diastolic images were used in this study. There have been studies which investigated the impact of using diastolic and systolic images on prosthesis sizing (Bertaso et al. 2012; Blanke et al. 2012; De Heer et al. 2011). Bertaso et al. (Bertaso et al. 2012) measured the difference of aortic annulus size between diastole and systole, and found that the difference was not significant enough to change prosthesis size selection; while in de Heer et al.'s study (De Heer et al. 2011), the opposite conclusion was reached. In Blanke et al.'s study (Blanke et al. 2012), the annulus was measured throughout the full cardiac cycle, and it turned out that the phase in which the annulus has the biggest size would be the most suitable phase for prosthesis selection. However, this ideal phase can be diastolic or systolic depending on the patient. The method presented in this study can be used for automatic annulus measurement in patients whose ideal phase is in diastole.

In our study, two kinds of CT scanners (Aquilion ONE scanner and Somatom Definition Flash scanner) with different acquisition protocols were

used from two hospitals. The patients who were scanned in hospital A had a higher image quality and a lower amount of calcium. Image quality had an impact on our automatic tool. The angulation results were better in the patients from hospital A, where an Aquilion ONE scanner was used. However, the 3 patients with the heavy calcifications did not show higher error, which indicates that our framework is not influenced by calcification.

The current study has a number of limitations. Firstly, given the limited number of data sets, the robustness of the method cannot be adequately assessed. We plan to investigate this in a more extensive study with more data. Secondly, the automatic measurement of the sinotubular junction, sinus of Valsalva and LVOT have been developed in our methodology, but not validated in this study. Finally, the optimal projection curve has not been compared with the actual projection during the TAVR procedure in the Cath lab.

5.5 Conclusion

Our newly developed methodology of automatic aortic annulus quantification on CTA images has been demonstrated to be accurate compared to the semi-automatic results. A fully automatic optimal X-ray projection curve prediction algorithm based on CT image was described. Our methodology provides physicians with information about the size and orientation of the aortic annulus in detail, which can help with the prosthesis selection in the pre-operative planning of TAVR.

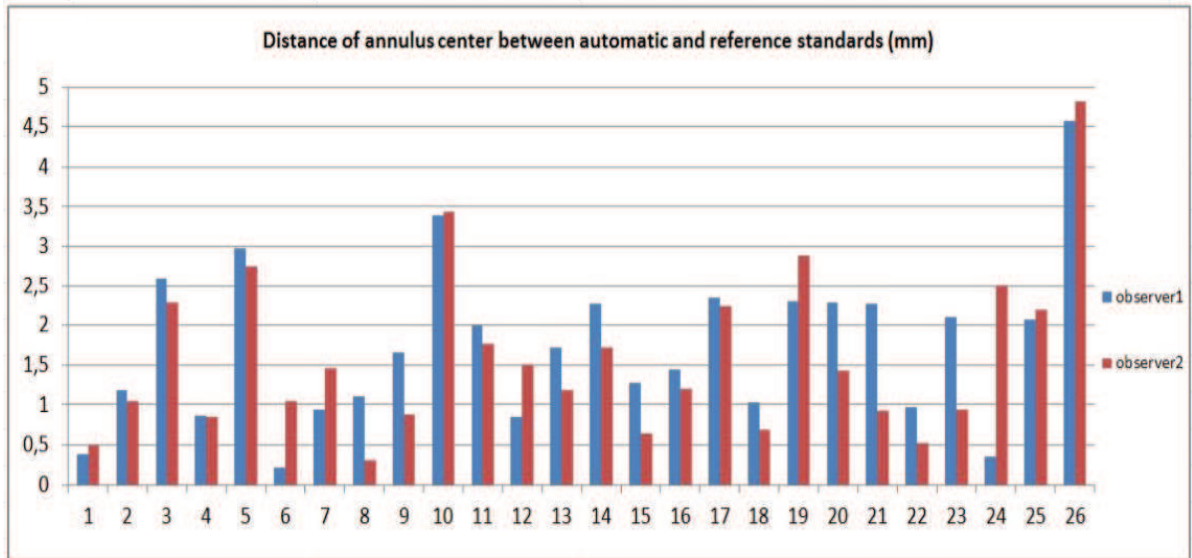
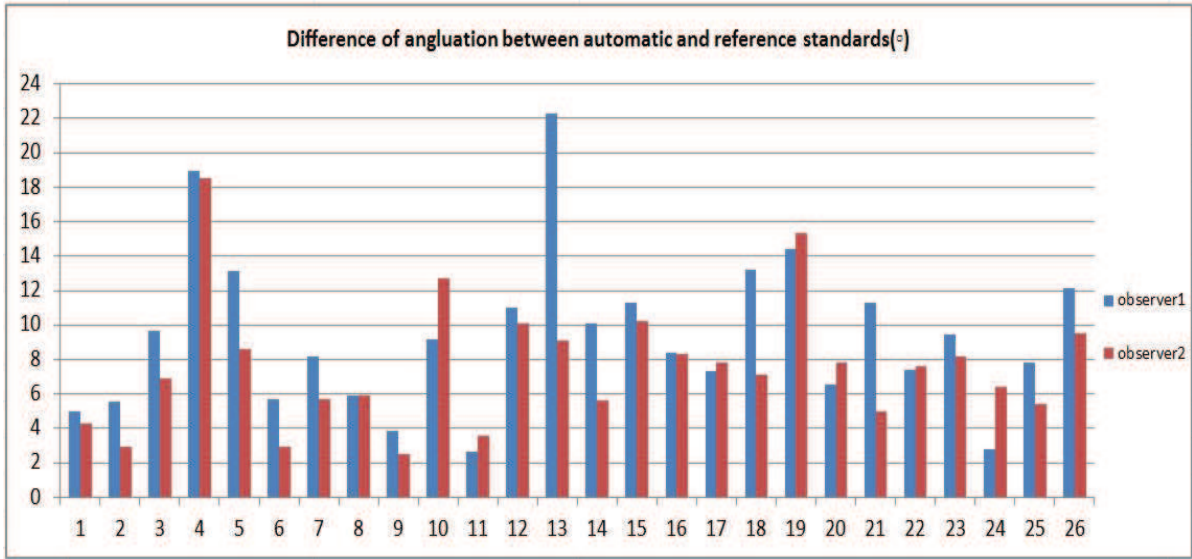


Figure 5.3 - The difference in the degree of the aortic annulus orientation between automatic and the observers.

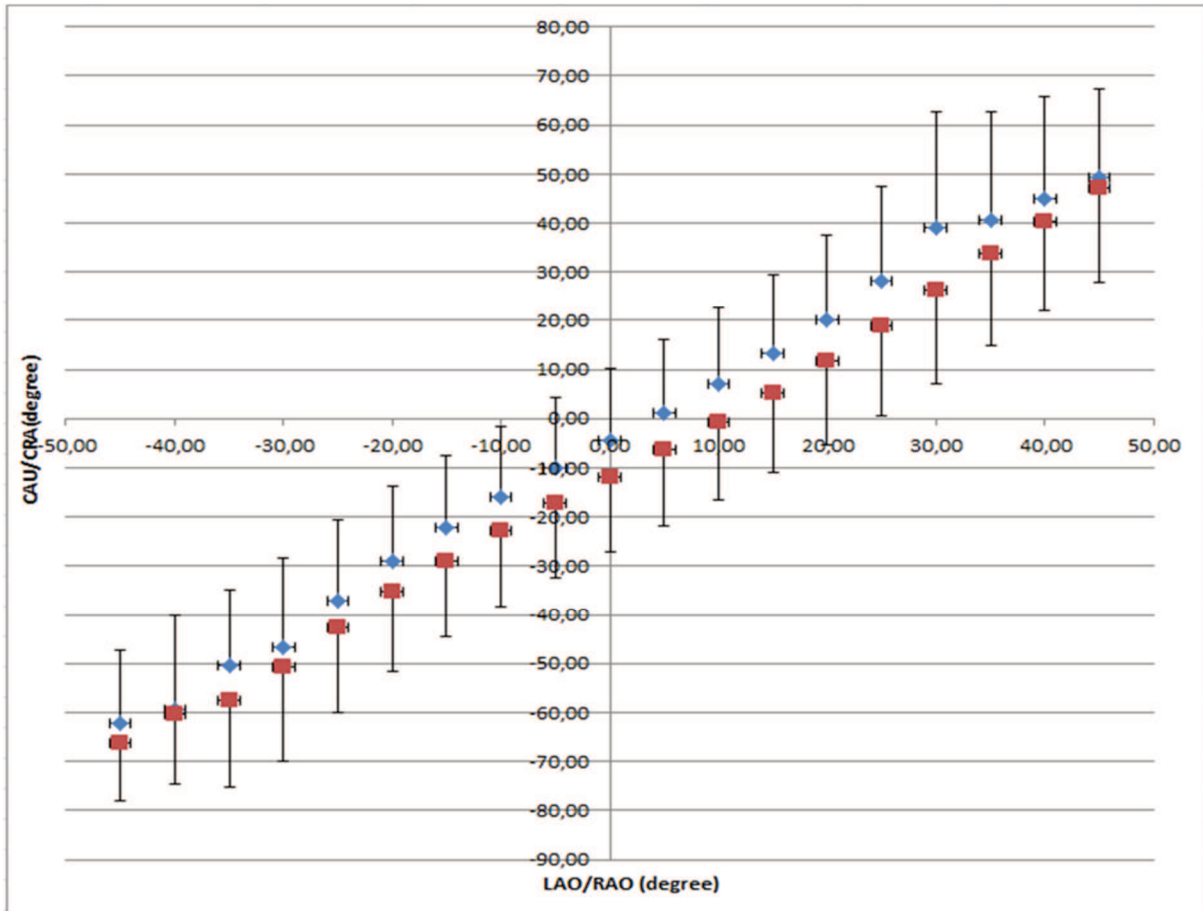


Figure 5.4 - Optimal projection curve: the mean optimal projection curve of the CAU/CRA angulation of automatic measurement (blue) and observer's measurement (red). The horizontal bars above the blue dots show the SDs of automatically extracted CAU/CRA of all the patients. The bars beneath the red dots represent the SDs of the observer's measurement.

Aortic annulus	unit	Automatic measurement			Observer 1			Observer 2		
		mean	SD	95% CI	mean	SD	95% CI	mean	SD	95% CI
Area	cm ²	4.8	1.0	4.4 to 5.2	4.7	1.0	4.3 to 5.1	5.1	1.0	4.7 to 5.6
Radius	mm	12.3	1.3	11.7 to 12.8	12.1	1.3	11.6 to 12.7	12.8	1.3	12.2 to 13.2
Diameter	mm	24.5	2.6	23.5 to 25.6	24.3	2.6	23.2 to 25.3	25.5	2.6	24.4 to 26.5
Long-axis diameter	mm	30.5	4.4	28.8 to 32.3	29.9	3.5	28.5 to 31.3	31.1	3.3	29.8 to 32.5
Short-axis diameter	mm	21.4	2.6	20.4 to 22.4	21.1	2.5	20.1 to 22.1	22.2	2.5	21.2 to 23.1
perimeter	mm	80.3	9.5	76.4 to 84.1	78.5	8.2	75.2 to 81.8	82.1	8.0	78.9 to 85.3

Table 5.3 Results of the detection of aortic annulus size from automatic measurement and reference standard.

Aortic annulus	unit	Automatic VS Observer 1		Automatic VS Observer 2		Observer 1 VS Observer 2	
		Correlation	Difference (mean ± SD)	Correlation	Difference (mean ± SD)	Correlation	Difference (mean ± SD)
Area	cm ²	0.92	0.1 ± 0.4	0.89	0.4 ± 0.5	0.97	0.5 ± 0.2
Radius	mm	0.91	0.1 ± 0.5	0.88	0.5 ± 0.6	0.97	0.6 ± 0.3
Diameter	mm	0.91	0.2 ± 1.0	0.88	1.0 ± 1.2	0.97	1.2 ± 0.6
Long-axis diameter	mm	0.85	0.7 ± 2.3	0.78	0.6 ± 2.8	0.94	1.2 ± 1.2
Short-axis diameter	mm	0.82	0.3 ± 1.5	0.78	0.8 ± 1.7	0.96	1.0 ± 0.7
Perimeter	mm	0.82	1.8 ± 5.5	0.81	1.8 ± 5.5	0.97	3.6 ± 2.0

Table 5.4 Results of aortic annulus size measurement comparing the automatic measurement to reference standard.

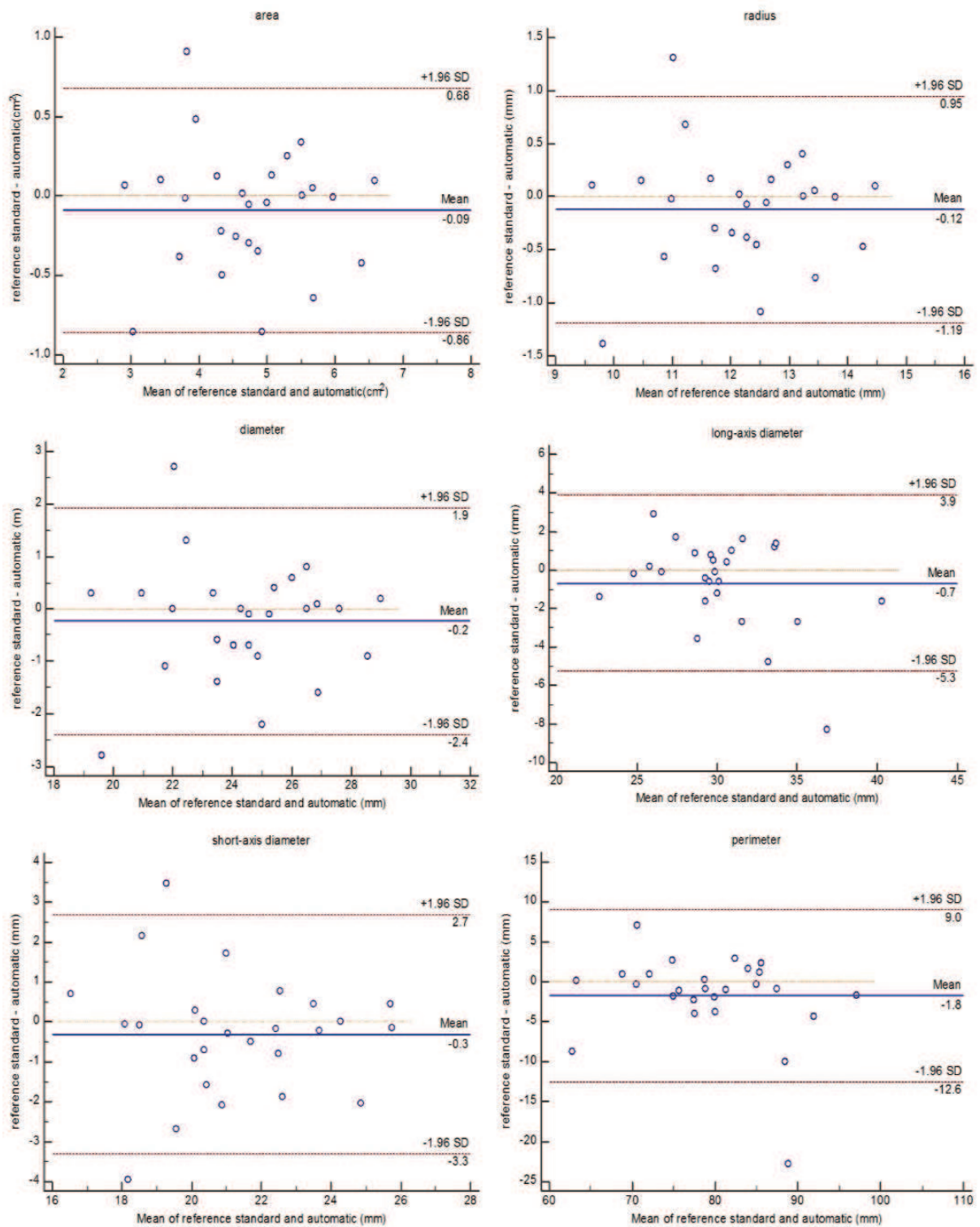


Figure 5.5 Bland-Altman plots of aortic annulus parameters

6

Fully automatic volume quantification of aortic valve calcium in coronary computed tomography angiography

Xinpei Gao, Pieter H. Kitslaar, Michiel A. de Graaf,
Alexander Broersen, Shengxian Tu, Boudewijn P.F. Lelieveldt,
Arthur J.H.A. Scholte, Jouke Dijkstra, Johan H.C. Reiber.

Abstract

Background: Aortic valve calcium quantification has significant meaning for the prognosis of coronary and cardiovascular disease. The extent of calcium is also correlated to the occurrence of paravalvular regurgitation after the procedure of trans-catheter aortic valve replacement. In this study, we evaluated a new fully automatic approach to detect and quantify the presence and degree of aortic valve calcium.

Methods: This retrospective study consisted of 68 patients who went through computed tomography angiography because of potential coronary artery disease. The first step is the automatic detection of the aortic root. Next, double-oblique images were automatically reconstructed to properly display the aortic valve. Finally, the calcium on the valve was segmented by thresholding, and the volume score was calculated. For the validation, a reference standard was set by an experienced cardiologist using a semi-automatic method.

Results: In this study, the median of the reference standard calcium volume was 0.54 mm³ (range: 0 to 1131.23 mm³, 25th-75th percentile: 0 to 12.00 mm³). The median of the automatic calcium volume score was 0.46 mm³ (range: 0 to 1136.17 mm³, 25th-75th percentile: 0 to 11.22 mm³). The median difference was 1.82 mm³ (25th-75th percentile: 0 to 5.08 mm³), with the Spearman rank correlation coefficient of 0.81 ($p < 0.001$). The Bland-Altman analysis illustrated that the bias between the automatic result and the reference measurement was -1.1 mm³ with limits of agreement between -16.2 and +14.1 mm³. The specificity of our automatic approach was 82.4%; the sensitivity was 85.3%. The mean processing time was 90 seconds.

Conclusions: This study demonstrated that a new fully automatic approach for aortic valve calcium quantification is accurate.

6.1 Introduction

The existence of aortic valve calcium (AVC) in contrast-enhanced computed tomography is a first indication for the presence of coronary and cardiovascular related diseases (Cueff et al. 2010; Kamperidis et al. 2014; Owens et al. 2012). AVC was found to correlate significantly with subclinical atherosclerosis (Owens et al. 2012). Furthermore, it can be used to appraise the extent of aortic stenosis (Cueff et al. 2010). In recent years, AVC has also proven to be related to paravalvular regurgitation or mortality after trans-catheter aortic valve replacement (TAVR) (Bettinger et al. 2015; Sinning et al. 2013). Therefore, the quantification of AVC has become an important indication. However, quantifying the AVC can be complicated. The direction of the aortic valve plane is usually oblique to the axial CT slices, which requires multiple steps of manual interactions to obtain a proper plane parallel to the valve. To reduce the manual interaction and improve the workflow, an automatic AVC quantification tool for contrast-enhanced CT scans would be preferred.

Therefore a new fully automatic approach to quantify calcium on the aortic valve was developed in this study. The accuracy of the method was appraised by comparing the calcium volume score with the results of an experienced cardiologist using a semi-automatic tool.

6.2 Methods

Patient cohort and CT protocol

This study used the same coronary computed tomography angiography (CCTA) image database as described in Kamperidis et al. (Kamperidis et al. 2014). The CCTA images of the patients were collected at Leiden University Medical Center in the period of November 2007 to April 2010. The patients were referred for a CCTA examination by the treating physician on the basis of standard clinical procedures to estimate the possible presence of coronary artery disease. Two different scanners were used, one was a 64-slice system with 64×0.5 mm collimation, and the other one a 320-slice system with 320×0.5 mm collimation, both from Toshiba Medical Systems, Japan. For the 64-slice scanner, the reconstruction parameters were 120kV and 300 mA, 0.3mm, reconstruction at 75% of the RR interval. For the 320-slice scanner, the reconstruction parameters were 120kV and 400 to 580 mA according to the patient's body mass index (BMI) and thoracic anatomy, 0.5 mm with 0.25 mm increment, reconstruction also at 75% phase of the R-R interval.

Automatic aortic valve calcium measurement

Automatic segmentation of aortic root

The automatic AVC measurement approach was implemented based on the algorithms that were previously developed for whole-body CT scans (Gao, Kitslaar, Budde, et al. 2016; Gao, Kitslaar, Scholte, et al. 2016). The approach follows the subsequent steps: First, the aortic root was segmented automatically using a registration-based algorithm (Kirişli et al. 2010). Second, the initial segmentation was refined according to the intensity distribution of the original images (Gao, Kitslaar, Scholte, et al. 2016).

Automatic detection of centerline and annulus plane

Figure 6.1(a) interprets the aortic root by a diagram. The aortic annulus plane was calculated from the segmentations of step 6.2.2.1. The 2D cross-sectional contours were calculated from the 3D surface of the segmentation from the ascending aorta into LVOT along the direction of the aortic annulus (Figure 6.1(b)). The area curve diagram was calculated from the 2D contours. According to Figure 6.1(a), starting from the aortic annulus plane up into the ascending aorta, the Sino-tubular junction plane is the first valley point along the area curve after the aortic annulus (Figure 6.1(c)).

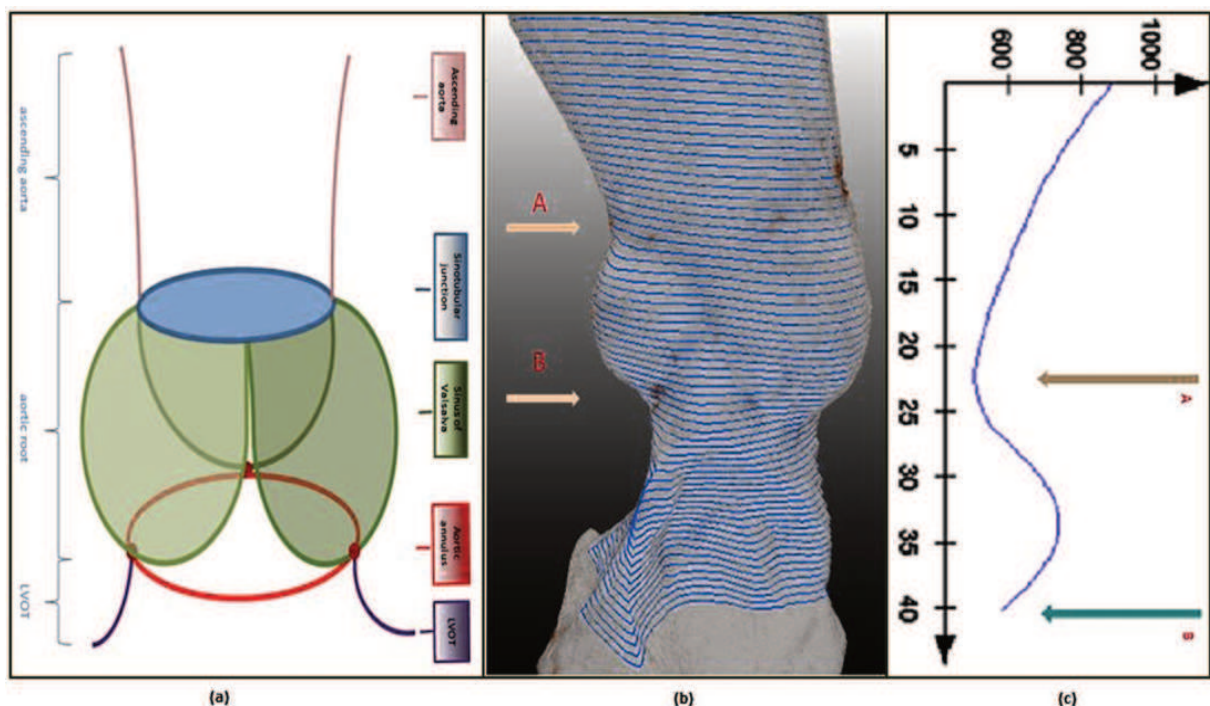


Figure 6.1 Automatic detection of annulus plane: (a) A schematic representation of the anatomical structure of the ascending aorta, aortic root and LVOT. (b) The 2D cross-sectional contours obtained from the 3D segmentation from ascending aorta into LVOT. Arrow A – sino tubular junction, arrow B – aortic annulus. (c) The area curve of 2D cross-sectional contours along the aortic root: arrow A - sino tubular junction, arrow B - aortic annulus. (y axis - mm, x axis- mm² , the curve range is from ascending aorta (40mm above aortic annulus) to aortic annulus.

Automatic detection of the calcium

With the aortic annulus orientation and location from the previous step, double oblique reformatted image slices (in-plane resolution 0.39mm × 0.39mm and field of view 100mm × 100 mm) parallel to the aortic annulus were created from the original image volume to clearly visualize the detailed structure of the aortic valves and the localization of the calcium in and around the aortic root (Figure 6.2). The slab thickness was set to 3 mm according to the previous study (Kamperidis et al. 2014). Within the region of the aortic root detected, a fixed threshold was used to segment the calcium. A cutoff value of 130 Hounsfield units (HU) is frequently used for the segmentation of the calcium in the coronary artery in non-contrast CT images (Agatston et al. 1990). However, in contrast images, the HU value of contrast-enhanced vascular structures can be all above the level of this value. In the work by Ewe et al. (Ewe et al. 2011) and Kamperidis et al. (Kamperidis et al. 2014), 800 HU was considered as a reasonable value for the calcium threshold in CCTA images and generated quantification results correlated to clinical outcome. In our study, 800 HU was also used as the threshold value. The volume of the voxels above this threshold in the reformatted images was used to compute the AVC volume.

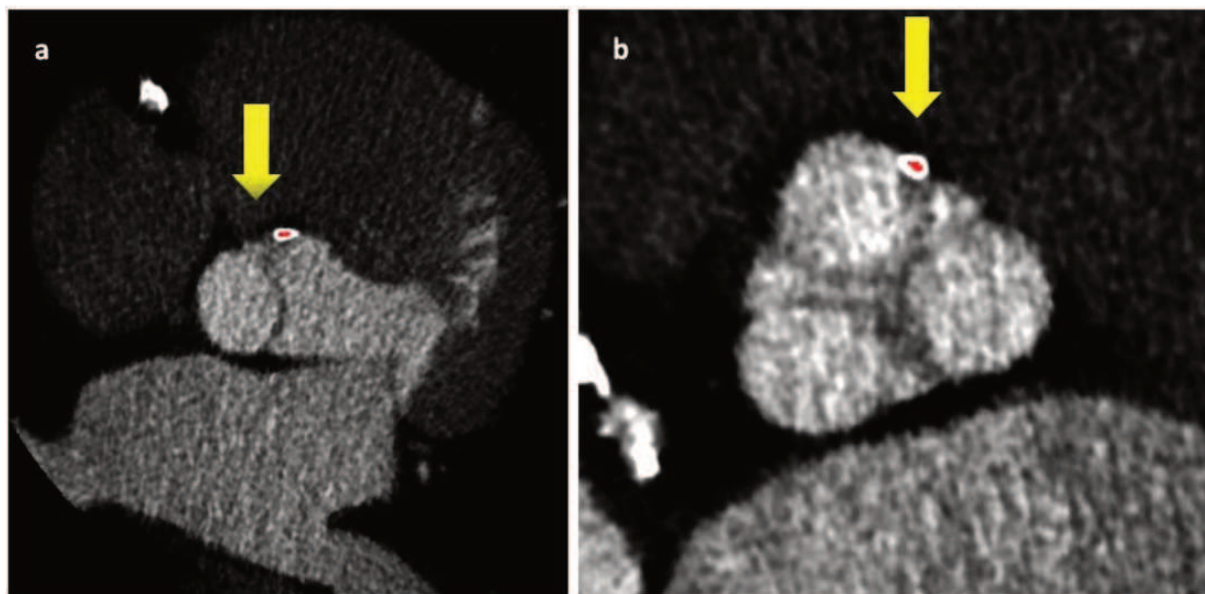


Figure 6.2. Aortic valve calcium in the same position in one patient in different views: (a) axial view (b) double oblique reformatted view. In Figure b, the location of the calcium relative to the aortic valve is much easier to determine than in Figure a.

Reference standard

In the study of Kamperidis et al. (Kamperidis et al. 2014), quantification of AVC was implemented by a semi-automatic image post processing tool (customized research version of CalcScore V1.1.1, Medis specials bv). The original image was first re-oriented manually to obtain a double oblique

reformatted view. In this view, the three lowest points of the aortic valve cusps appear at the same time (according to the definition of the aortic annulus). A 3 mm slab thickness was used in this tool according to the reference standard for scoring coronary artery calcium. Next, the user manually annotated the calcium which was in the aortic valve.

Statistical analysis

If normally distributed (based on the Shapiro-Wilk test), the error of the automatic results was quantified by average difference and standard deviation, meanwhile the correlation analyzed by the Pearson correlation coefficient. Otherwise, the differences were expressed by median and interquartile range, and the correlation by Spearman rank correlation. The median difference is the median of all absolute differences. Bland-Altman plots were generated to show the deviation and the limits of agreement. P-values lower than 0.05 were deemed as statistically significant. Specificity and sensitivity were calculated for the classification of AVC and no-AVC cases with the number of true positive (TP), true negative (TN), false positive (FP) and false negative (FN) cases.

Implementation

The whole framework was implemented in the MeVisLab (version 2.7.1, MeVis Medical Solutions AG, Germany) environment.

The statistical analyses were carried out with SPSS (version 20.0, SPSS Inc., USA) along with MedCalc (version 15.6, Belgium).

6.3 Results

Patient characteristics

In total, 68 patients were included. According to the reference standard, 34 were with AVC, and 34 without AVC (selected randomly); the baseline characteristics are presented in Table 6.1.

	Total (68)
Age (years)	61 ± 11
Gender (% male)	43 (63%)
Diabetes	19 (28%)
Hypertension [†]	33 (49%)
Hypercholesterolemia [‡]	28 (41%)
Family history of CAD [*]	21 (31%)
Smoking	14 (21%)
Obesity	17 (25%)

Table 6.1. Patient characteristics

Data are represented as mean \pm SD, median (interquartile range) or as number and percentages of patients.

†Defined as systolic blood pressure \geq 140 mm Hg and/or diastolic blood pressure \geq 90 mmHg or the use of antihypertensive medication.

‡Defined as serum total cholesterol \geq 230 mg/dL or serum triglycerides \geq 200 mg/dL or treatment with lipid lowering medication.

*Defined as the presence of coronary artery disease in first-degree family members at age $<$ 55 years in men and $<$ 65 years in women.

CAD: coronary artery disease

Aortic valve calcium score

According to the Shapiro-Wilk test, neither the results of the reference standard nor our automatic approach was normally distributed. The median calcium volume score of the reference standard was 0.54 mm³ (range: 0 to 1131.23 mm³, 25th-75th percentile: 0 to 12.00 mm³). The median of the automatic calcium volume score was 0.46 mm³ (range: 0 to 1136.17 mm³, 25th-75th percentile: 0 to 11.22 mm³).

Automatic aortic valve calcium score evaluation

The median difference of the calcium volume between the automatic measurement and reference standard for the patient cohort in this study was 1.82 mm³ (25th-75th percentile: 0 to 5.08 mm³). The Spearman rank correlation coefficient between the results of the two measurements was 0.81 ($p < 0.001$). In Figure 6.3, two Bland-Altman plots of all the 68 patients are shown. Figure 6.3A shows the plot of the full range of quantified volumes (0 to 1200 mm³). Figure 6.3B is a magnified plot of the volume range from 0 to 100 mm³ excluding a seriously calcified AVC case whose calcium volume score greatly differs from the other patients. The Bland-Altman analysis showed that the bias between the automatic and the ground truth is -1.1 mm³ with limits of agreement between -16.2 mm³ and +14.1 mm³.

Of the 34 patients without AVC, the automatic approach also did not detect any calcium in 28 patients (specificity: 82.4%). For the 34 patients with calcium on the aortic valve, the automatic approach also assigned a non-zero score to 29 patients (sensitivity: 85.3%). Table 6.2 shows the contingency table of the results.

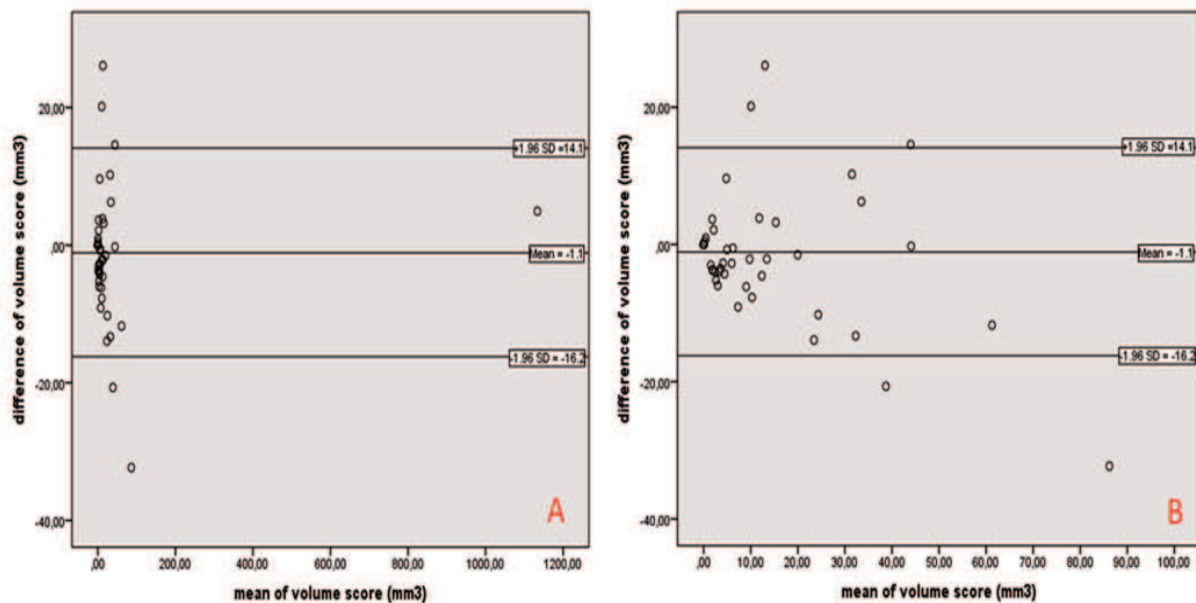


Figure 6.3. Bland-Altman plot of aortic calcium volume score. Figure A is the plot including all the results. Figure B is the plot within the magnified view of the range from 0 to 100 mm³. Difference of volume score = automatic measurement – reference standard. Mean of volume score = (automatic measurement + reference standard)/2.

		reference standard	
		calcium	no-calcium
automatic measurement	calcium	TP = 29	FP = 6
	no-calcium	FN = 5	TN = 28

Table 6.2. The contingency table of all the patients: true positive (TP), true negative (TN), false positive (FP) and false negative (FN)

Time needed for the computation

The automatic quantification approach needs on average 90 seconds to segment and quantify the calcium in a single CCTA scan on a typical workstation.

6.4 Discussion

Two studies have been published related to the aortic valve calcium quantification, Jilaihawi et al.'s semi-automatic method (Jilaihawi et al. 2014) and Grbic et al.'s automatic methods (Grbic et al. 2013). Grbic et al. discussed an automatic method to extract the aortic valve model including calcium. The Dice Similarity Coefficient was analyzed, but the calcium scoring was not presented. Jilaihawi et al. investigated the clinical impact of a semi-automatic tool for aortic valvar calcium quantification, which proved that both leaflet and left ventricle outflow tract calcium can predict

paravalvular leakage. However, no automatic quantification of calcium scoring in aortic valve has been evaluated.

In this study, a fully automatic approach to quantify aortic valve calcium scoring on CCTA scans was presented and evaluated in this study. Physicians will be able to use this to do the batch measurement in large population cohort studies.

With the same threshold set to 800 HU as the semi-automatic method, the AVC quantification results depend on the automatic detection accuracy of the aortic root. The aortic root was segmented successfully in all the patients by visual examination, which indicated that the algorithms in our previous studies (Gao, Kitslaar, Budde, et al. 2016; Gao, Kitslaar, Scholte, et al. 2016) developed especially for TAVR-related patients, can also be used in CCTA images scanned for diagnosis of CAD with different CT protocol and different anatomy.

We evaluated the automatic calcium segmentation results by comparing the median and Spearman rank correlation with semi-automatically obtained reference standard values. The correlation coefficient was excellent with the number 0.81. The left panel in Figure 6.3 showed that most of our volume scores were within a small range [0,100] with a single heavy calcified patient in the range [1000, 1200]. Bland-Altman plots show the bias between automatic measurement and reference standard. The range 0 - 1200 mm³ included all the patients. The magnified plot in range 0 - 100 mm³ enables a more detailed view of the results. In Figure 6.3A, the serious calcified patient's bias was within limits of agreement. Figure 6.3B showed that when the volume score is larger, the difference between the automatic measurement and reference standard is also larger.

The classification of AVC is important for a calcium score quantification system for risk assessment and cardiovascular disease prediction. For our system, there were 6 FP and 5 FN cases. The specificity was 82.4% and sensitivity 85.3%.

The main likely cause of the 5 FN patients and the 6 FP patients was the partial volume effect. This generated a difference between our results and the reference standard since a double oblique reconstruction of the image was used. Rutten et al. (Rutten, Isgum, and Prokop 2008) described the influence of partial volume effect on coronary artery calcium scoring and prediction of risk factors due to small variations in starting position of MPR images. With a different starting position, the calcium distribution changed. This can lead to the variation of the calcium quantification results with a fixed threshold. Similarly, in our system, first, the center and direction of the aortic annulus were detected. The positions of the MPR images were defined by the two parameters. The bias of the annulus location and

orientation between our automatic approach and the reference standard can cause variations in the start positions and orientations.

In Figure 6.4, panel (a) &(c) show the multiplanar reconstruction (MPR) images in the reference standard, panel (b) & (d) show the MPR images of the same patient by the automatic approach. The locations of the calcium were different, and the intensity of the calcium changed too. This patient was considered to have no calcium in the reference standard, but had calcium in the automatic approach.

To investigate the effect of a change in orientation we applied a 5-degree orientation difference in MPR images of the same patient. The 5 degrees was chosen based on work by Tzikas et al. (Tzikas et al. 2010), where a 10-degree cut-off is used to distinguish accurate measurements while evaluating the angular difference of aortic annulus orientation. In Figure 6.5 the six MPR images show the aortic root of the same patient. The calcification distribution in the aortic valve leaflets changed when the reconstruction orientation changed for 5 degrees (top versus bottom row). This can lead to the variation of the calcium quantification results as proven by Rutten et al. (Rutten, Isgum, and Prokop 2008). The difference of the calcium volume score for these two orientations is 8.39 mm^3 , which is much higher than the median and mean error of our approach.

In the ground truth measurement, the region of the aortic root was defined manually. The definition of the top of the region was different. There is no standard of the definition of AVC as far as we know. According to Hanneman et al.'s description (Hanneman et al. 2015), the sino-tubular junction is the highest level at which the aortic valve cusps and commissures are attached to the aortic wall. In order to include all the aortic valve cusps in our automatic method, we used the sino-tubular junction. In the reference standard, the coronary ostium were used. When there was calcium beyond the coronary ostium inside the aortic root, the results can be different in our automatic approach compared with the reference standard. This effect caused 2 false positive (FP) cases.

There are several aspects that can be improved in this study. Firstly, the quantification results of AVC were assessed only by comparing the quantified volumes with a manual reference standard that has shown to vary with small changes in image orientation. The clinical value of our automatic method can be further evaluated by directly analyzing the relationship between the automatic calcium measurement and risk factors of a patient. Secondly, the performance of the automatic algorithm needs to be tested on patients with a broader range of AVC. Finally, the segmentation of the calcium into separate valves, which reflects the

distribution of calcium, can be realized in future based on the extension of the methods described in this study.

In conclusion, a fully automatic aortic valve calcium quantification approach was established and evaluated in this study. The evaluation proved that the approach is accurate.

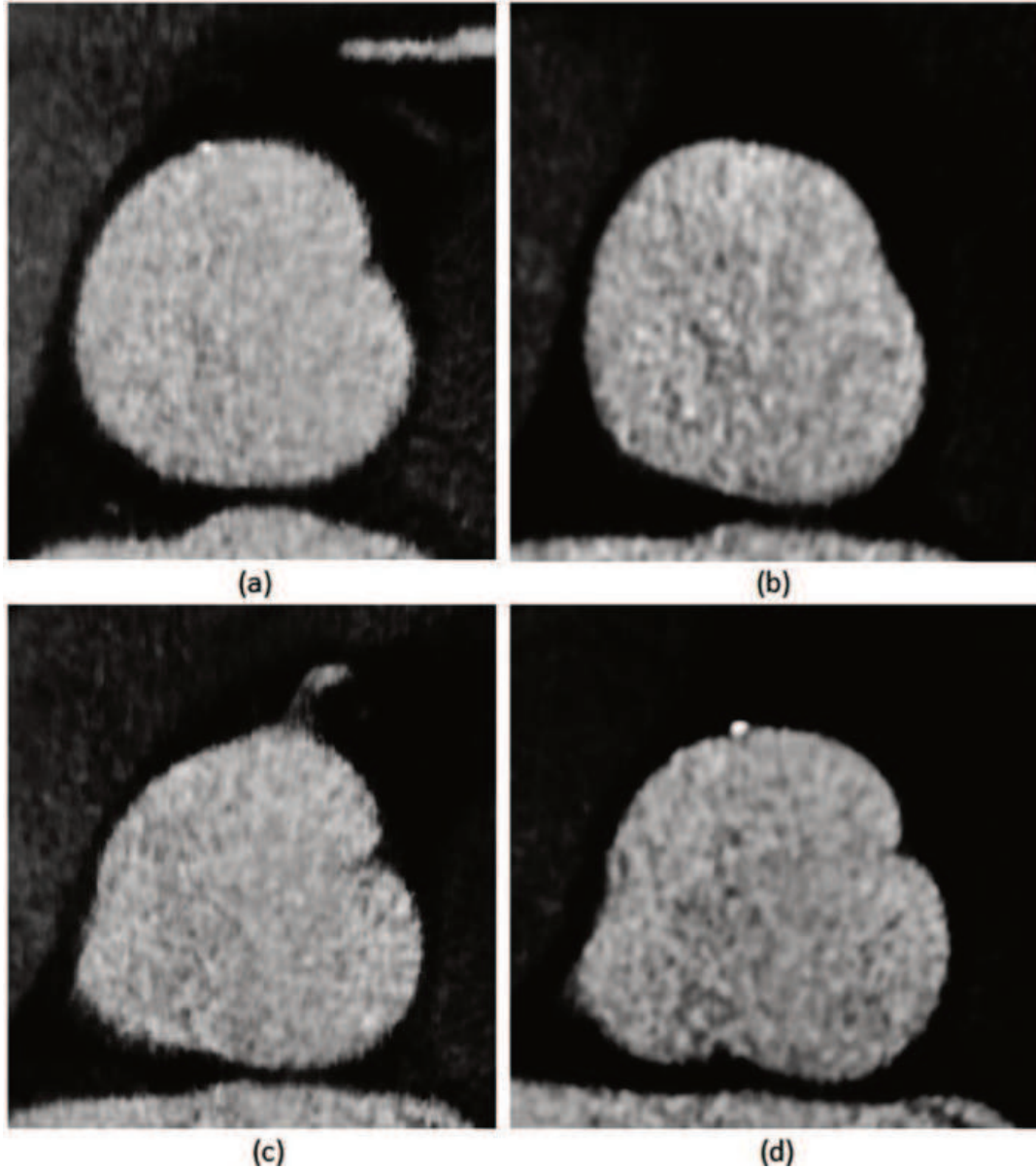


Figure 6.4. Multiplanar reconstruction (MPR) images of the same patient in reference standard and the automatic approach. (Image (a) & (c) are the reference standard, image (b) & (d) are the automatic measurement)

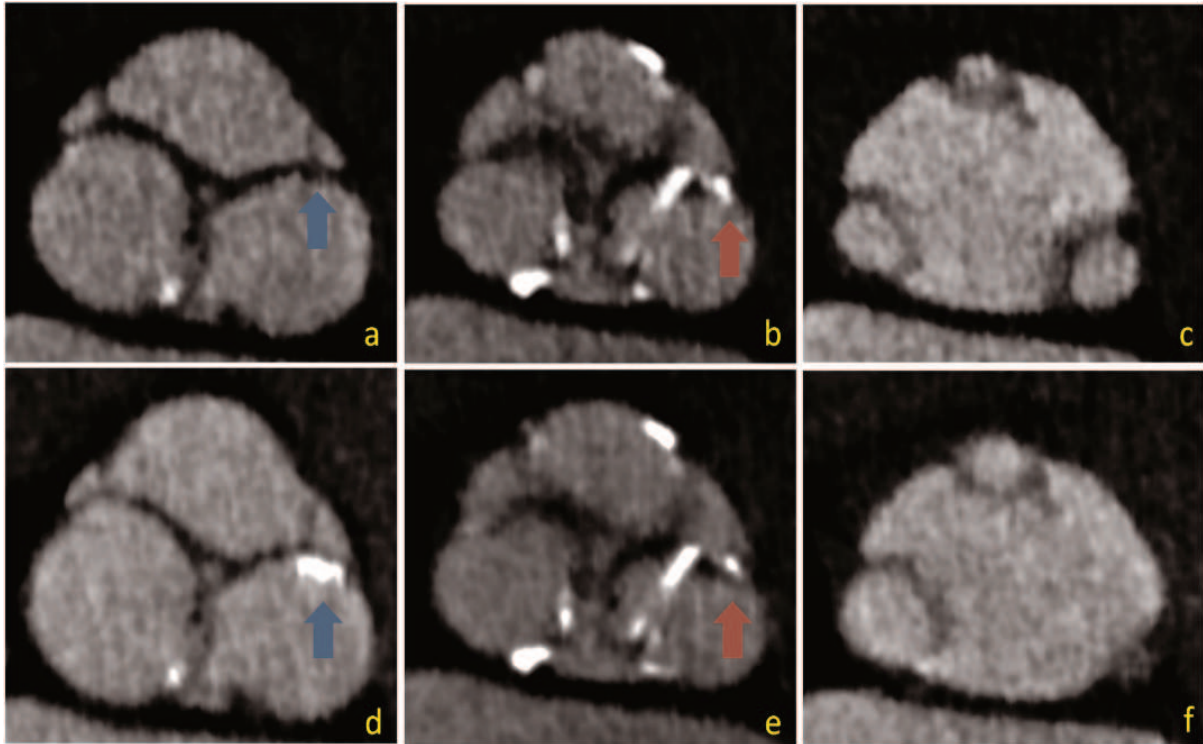


Figure 6.5. MPR images of the same CCTA image with the same slice thickness 3 mm and different reconstruction orientations. The angle between the two different orientations was 5 degrees. a. b. c. belong to one MPR image. d. e. f. belong to the MPR image of another orientation. The six different MPR images were both showing the aortic root of the same patient, the calcifications were not of the same size in the spots pointed by the arrow. The arrows of the same color denoted the same position in different MPR images of the same CCTA image.

7

Automated quantification of thoracic aorta dilatation on baseline and follow-up computed tomography angiography

Xinpei Gao, Sara Boccalini, Pieter H. Kitslaar,
Ricardo P.J. Budde, Shengxian Tu,
Boudewijn P.F. Lelieveldt, Jouke Dijkstra, Johan H.C. Reiber.

Abstract

Background Patients with aortic pathologies will undergo lifelong imaging surveillance to determine aortic diameters and their changes over time. According to the guidelines, the measurements of the aorta should be performed at predefined anatomical landmarks and reported accordingly. A framework which can automate the calculation of the changes of the aortic diameters based on multiple scans of the same patient would effectively decrease measurement time and most likely reduce inter-methods and inter-observer variabilities. Notwithstanding, to the best of our knowledge there is no such tool available for thoracic aorta. In this study, we describe and present a validation of an innovative tool for the automatic quantification of thoracic aorta dilatation in baseline and follow-up CTA images.

Methods Patients who underwent two contrast CT scans of the thoracic aorta were included. Diameters of baseline and follow-up scans are automatically generated by the tool, based on multiple landmarks defined on the baseline scans by two operators, were compared with manual measurements performed with the double oblique technique. Bias and correlations were calculated between the methods and, for the automatic framework, between the operators. Bland Altman plots for each location were drawn.

Results Twenty-nine patients were included. The automatic analysis failed in two cases during the centerline extraction and segmentation procedure, which were excluded from further analysis. Our tool showed excellent correlation and small error with the manually generated reference standard, especially for proximal aortic arch (baseline: 0.98, 0.19 ± 1.30 mm; follow up: 0.93, 0.44 ± 2.21 mm), mid descending aorta (baseline: 0.95, 0.37 ± 1.64 mm; follow up: 0.94, 0.37 ± 2.06 mm), and diaphragm (baseline: 0.98, 0.30 ± 1.14 mm; follow up: 0.96, 0.37 ± 1.80 mm). The inter-observer variability was quite low with the errors of the diameters all lower than or around 1mm, and correlations all higher than 0.95. The automatic tool reduced the processing time by half (10-12 minutes auto vs 22 minutes manual).

Conclusion For the first time, a fast and automatic tool was able to derive diameters of baseline and follow-up scans of the thoracic aorta as well as their differences with high accuracy and reproducibility, was presented.

Submitted.

7.1 Introduction

Aortic aneurysms are the second most frequent disease of the aorta after atherosclerosis. The estimated risk of rupture or dissection depends on the maximum diameter of the aneurysm which is also the most important parameter to decide if and when to intervene with surgery or percutaneous intervention (Erbel et al. 2014b; Hiratzka et al. 2010). For patients with aortic dilatation who do not meet the criteria for intervention, imaging follow-up is recommended to monitor diameters at intervals that vary depending also on the underlying aortic pathology. In genetic diseases that affect the aorta, the rate of enlargement progression is higher than in the general population, thus requiring more frequent follow-up. Focal aortic dilatations/aneurysms are a manifestation of a diffuse aortic pathology and therefore the entire aorta, not only the enlarged segment, should be assessed both at baseline and at follow up. To reduce variability between institutions and/or operators, measurements of the aorta should be performed at several specific predefined landmarks and reported accordingly (Erbel et al. 2014b; Goldstein et al. 2015; Hiratzka et al. 2010).

Providing rapid and high resolution images of the entire aorta, CT is the imaging modality of choice to measure aortic diameters both at diagnosis and follow up. Measurements have to be performed in a plane perpendicular to the long axis of the vessel that can be identified manually or by semi-automatic or automatic software (Erbel et al. 2014b). The manual technique requires a workstation for multiplanar reconstructions, knowledge of how to obtain the correct plane of the aortic anatomy as well as the positions of specific landmarks. Moreover for each exam and at all locations, the operator must repeat the process to define the plane perpendicular to the long axis of the aorta ensuing a very time consuming post-processing procedure, especially when the baseline scans have to be reassessed as well. Several commercially available semi-automatic and automatic software are able to detect the aortic centerline and aortic diameters reducing the reporting time and measurement variability especially among non-expert readers (Biesdorf et al. 2012; Entezari et al. 2013; Kauffmann et al. 2011, 2012; Lu et al. 2010). However the reliability of accurate aortic diameter assessment by these published methods has been deemed so low, that previously published thresholds for intervention based on aortic growth over time have been removed from more recent guidelines (Erbel et al. 2014b).

A single framework that would be able to automate the calculation of the differences of aortic diameters from multiple scans of the same patient, would dramatically reduce reporting time and likely improve measurement

reproducibility thereby reducing intermethod, intraobserver and intraobserver variabilities. However, to the best of our knowledge there is no such tool for the thoracic aorta available.

The aim of our study was to analyze the accuracy and reproducibility of our newly developed tool for the automatic assessment of thoracic aorta diameter and the differences over time by comparison with manual measurements.

7.2 Methods

Study population and CT protocol

In this this single-center retrospective study, for which a waiver was received from the local Medical Ethics Committee, two CT scans of patients who had shown an increase of thoracic aorta diameters over time were included. To identify these patients, the PACS of the Erasmus MC was searched for radiological reports of CT scans performed between 2006 and March 2016 and included predefined terms. These terms were: "more dilated", "increase in diameter", "increased dilatation", "wider dilatation", "wider aneurysm", and "change in diameter". Patients with reports containing any of these search phrases were eligible for inclusion regardless of the amount of diameter increase. Next, the quality of the corresponding CT scan and of the one used as a comparison for clinical purposes was subjectively assessed and only patients who two contrast enhanced CT scans with quality had judged acceptable to perfect were included. Whenever the two so identified scans did not have sufficient quality but the patient had undergone prior and/or later scans that met this criterion, the latter were included. In case multiple exams with adequate quality were available, the two with the longest time period in-between were selected. All scans that did not have thin slice reconstructions with angio or soft tissue kernels of the entire thoracic aorta were excluded. Patients with congenital anatomical variations of the aorta were also excluded, with the exception of mild aortic coarctation. All patients who had been operated upon with replacement of any part of the ascending aorta and/or aortic arch prior to the CT scans, were excluded as well. On the other hand, patients operated for aortic coarctation with end-to-end anastomosis or small patches were included.

Patient demographics were retrieved from the electronic patient files. Technical parameters of the CT scans including date, scanner, ECG gating, type of gating, kV, mAs, reconstruction slice thickness, kernel, contrast medium and contrast injection protocol were collected. For the scans performed with ECG-gating also the phase of the cardiac cycle

(approximated at 5% intervals) of the reconstruction employed for manual measurements was noted and whenever possible the same phase was chosen to assess the two scans of a single patient. For prospectively ECG-triggered high-pitch spiral acquisitions the cardiac phase at the level of the aortic valve was considered.

Reference standard

Manual measurements were performed by a radiologist with four years of experience in cardiovascular imaging. For this purpose CT datasets were exported to a multimodality workstation (Syngo.via, Siemens). Measurements were performed on planes perpendicular to the centerline of the aorta that were identified with the double-oblique method by manually rotating the axes. Inner-edge to inner-edge diameters were manually defined.

The maximal diameter was measured. All older scans were assessed first. The more recent scans were assessed at least two weeks after the first ones, by the same radiologist blinded to the results of the first dataset. The time needed to perform all the measurements on one dataset was recorded and the average calculated.

Diameters at different anatomical locations along the aorta

To assess changes of aortic dimensions over time, diameters were measured at multiple and standardized anatomical locations in accordance with the 2014 guidelines of the European Society of Cardiology (ESC) for the diagnosis and treatment of aortic diseases (Erbel et al. 2014b). Diameters were therefore calculated at seven prescribed anatomical locations along the thoracic aorta: sinotubular junction (STJ), mid ascending aorta (MAA), proximal aortic arch (PROX), mid aortic arch, proximal descending thoracic aorta (DIST), mid descending aorta (DESC) and diaphragm. STJ was measured as the connection of the aortic root and the ascending aorta, MAA at the level of the pulmonary trunk, PROX at the origin of the brachiocephalic trunk. The mid aortic arch was located between the left carotid artery and the left subclavian artery; after the left vertebral artery if it had a separate origin from the aorta. DIST was measured at approximately 2 cm distal to the left subclavian artery. However if at this level there was either a dilatation or a steep bending of the aorta, the plane was moved closer to the left subclavian artery. DESC location was placed at the same level as the MAA.

The same landmarks and location were employed for both manual and automatic measurements.

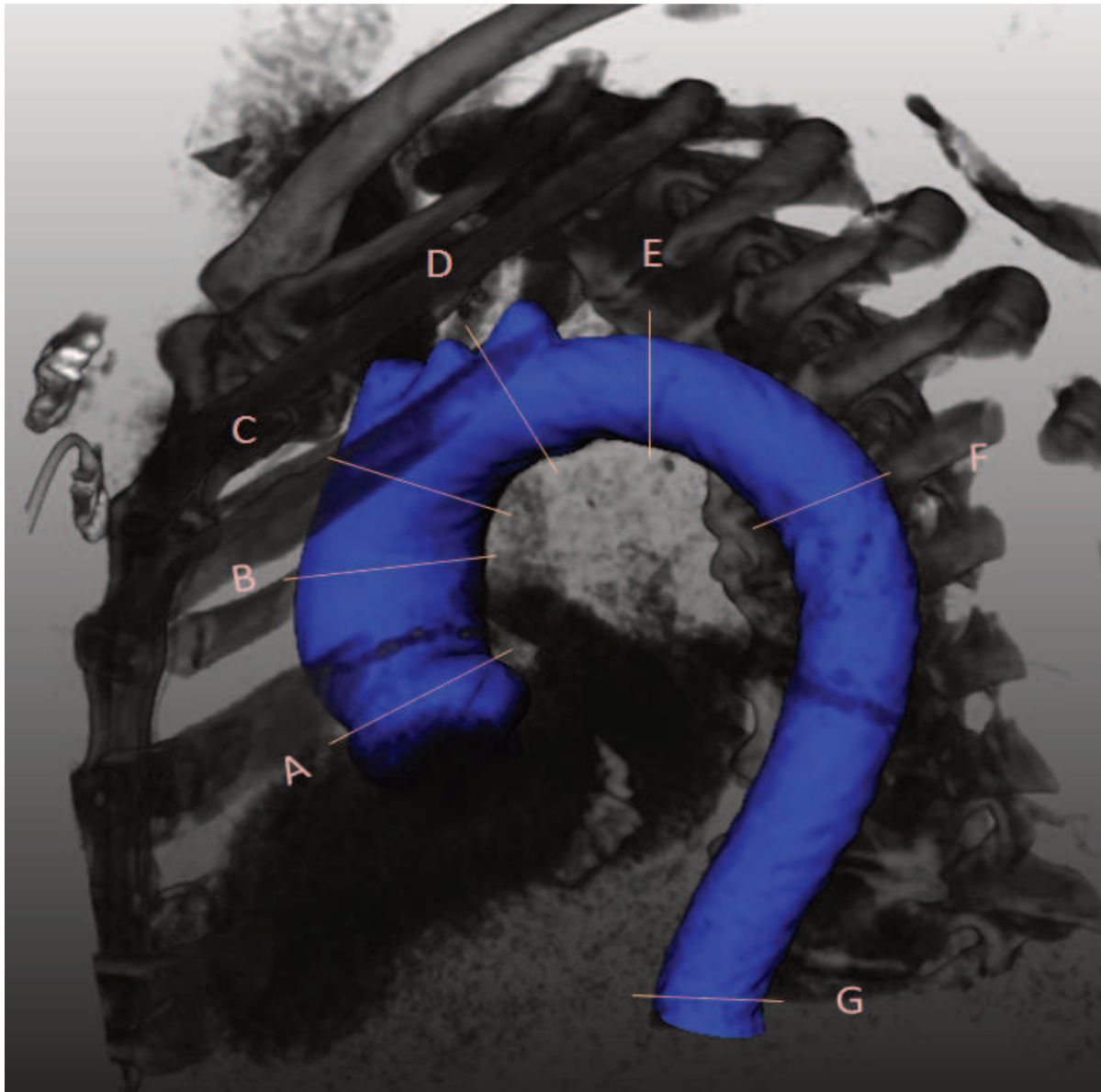


Figure 7.1.3D reconstruction of the thoracic aorta showing the level of the 7 locations where measurements were performed

Automatic aorta dilatation quantification framework

Framework overview

The whole framework was constituted by multiple steps of which the main ones are as follows (Figure 7.2). Firstly the thoracic aorta was segmented from baseline CTA images automatically. In the next step, follow-up images were automatically aligned to baseline image by registration. Subsequently, with the segmented contour of the baseline CTA scan as initial contour, the contour of the thoracic aorta of the follow-up CTA scan was extracted by deforming the initial contour. Finally, based on

the manually defined positions of the seven landmarks along the thoracic aorta on the baseline scan, the maximal diameters of these locations in baseline and follow-up images were calculated.

The automatic framework was implemented in the MeVisLab platform (version 2.7.1, MeVis Medical Solutions AG, Bremen, Germany) using C++ and Python code, and integrated in an in-house tool (AortaDilatationViewer 1.0, LKEB, Leiden, Netherlands).

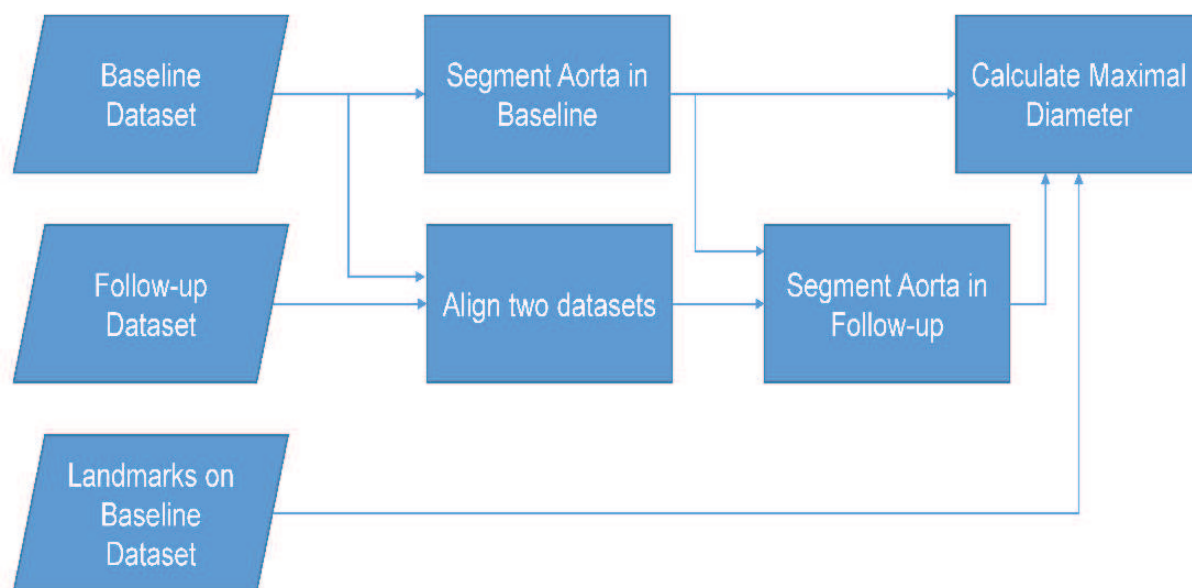


Figure 7.2. Workflow of the automatic aorta dilatation quantification framework

Preprocessing

If the length of the baseline and follow up scans were longer than the region of the thoracic aorta, for instance extended to the femoral arteries, or if the baseline and follow up images had a different length of the aorta that was imaged, datasets were manually adjusted. To minimize the automatic processing of the framework, we manually removed unnecessary images along the z-axis and when the baseline and follow up scans had had a different length of the aorta that was imaged, images from the longer scan were removed until the included anatomical region was the same as in the shorter.

Automatic segmentation of the thoracic aorta of the baseline CTA

The automatic thoracic aorta segmentation scheme in CTA images was based on the centerline extraction and contour detection methods. The centerline extraction method was similar to the algorithm we developed and previously described (Gao et al. 2014), based on wave-propagation algorithm, Gaussian probabilistic distribution model and Dijkstra shortest path algorithm. The previous automatic landmark detection algorithm was

modified from detection of two femoral end points to one aortic end point. The contour detection method was implemented by deformable subdivision surface model fitting algorithm (Kitslaar et al. 2015). In figure 7.2 the result in 3 dimensional grids and 2 dimensional axial views is shown.

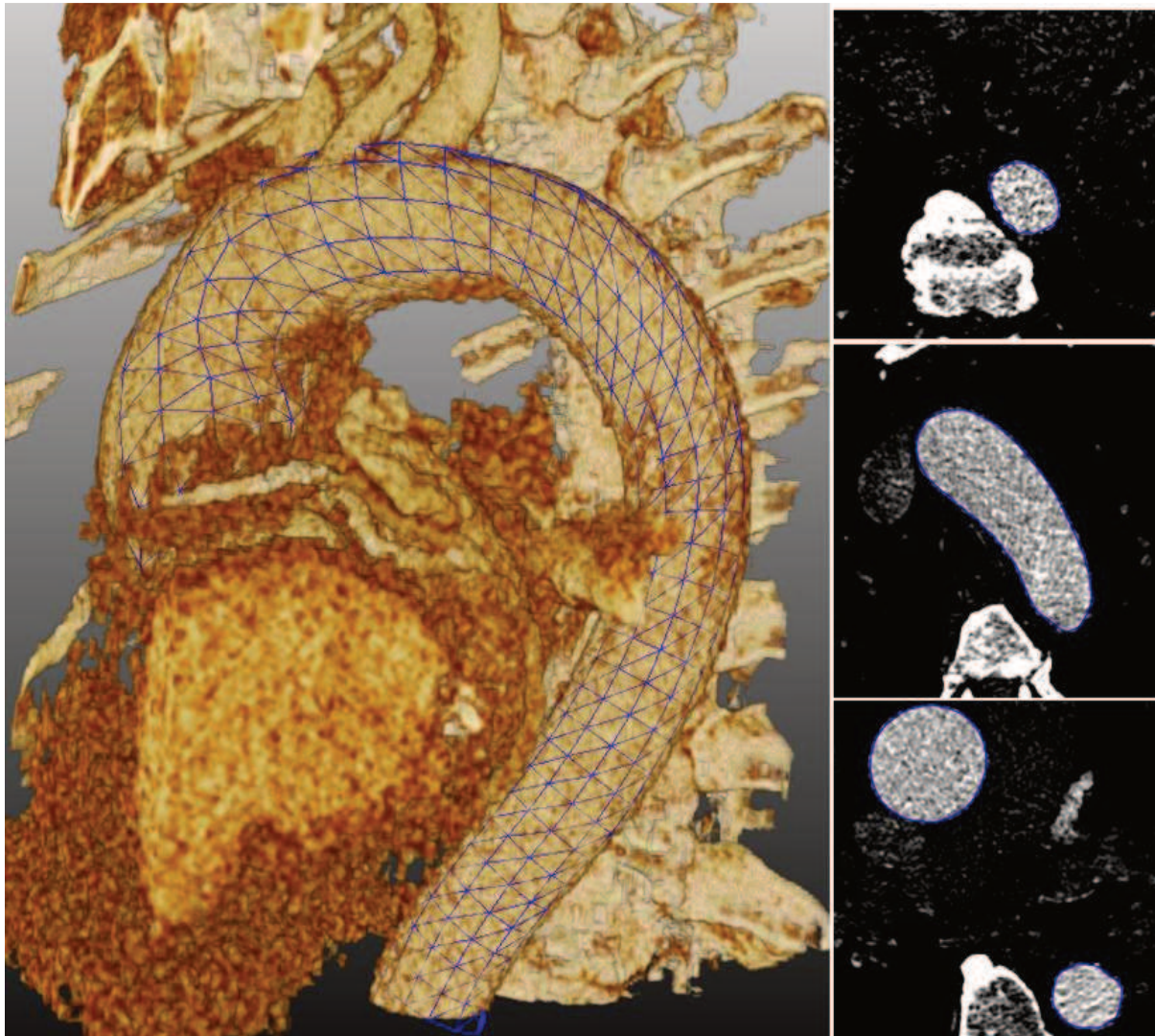


Figure 7.2. 3D grid and 2D axial views showing the result of automatic segmentation

Automatic alignment of baseline and follow up CTA

Automatic alignment was implemented by the registration algorithms. The follow-up image (the moving image) is deformed to fit the baseline image (the fixed image) by registration to find an optimal coordinate transformation. The optimal transformation is obtained while the bias of alignment reaches minimum value. A mask including aorta and surrounding structures was generated by minimum bounding box of the segmented thoracic aorta in the baseline CTA. The mask was used as the mask for the fixed image during registration. The follow-up image was coarsely aligned to the baseline image by rigid transformation at first. Afterwards, affine transformation was implemented for refinement.

Automatic segmentation of the thoracic aorta in follow up CTA

The aligned follow up CTA image was processed by a centerline-based adaptive threshold method (Gao, Kitslaar, Budde, et al. 2016) to reduce the influence of the surrounding tissues in the background, such as high intensity tissue like bone, and low intensity tissue like muscle. With this result image as cost function image and baseline aorta contour as initial contour, the follow-up aorta contour can be obtained by deforming the initial contour according to the intensity of the cost function image. After the segmentation, a region-growing algorithm was used to detect the aortic arch and its branches, in particular at the point of emergence, in detail.

Definition of landmarks for automatic diameter assessment

With the in-house tool, the user could manually annotate the position of the landmarks in multiplanar reconstructions of the baseline scan of each patient. Thereafter the cross-sectional contours of the aorta could be detected by intersecting the landmark plane with the 3D contour, and then the maximum diameter could be calculated automatically. The software automatically identified the same locations and derived the aortic diameter at that level on the follow-up scan.

Visualization of aortic diameters change over time

To improve the visualization of the size change of the aorta, several graphic solutions were implemented in the software and are presented in Figures 7.3 and 7.4.

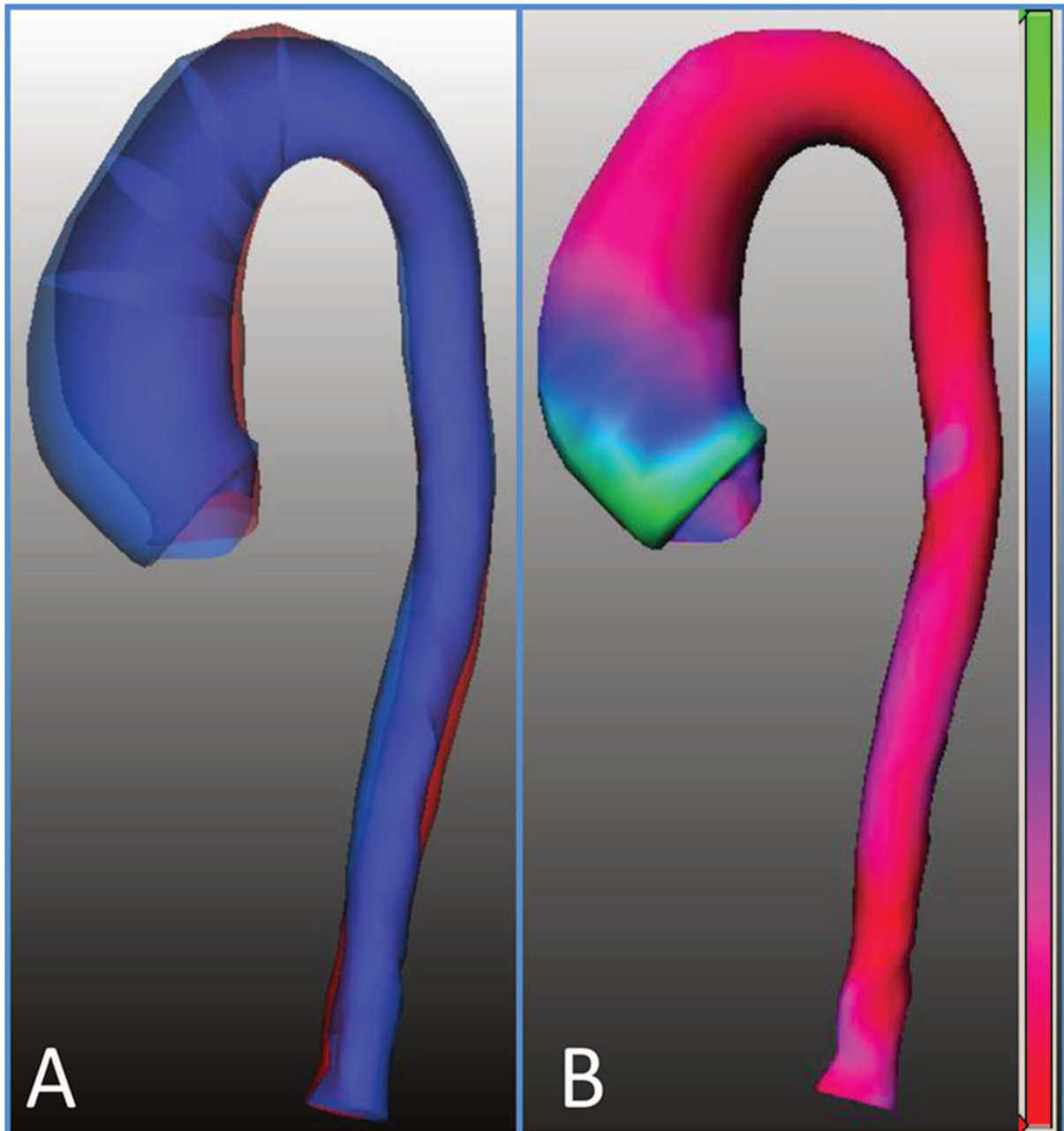


Figure 7.3 Tools for the visualization of the size change of the aorta. In A superimposed 3 dimensional views of the surfaces of the thoracic aorta based on the automatically segmented contour of both baseline (in red) and follow-up (in blue) CTA images. In B the automatically calculated changes in diameters between baseline and follow-up scans are represented with colors (red, blue and green indicate 0, 5 and 10 mm difference in diameters respectively) for an immediate and comprehensive overview of the results.

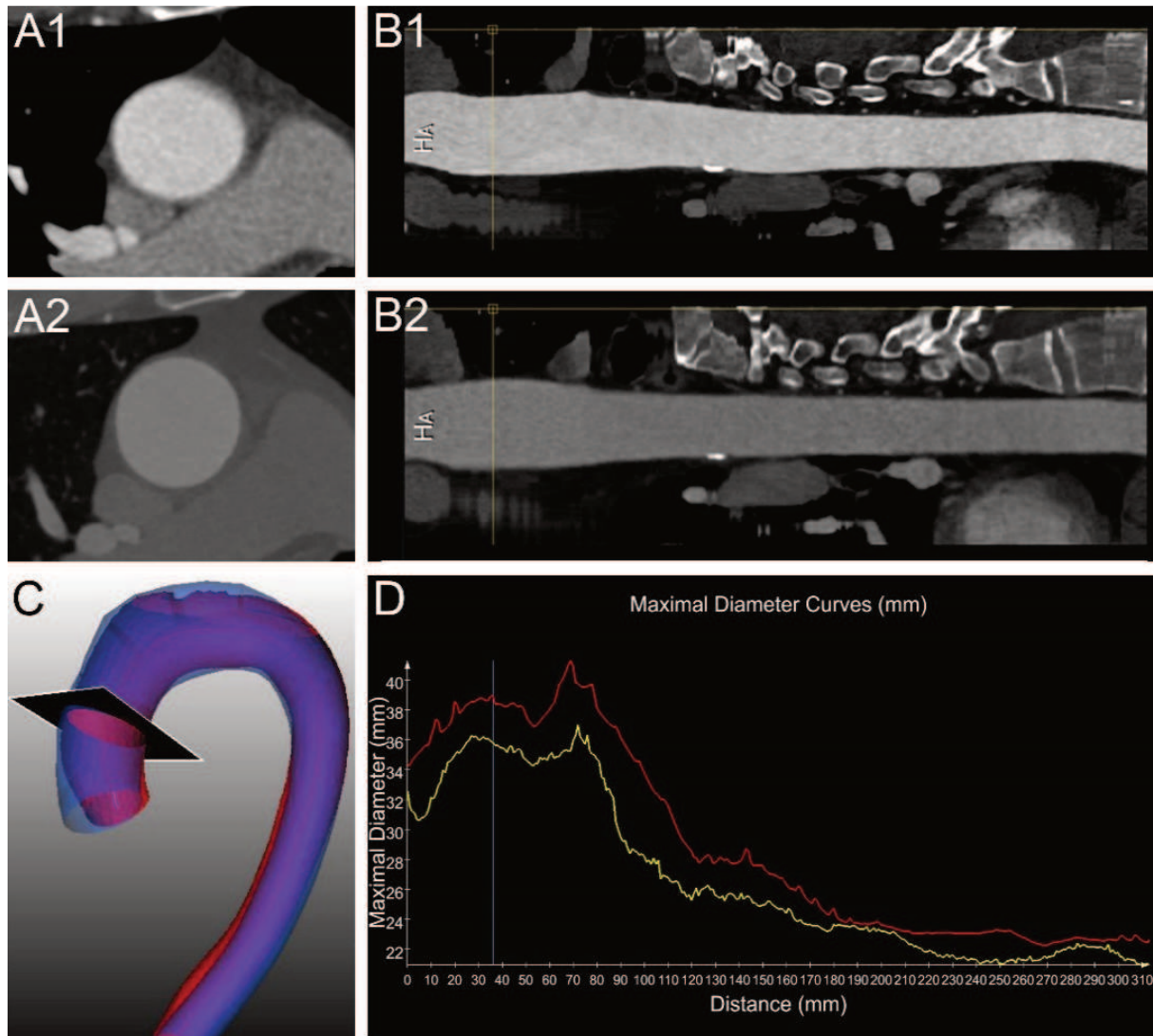


Figure 7.4 Tools for the visualization of the size change of the aorta. Cross-sectional views of the aorta (A1 and A2) and straightened MPR reconstructions (B1 and B2) of the aligned baseline (A1 and B1) and follow-up (A2 and B2) images. In C superimposed 3 dimensional views of the surfaces of the thoracic aorta based on the automatically segmented contour of both baseline (in red) and follow-up (in blue) CTA images. In D the two diameters curves (baseline in yellow and follow-up in red), starting from the sinotubular junction, drawn together on the same graph. The black plane in C shows the level where the cross-sectional diameter indicated by the yellow lines in B1 and B2 and by the blue line in D was calculated.

Inter-observer variability

To analyze the inter-observer variability of the in-house tool, two observers used the in-house tool to annotate the seven aortic landmarks manually on the baseline scan of each patient. Based on these annotations the software automatically generated the following clinical parameters: maximum diameters at the level of the landmarks in baseline and follow-up CTA images, and the progression of the diameters. The inter-observer variability was calculated by comparing the two groups of results. One

observer had 5 years of experience in cardiovascular imaging, the second observer had 4 years of experience.

Statistical analysis

In this study, we used two software SPSS (version 20.0, SPSS Inc., Chicago, IL, USA) and MedCalc (version 15.6, Ostend, Belgium) in the statistical analyses. Quantitative data was analyzed by the mean, standard deviation, and intraclass correlation coefficient (ICC). To visualize the bias between the automatic results from the in-house tool and the reference standard, Bland-Altman plots were drawn. The significance level of the p-value was 0.05.

7.3 Results

Patient population

Twenty-nine patients that had two contrast enhanced CT scans with reasonable to perfect quality of the thoracic aorta were included (23 males; average age $55,5 \pm 14,3$ years). Patient characteristics are summarized in table 7.1.

Four patients had a known congenital aortic disease (2 coarctation and 2 Ehlers-Danlos type 4) and five patients had a bicuspid aortic valve. Six patients had undergone an aortic valve replacement, one a Ross procedure and one an end-to-end anastomosis to correct aortic coarctation.

	Total(n=29)
Male	23(79%)
Age (mean, SD, range) in years	55,5±14,3(25-82)
Height (mean, SD, range) in Kg	1,75±0,1(1,5-1,9)
Weight (mean, SD, range) in m	82,6±18(50-117)
BMI (mean, SD, range)	27,2±6,9(16,9-52,7)
Congenital aortic valve/aortic diseases	
- Ehlers-Danlos 4	2
- BAV	5

- coarctation	2
<hr/>	
Risk factors for cardiovascular diseases	
- Smoking	6 (3 past smokers)
- Hypertension	12
- Diabetes	4
- Hypercholesterolemia	8
<hr/>	
Previous related surgical procedures	
- Aortic Valve Replacement	6
- Coarctation repair	1
- Ross procedure	1

Table 7.1. Patient population characteristics

CT scans technical parameters

In total 58 scans were included, 29 baseline and 29 follow up examinations. The technical parameters are summarized in Table 7.2. All, but one, scans were acquired with scanners with more than 64 detectors. ECG gating or triggering was employed in most cases (52 scans; =90%). The slice thickness of assessed reconstructions was on average $1 \pm 0,2$ mm and only in two baseline exams the thickness was higher than 1mm.

	Baseline CT scans (=29n)	Follow-up CT scans (=29n)	Total CT scans (=58n)
Patient age at CT (average \pm SD; range) [years]	50,1 \pm 13,7; 22-71	53,4 \pm 14; 24-78	51,7 \pm 13,8
Time difference between CT scans		1187,9 \pm 622,4; 344-2558	

(average \pm SD; range) [days]			
Scanner			
- Sensation 16	1	0	1
- Definition	3	0	8
- Definition AS+	8	0	13
- Definition Flash	12	1	1
- Definition Edge	1	0	1
- Sensation 64	2	1	3
- Somatom Force	2	15	17
kV (average, \pm SD; range) [kV]	106,2 \pm 14,5; 70-120	95,9 \pm 12,9; 70-120	101 \pm 14,6 2
- 70 kV	1	1	8
- 80 kV	2	6	6
- 90 kV	1	5	24
- 100 kV	12	12	2
- 110 kV	0	2	16
- 120 kV	13	3	
Slice thickness (average, \pm SD; range) [mm]	1 \pm 0,2; 0,75-2 2	0,97 \pm 0,1; 0,75-1 3	1 \pm 0,2 5 51
- 0,75 mm	1	26	1
- 1 mm	1	0	1
- 1,5 mm		0	
- 2 mm			
Kernel			
- B20f	9	2	11
- B25f	1	0	1
- B26f	10	1	11
- Bv40	2	15	17
- I26f	6	11	17
ECG-gating			
- not gated	6	0	6
- unknown protocol	1	2	3
- retrospective	2	1	3
- prospective	7	5	12
- prospective high-pitch	12	21	33

Phase of the cardiac cycle			
- 0%-20%	2	4	6
- 25%-40%	5	12	17
- 45%-60%	5	9	14
- 65%-80%	11	3	14

Table 7.2. CT scans technical parameters

Success rate of registration and segmentation

Out of the 29 patients, 2 patients were excluded from further analysis. In the first patient, the automatic centerline extraction failed in the baseline image; and in the second patient, the region growing step failed in the baseline image.

Accuracy of the tool

Table 7.3 shows the mean and standard deviation of the maximal cross-sectional diameters at different landmarks by manual measurement and automatic measurements from two observers.

As shown in Table 7.4, for observer 1 the mean differences between the manual measurement and the automatic measurement at different landmarks were all lower than 1mm except at the mid aortic arch, the mid ascending aorta and the sinotubular junction. In the baseline and the follow-up scans, the ICC were all higher than 0.90.

As shown in Table 7.4, also for observer 2 the mean differences at different landmarks were all lower than 1mm except at the mid aortic arch and the sinotubular junction. The ICC coefficients for baseline diameters were all higher than 0.90.

Bland Altman plots for the differences between the two observers and the automatic results combining data from the baseline and follow-up scans for each of the seven locations are shown in Figure 7.5-7.6.

Maximal diameter (mm)	Baseline			Follow up		
	Manu al	Automat ic 1	Automat ic 2	Manu al	Automat ic 1	Automatic 2
Sinotubular junction	37 ± 5	40 ± 5	39 ± 5	39 ± 5	42 ± 5	42 ± 4
Mid ascending aorta	44 ± 5	43 ± 6	44 ± 6	47 ± 6	45 ± 6	46 ± 6
Proximal aortic arch	37 ± 5	37 ± 4	38 ± 5	39 ± 4	39 ± 4	39 ± 4
Mid aortic arch	29 ± 3	30 ± 5	30 ± 5	30 ± 4	33 ± 5	32 ± 5
Proximal descending aorta	27 ± 5	27 ± 5	27 ± 5	29 ± 7	30 ± 6	29 ± 6
Mid descending aorta	26 ± 4	26 ± 4	26 ± 4	27 ± 4	28 ± 5	27 ± 5
Diaphragm	24 ± 4	24 ± 5	24 ± 4	25 ± 4	25 ± 5	25 ± 5

Table 7.3. Average diameter in different locations along the aorta. Manual = measurements performed manually with the double oblique method by observer 1. Automatic 1 and Automatic 2 = automatically calculated diameters based on the locations identified on the baseline scan by observer 1 and 2 respectively. Data as mean ± SD.

Maximal diameter Automatic 1 vs Manual		Sinotubular junction	Mid ascending aorta	Proximal aortic arch	Mid aortic arch	Proximal descending aorta	Mid descending aorta	Diaphragm
Baseline	Mean difference \pm SD [mm]	2.22 \pm 2.19	1.07 \pm 2.20	0.19 \pm 1.30	1.15 \pm 2.33	0.22 \pm 0.97	0.37 \pm 1.64	0.30 \pm 1.14
	ICC	0.95	0.96	0.98	0.91	0.99	0.95	0.98
Follow-up	Mean difference \pm SD [mm]	2.96 \pm 2.64	1.30 \pm 2.45	0.44 \pm 2.21	2.37 \pm 2.59	0.93 \pm 2.79	0.37 \pm 2.06	0.37 \pm 1.80
	ICC	0.92	0.96	0.93	0.90	0.95	0.94	0.96
Maximal diameter Automatic 2 vs Manual		Sinotubular junction	Mid ascending aorta	Proximal aortic arch	Mid aortic arch	Proximal descending aorta	Mid descending aorta	Diaphragm
Baseline	Mean difference \pm SD [mm]	1.96 \pm 1.79	0.44 \pm 1.65	0.56 \pm 1.22	1.19 \pm 1.92	0.00 \pm 1.41	0.37 \pm 2.02	0.41 \pm 1.05
	ICC	0.97	0.97	0.98	0.94	0.98	0.93	0.98
Follow-up	Mean difference \pm SD [mm]	3.15 \pm 2.57	0.26 \pm 2.01	0.85 \pm 2.09	2.26 \pm 2.57	0.59 \pm 2.56	0.04 \pm 2.30	0.30 \pm 1.56
	ICC	0.92	0.97	0.94	0.91	0.96	0.93	0.97

Table 7.4. Assessment of automatic framework compared with manual results. The automatic results were generated based on landmarks defined by observer 1 (Automatic 1) and observer 2 (Automatic 2).

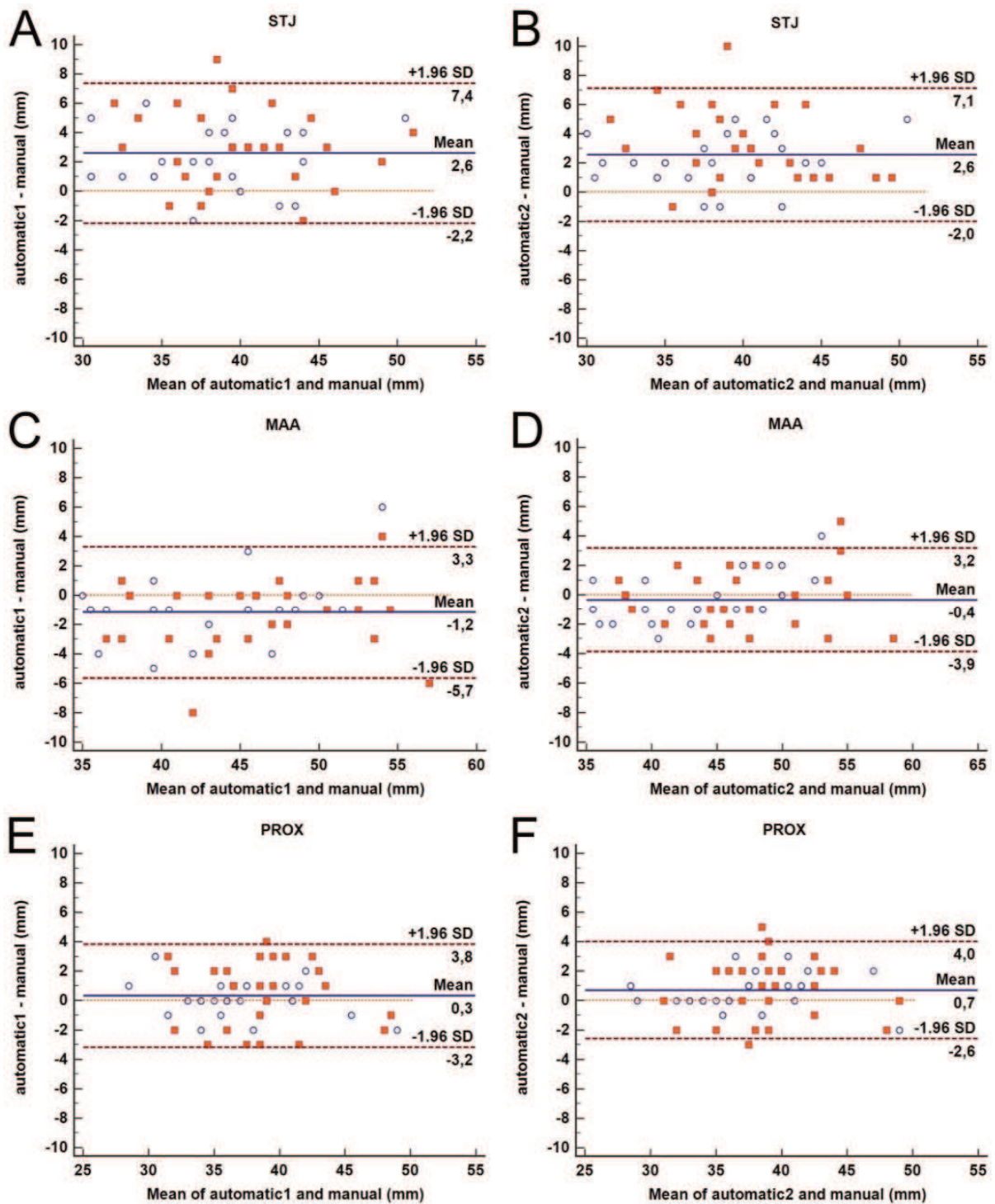


Figure 7.5. Bland-Altman plots representing the difference between automatic and manual measurements at sinotubular junction (A-B), MAA (C-D) and PROX (E-F). Blue circles: baseline diameters. Red squares: follow-up diameters.

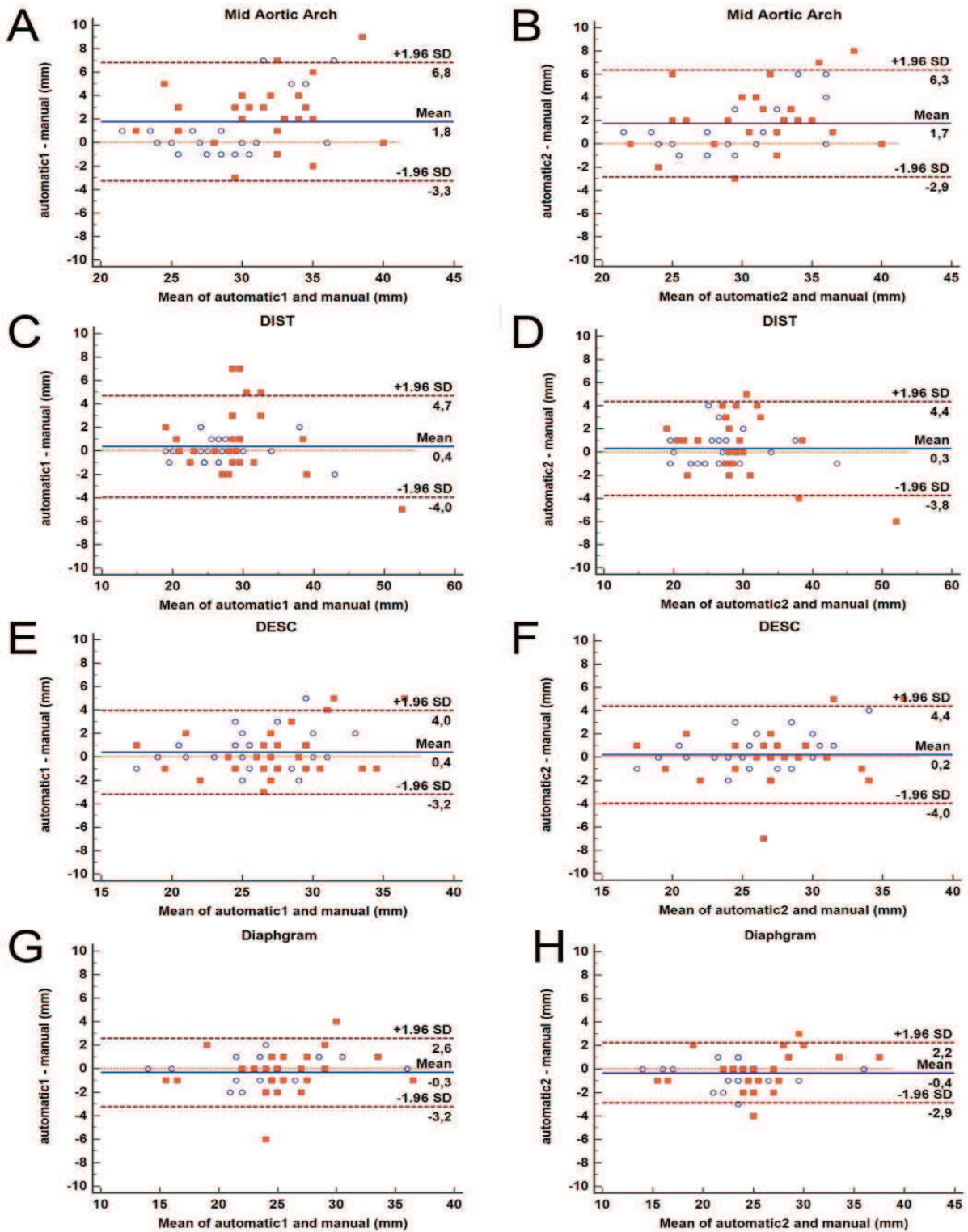


Figure 7.6. Bland-Altman plots representing the difference between automatic and manual measurements at mid aortic arch (A-B), DIST (C-D), DESC (E-F) and diaphragm (G-H). Blue circles: baseline diameters. Red squares: follow-up diameters.

Inter-observer variability

The inter-observer variability of the automatic framework is shown in Table 7.5. The automatic framework showed low inter-observer variability. The mean differences were all lower than 1 mm or around 1 mm at all the landmark locations, and the ICC values all higher than 0.90.

Maximal diameter Automatic 1 vs Automatic 2		Sinotubular junction	Mid ascendin g aorta	Proxima l aortic arch	Mid aorti c arch	Proximal descendin g aorta	Mid descendin g aorta	Diaphr agm
Baselin e	Mean differenc e \pm SD [mm]	0.26 \pm 1.35	0.63 \pm 2.40	0.37 \pm 1.21	0.04 \pm 2.03	0.22 \pm 1.25	0.00 \pm 1.62	0.11 \pm 0.75
	ICC	0.98	0.96	0.98	0.95	0.99	0.96	0.99
Follow- up	Mean differenc e \pm SD [mm]	0.19 \pm 1.62	1.04 \pm 1.93	0.41 \pm 1.15	0.11 \pm 1.22	0.33 \pm 1.36	0.33 \pm 1.52	0.07 \pm 0.92
	ICC	0.97	0.98	0.98	0.98	0.99	0.97	0.99

Table 7.5. Assessment of automatic framework compared with manual results. The automatic results were generated based on landmarks defined by observer 2.

Time consumption for automatic and manual measurements

The overall mean time to manually measure the all the diameters on both baseline and follow up scans was 22.3 minutes (11.4 minutes for baseline, 10.9 minutes for follow up exams). The average time for automatic measurement of both baseline and follow up diameters was about 10 - 12 (4 minutes for landmark annotation, 2 minutes for the automatic processing of baseline images, 6 minutes for the automatic measurement of the follow up images and comparison with baseline).

7.4 Discussion

The natural history of the aorta and aortic aneurysms is to enlarge over time. The rate of (possibly lethal) complications, such as rupture and dissection, increases as the diameter of the aneurysm grows. Therefore these patients will undergo surveillance with imaging techniques at regular intervals until the dilatation has reached a threshold for which it is safer to intervene than to wait and varies depending on the involved aortic segment and underlying aortic pathology (Erbel et al. 2014b). CT is the imaging modality of choice for this purpose. Also the rate of enlargement over time varies depending on the same variables and is estimated to be 0.07 cm/year for the ascending aorta and 0.19 cm/year for the descending aorta in the general population without genetic aortic pathology (Davies et al. 2002). In the 2010 guidelines of the ACCF/AHA/AATS/ACR/ASA/SCA/SCAI/SIR/STS/SVM (Hiratzka et al. 2010) intervention was proposed also before the absolute threshold sizes were reached, as long as a growth rate higher than expected, for instance of more than 0.5 cm/year for aneurysms without an associated genetic aortic pathology, was demonstrated. In the more recent ESC guidelines (Erbel et al. 2014b) growth thresholds have been removed due to the high variability of aortic measurements. To improve accuracy it has been suggested to derive diameters on planes perpendicular to the long axis of the aorta and at predefined and specific landmarks. Although the double-oblique technique has been regarded and used as the reference standard for aortic measurements, it has been associated with intra and interobserver variabilities (defined as mean difference \pm SD) as high as $-0,8\pm 1,3$ mm and $1,3\pm 2$ mm respectively and absolute difference values of up to 11 mm (Quint et al. 2013). It has also been demonstrated that the experience of the observers plays an important role in reducing the variability (Rengier et al. 2009). Therefore notwithstanding standardization of the measurements it is suggested that only differences over time of more than 5 mm should be considered relevant (Erbel et al. 2014a). Moreover, time consumption is an important limitation to the applicability of the double oblique method in daily clinical practice since at all locations and for each exam the axes have to be adjusted to obtain a plane perpendicular to the centerline of the aorta.

Several automatic software packages for aortic measurements have been validated and showed lower intra and interobserver variability and reduced measurement time compared to manual measurements (Biesdorf et al. 2012; Entezari et al. 2013; Kauffmann et al. 2011, 2012; Lu et al. 2010). Only a very limited number of studies described an automated segmentation tool for the thoracic aorta, due to the more complex anatomical structure of the thoracic aorta compared to the abdominal aorta (Biesdorf et al. 2012; Entezari et al. 2013; Lu et al. 2010).

In the study by Biesdorf et al. (Biesdorf et al. 2012) the aortic arch was segmented by three approaches: model-based approach, 2D joint approach and 3D joint approach. The error of the maximal diameter in the ten 3D CTA images with pathologies of the aorta was 2.24 ± 0.72 mm for

the model-based approach, 1.51 ± 0.66 mm for the 2D joint approach, and 1.52 ± 0.69 mm for the 3D joint approach. In the seven 3D CTA images with severe pathologies, the error was 5.45 ± 2.98 mm for the model-based approach, 3.34 ± 2.23 mm for the 2D joint approach, 2.04 ± 0.83 mm for the 3D joint approach. In Lu et al.'s study (Lu et al. 2010) the ascending aorta was semi-automatically measured by two observers to assess the inter-observer variability of the tool. The inter-observer variability was 1.1 mm during the first session of measurements, and 1.2 mm during the second session. However, no comparison against manual reference standard was performed. The tool by Entezari et al. (Entezari et al. 2013) which can segment the thoracic aorta semi-automatically was the one with the most similar features to our study, however it only segmented and measured the thoracic aorta diameters without automatic comparison between two exams of the same patient. The maximum diameters were measured manually and semi-automatically in multiple locations and the mean difference was calculated: all the differences were less than 1mm, except at the sinotubular junction and proximal aortic arch.

Our study not only estimates the accuracy of the automatic diameter measurement tool, but also evaluates the inter-observer variability. For baseline scans all the differences between manual and automatic measurements performed by the two observers were smaller than 1 mm except at the sinotubular junction, mid ascending aorta (only for one observer) and mid aortic arch. The ICC values were all higher than 0.90. The inter-observer variability was less than 1mm with ICC values higher than 0.95 at all locations. The fully automatic contour detection algorithm in our tool for the baseline thoracic aorta has at least similar or even better accuracy and reproducibility compared to the published semi-automatic tools listed above.

To the best of our knowledge, only one study was published presenting a software that allows automatic calculation and comparison of baseline and follow up abdominal aneurysms volume and diameters (Kauffmann et al. 2012). The software described by Kauffman et al. relies on the semi-automatic segmentation of both datasets with the operators' intervention at multiple steps such as the user definition of the aortic lumen location and the correction of aortic contours. In our framework, the segmentation is fully automatic. Kauffman et al.'s study evaluated the inter-observer variability between a senior radiologist and one of three medical students: the mean difference between different observers was 0.07 mm, the ICC values between the senior radiologist and the three medical students for baseline and follow-up examinations were in the range from 0.989 to 0.998. However in this study the performance of the software was not compared to a reference standard. They mentioned that in their previous study (Kauffmann et al. 2011), the accuracy of the software was estimated by comparing the maximal diameter obtained by the semi-automated software to manual measurement, with a mean error of 1.1 ± 0.9 mm. To the best of our knowledge there have been no descriptions of a framework that can automatically align the baseline and follow-up CT datasets of the thoracic

aorta of the same patient and measure the diameters of both scans at the same time.

Compared to the published studies, our framework presents the following new features: 1) The centerline extraction and the contour detection steps in the framework are both fully-automatic without requiring user interaction; 2) The landmark locations can be automatically detected in the follow-up images; 3) The contours of both the baseline and follow up images can be automatically detected and compared; 4) The dilatation of the aorta (difference in diameters) between the baseline and the follow up, can be visualized in color coding on a 3D reconstruction which gives an instantaneous overview of all relevant information; 5) The maximum diameter of the mid aortic arch was quantified automatically for the first time.

For the automatic detection of the follow up thoracic aorta diameters at the level of the landmarks identified on the baseline scan, which has never been implemented in previous studies, the accuracy was evaluated by comparing the maximal diameter at different locations to the manual measurements. For both observers all the differences were smaller than 1 mm except at the sinotubular junction, and mid aortic arch; for one observer they were higher than 1 mm also at mid ascending aorta. The inter-observer variability was less than 1 mm at all locations except at mid ascending aorta (1.04 mm), while the ICC were all higher than 0.95. The accuracy and reproducibility of measurements on follow-up scans of the thoracic aorta proved to be comparable to the results on baseline datasets.

There are some limitations in this study. Firstly, the patient number in this study is relatively small due to the strict inclusion criteria (patients with clinical reports indicating changes in aortic diameters; no congenital aortic anomalies or previous surgery; both baseline and follow-up scans with reasonable to high quality and thin slices reconstructions). Especially the choice to include a priori only scans with reasonable to high quality does not reflect real world variability and further studies are needed to validate the software with a broader spectrum of scans quality. Thirdly, measurements were not compared to a real gold standard. However this is a general issue for studies regarding aortic diameters assessment with imaging techniques since, even if the patients underwent surgery during which aortic dimensions were derived, measurements performed in this setting cannot be considered the gold standard.

7.5 Conclusion

In conclusion, for the first time, an automatic tool which is able to align the baseline and the follow up images to measure the thoracic aorta was developed and evaluated. The tool has high accuracy and reproducibility, especially in the locations PROX, DESC, and diaphragm. The automatic calculation time was half that of the manual measurement time.

8

Summary and conclusions

8.1 Summary

In recent years, trans-catheter aortic valve replacement (TAVR), also known as Trans-catheter aortic valve implantation (TAVI), was demonstrated to have a low risk-benefit ratio as an alternative therapy for surgical aortic valve replacement (SAVR) in high risk elderly patients. During a TAVR procedure, the vascular access route and aortic root are not directly visible for the treating physician. Pre-operative imaging is necessary to evaluate the aorto-femoral vascular access and the aortic root. For vascular access, the vessel size and tortuosity are important parameters. For the aortic root, the size, the degree of calcification and the delivery direction are important parameters; these measurements can assist the cardiologist in selecting and delivering the appropriate prosthesis. Over-estimating or under-estimating the size of the vascular access and the aortic root can result in severe complications, such as peripheral arterial disease, aortic valve rupture, prosthesis migration and paravalvular regurgitation. This thesis focuses on the development and evaluation of fully automatic pre-operative planning methods for TAVR based on CT images. In addition, automatic pre-operative measurement of aorta dilatation is developed and validated.

To measure the size of the aorto-femoral vascular access in whole-body CTA imaging, at first the location of the access vessel needs to be identified manually, which can be time-consuming because of the long length and the high tortuosity of the vasculature. Chapter 2 describes a novel and fully automatic centerline extraction method of the vascular access from the left and right femoral arteries to the aortic root. First, the CTA Images were corrected for contrast inhomogeneity. Second, a wave propagation algorithm was developed to extract the aorta from an automatically detected anatomical landmark in the aortic arch towards the femoral arteries. Finally, the cost image resulting from a wave propagation algorithm was used to extract the centerlines using Dijkstra's algorithm. Based on visual inspection, the method succeeded in 91.7% of the patients with no need for user interaction. The average mean error compared with the manual reference standard was 1.63 ± 0.40 mm. Based on this vessel localization, a fully automatic tool was developed that seamlessly integrates these measurements into the TAVR clinical workflow.

In Chapter 3, a fully automatic aorto-femoral vascular access segmentation framework was proposed for the pre-operative planning of trans-femoral aortic valve replacement. Its main component is the 3-dimensional deformable subdivision surface model fitting method. Two observers generated ground-truth contour data to benchmark the

automated method. The average Dice similarity indices between the automated segmentations and observer 1 for different vessel segments (left ilio-femoral artery, right ilio-femoral artery and the aorta) were all higher than 0.97; the Dice indices between the automatic measurements and the observer 2 were all higher than 0.95. The inter-observer variability was in the range of 0.95 to 0.97. Comparing the automated segmentation to observer 1, the mean error of the minimal diameter of the lumen in the ilio-femoral artery was 0.32 ± 0.49 mm ($p < 0.001$); In comparison to observer 2, the mean error was 0.51 ± 0.71 mm ($p < 0.001$). This demonstrates that the accuracy of the automated segmentations was in the same, clinically acceptable range as the inter-observer variability.

The difficulty of the aortic root segmentation in CTA image is its complex 3-dimensional geometrical structure. Manual segmentation is complex, time consuming and prone to variations between observers. In Chapter 4, a new method for automatic aortic root segmentation was introduced. The method was composed of 4 components: (1) the cardiac image was resampled for computational complexity reduction. The heart region was masked out by deformable subdivision surface model fitting.;(2) An atlas-based based method was used to segment the aortic root from the cardiac image. The most similar atlas to the patient anatomy was selected based on the similarity (the mutual information) between atlas and the patient's image.;(3) The segmentation result from the previous step was transferred to the whole body CTA image by affine registration; and (4) Refinement by deformable subdivision surface model fitting. The mean Dice index between the automatic segmentation and the reference standard was 0.97 ± 0.02 . This novel framework reduced the time of registration, meanwhile delivering acceptable accuracy.

Automatic sizing of the aortic annulus and determination of the optimal angulation of the C-arm X-ray projection are essential to select and deliver the appropriate prosthesis in the aortic valve for the TAVR procedure. In clinical practice, multi-planar reconstruction of the image data is required to manually measure the size and the dimension of the aortic annulus. In Chapter 5, we presented a fully automatic method to quantify the size parameters and the optimal projection curve of the aortic annulus. The method is based on the segmentation of the aortic annulus by atlas-based algorithm and the calculation of the annulus direction by principal component analysis. 26 patients were included in a retrospective validation study. The error of the automatic tool was assessed on the clinical parameters: 0.1 ± 0.4 cm² for the area, 0.1 ± 0.5 mm for the radius, 0.7 ± 2.3 mm for the long-axis diameter, 0.3 ± 1.5 mm for the short-axis diameter and 1.8 ± 5.5 mm for the perimeter; the correlation coefficients

between the automatic measurements and the reference standard were 0.92 for the area, 0.91 for the radius, 0.85 for the long-axis diameter, 0.82 for the short-axis diameter and 0.82 for the perimeter (all $p < 0.001$), respectively. The mean error of the optimal projection curves was 6.4° in the cranial/caudal (CRA/CAU) direction. For each patient, the average computation time was around 60 seconds, while it would take a physician about 600 seconds to manually quantify the aortic annulus. As such, the developed tool can provide accurate results, reducing analysis time and minimizing manual interaction.

Aortic valve calcium quantification plays an important role in the prognosis of coronary and cardiovascular disease. The extent of calcium is also correlated to the occurrence of paravalvular regurgitation after transcatheter aortic valve replacement. To detect and quantify the presence and extent of the aortic valve calcium, in Chapter 6, a fully automatic approach was developed. The calcium on the valve was segmented by thresholding after the segmentation of the aortic root and the reconstruction of the double-oblique view of the aortic valve. Finally, the calcium volume score was calculated. To validate the automated scores, 68 CTA data sets of patients with suspicion of having coronary artery disease, were used. The reference standard was the calcium volume score semi-automatically obtained by a cardiologist with a different, manual calcium annotation tool. The accuracy of our approach was assessed by comparing with this reference standard. The median difference was 1.82 mm^3 (25th-75th percentile: 0 to 5.08 mm^3), with a Spearman rank correlation coefficient of 0.81 ($p < 0.001$). Bland-Altman analysis showed that the bias between the automatic and the reference standard was -1.1 mm^3 with limits of agreement between -16.2 and $+14.1 \text{ mm}^3$. The specificity of our automatic approach was 82.4%; the sensitivity was 85.3%. The mean processing time was 90 seconds. In conclusion, we demonstrated that a new fully automatic approach for aortic valve calcium quantification is feasible.

The aorta is the main conduit for the blood in the human body and plays a key role in controlling the vascular resistance and heart rate. CT imaging is important in the diagnosis and pre-operative planning of patients with aortic disease. To be able to monitor aortic disease using CT, images from the same patient at different time points are required, as well as standardized measurement protocols and automated quantification tools to minimize systematic and random errors. In Chapter 7, we introduced an automatic aorta dilatation quantification framework. This framework works as follows: first, the thoracic aorta is segmented automatically from the baseline CTA image. Next, the follow-up image is automatically aligned to the baseline image by rigid and affine image registration. Subsequently,

with the segmented contour in the baseline CTA image as initial contour, the contour of the thoracic aorta in follow-up CTA image is extracted by deforming the baseline contour. Finally, the measurement positions along the thoracic aorta are manually defined, and the maximal diameters at these locations in the baseline and the follow-up images are calculated. In a validation study with CT data from 29 patients, the intraclass correlations of the maximal diameters were all higher than 0.90; the mean differences between the manual measurement and the automatic measurement at different landmarks were all lower than 2mm except at the mid aortic arch and the sinotubular junction.

Taken together, this thesis presented several fully automatic algorithms for the pre-operative planning of TAVR procedures, including the sizing of the vascular access and the aortic root, the location definition of the aortic annulus, the determination of the optimal angulation of the C-arm X-ray projection and the quantification of the aortic valve calcium. Also, an algorithm for the automatic quantification of thoracic aorta dilatation was developed. For all these developments, a clinically acceptable accuracy was demonstrated against expert annotated reference standards, while significantly reducing analysis time and effort.

8.2 Future work

TAVR is an innovative cardiovascular intervention procedure developed in recent years. The successful planning of TAVR requires accurate and reproducible measurements of the vascular access and aortic root. As a high-resolution 3D modality, CT provides comprehensive visualization and precise quantification of aorto-femoral vascular access and aortic root.

In this thesis, fully automatic pre-operative planning by CT images is discussed and demonstrated to be accurate. However, the performed validation in the aortic root was limited: the size parameters of the annulus are quantified and validated, but no other landmark planes were validated. Although the annulus parameters are the most important ones for prosthesis selection, other landmark planes such as the sinotubular junction, the left ventricle outflow tract and the sinus of valsalva may provide additional useful information.

In the current study, only diastolic images were measured, while in clinical imaging the whole cardiac cycle can be useful. It is still under discussion which phases should be suitable for aortic annulus measurement and other landmark planes. A further limitation of this work is the fact that we could not investigate robustness of the presented approaches with

respect to all the main CT vendors. Images from multiple vendors has been included in our study, but there are still some vendors not tested. Therefore, future work may further complement the current study by focusing on other anatomical planes, images of multiple cardiac phases and on cross-vendor robustness.

Since the durability of the bioprosthetic valve is 10-20 years, pre-treated patients will have high possibility to receive "valve-in-valve" procedure. As it is risky for the patient to receive cardiac surgery twice, TAVR may provide a good alternative. In those cases, the previous bioprosthetic valve appears as a high intensity structure inside the aortic root in CT imaging. This will make the size measurement of the aortic annulus and other landmark planes difficult. In the future, it will be important to test whether our automatic algorithms for pre-operative planning can be generalized to "valve-in-valve" procedures. Apart from aortic valve replacement, it is important to also automate the pre-operative planning of other heart valves during trans-catheter valve replacement, such as the mitral valve, the pulmonary valve and the tricuspid valve. The minimal-invasive surgery of these valves has been implemented successfully just in recent years. There are still uncertainty and difficulty for the physicians without experience to do pre-operative planning. Especially, the mitral valve has a different anatomical structure than other valves, as it only has two leaflets while others have three. As such, an alternative segmentation and quantification approach of the other valves will be needed for the prosthesis selection and delivery for these valves.

This thesis focuses mainly on size measurements based on image segmentation. For pre-operative planning of TAVR, this quantification from anatomical perspective is important, but there are also other issues to consider to reduce complications.

Aortic regurgitation is one of the main factors which influence the final outcome of TAVR. It can be caused by unsuitable size, misplacement or incomplete expansion of the prosthesis during TAVR. Simulation of the prosthesis implantation procedure can help to predict the occurrence of aortic regurgitation post TAVR, and therefore has potential to improve the selection, placement and expansion of the prosthesis. Furthermore, the design of the prosthesis model can be improved by adjusting the mechanical parameters during simulation. The personalized aortic root models described in chapter 4 could also be used as input for such simulation models, which ultimately may lead to the reduction of the mortality rate of TAVR. Not only will the aortic valve, the simulation of trans-catheter replacement of other valves also be helpful.

As to the direct evaluation of aortic regurgitation in patient, Echocardiography plays an important role. Echocardiography can visualize the peri-TAVR hemodynamic change by multiple modalities such as Doppler and Transesophageal echocardiography, thus illustrating the mechanism of aortic regurgitation such as the under-expansion or misplacement of the prosthesis. The severity of aortic regurgitation can be quantified too and used to make clinical decisions. The combination of multiple image modalities will make TAVR a more trustable technique.

9

Samenvatting en conclusies

9.1 Samenvatting en conclusies

In de afgelopen jaren is aangetoond dat de trans-katheter aortaklep vervanging (TAVR), ook bekend als trans-katheter aortaklep implantatie (TAVI), een veilige alternatieve behandeling is als vervanging van de chirurgische aortaklep vervanging (SAVR) in oudere hoge-risico patiënten. Tijdens een TAVR-procedure is de vasculaire toegang en de aortawortel niet direct zichtbaar voor de behandelende arts. Daarom is preoperatieve beeldvorming nodig om de aorto-femorale vasculaire toegang en de aortawortel te beoordelen. Voor vasculaire toegang zijn de grootte van de vaten en kronkeligheid belangrijke parameters. Voor de aortawortel zijn de grootte, de mate van verkalking en de afleverrichting belangrijke parameters; Deze metingen kunnen de cardioloog helpen bij het selecteren en plaatsen van de juiste prothese. Het overschatten of onderschatten van de grootte van de vasculaire toegang en de aortawortel kan leiden tot ernstige complicaties, zoals perifere arteriële ziekte, aortaklep breuk, prothese migratie en lekken van de klep. Dit proefschrift richt zich op de ontwikkeling en evaluatie van volautomatische preoperatieve planning methoden voor TAVR op basis van CT beelden. Daarnaast is automatische preoperatieve meting van aorta verwijding ontwikkeld en gevalideerd.

Om de grootte van de aorto-femorale vasculaire toegang in het CTA-beeld van het hele lichaam te meten, moet eerst de locatie van het toegangsvat handmatig worden bepaald, wat tijdrovend kan zijn door de grote lengte en de hoge kronkeligheid van het vat. Hoofdstuk 2 beschrijft een nieuwe en volautomatische middellijn extractie methode van de vasculaire toegang van de linker en rechter femorale arteriën naar de aortawortel. Ten eerste werden de CTA-beelden gecorrigeerd voor contrast-inhomogeniteit. Ten tweede werd een golf propagatie algoritme ontwikkeld om de aorta te extraheren vanuit een automatisch gedetecteerd anatomisch herkenningspunt in de aortaboog naar de femorale arteriën. Tenslotte werd het kostenplaatje dat geproduceerd wordt door het golf voortplanting algoritme gebruikt om de middellijnen te extraheren met behulp van het Dijkstra algoritme. Op basis van visuele inspectie was de methode succesvol in 91,7% van de patiënten zonder dat er gebruikersinteractie nodig was. De gemiddelde fout in vergelijking met de handmatige referentiestandaard was $1,63 \pm 0,40$ mm. Op basis van de locatie van het vat is een volledig automatische methode ontwikkeld die deze metingen naadloos integreert in de klinische workflow van TAVR.

In hoofdstuk 3 werd een volledig automatische aorto-femorale vasculaire toegangssegmentatie methode gepresenteerd voor de preoperatieve planning van trans-femorale aortaklep vervanging. De hoofdcomponent is

de 3-dimensionale vervormbare oppervlakte methode. Twee waarnemers genereerden de gouden standaard contouren om de automatische methode te valideren. De gemiddelde Dice-indexen tussen de automatische segmentaties en waarnemer 1 voor verschillende vaatsegmenten (linker ilio-femorale slagader, rechter ilio-femorale arterie en de aorta) waren allemaal hoger dan 0,97; De Dice-indexen tussen de automatische metingen en de waarnemer 2 waren ook allemaal hoger dan 0,95. De variatie tussen de waarnemer was in de range van 0,95 tot 0,97. In vergelijking met de automatische segmentatie van waarnemer 1, was de gemiddelde fout van de minimale diameter van het lumen in de ilio-femorale arterie $0,32 \pm 0,49$ mm ($p < 0,001$); In vergelijking met waarnemer 2, was de gemiddelde fout $0,51 \pm 0,71$ mm ($p < 0,001$). Dit laat zien dat de nauwkeurigheid van de automatische segmentatie in hetzelfde, klinisch aanvaardbaar bereik ligt, als de variatie tussen waarnemers.

De moeilijkheid van de aortawortel segmentatie in het CTA-beeld is zijn complexe 3-dimensionale geometrische structuur. Handmatige segmentatie is complex, tijdrovend en gevoelig voor variaties tussen gebruikers. In hoofdstuk 4 werd een nieuwe methode voor automatische aortawortel segmentatie geïntroduceerd. De methode was samengesteld uit 4 componenten: (1) het hartbeeld werd opnieuw met een lager resolutie herberekend om de complexiteit van de berekening te verminderen. Het hartgebied werd gemaskeerd door een vervormbaar oppervlakmodel; (2) Een atlas gebaseerde methode werd gebruikt om de aortawortel uit het hartbeeld te segmenteren. De best passende atlas voor de patiëntanatomie werd geselecteerd op basis van de gelijkheid (de wederzijdse informatie) tussen atlas en het beeld van de patiënt. (3) Het segmentatieresultaat van de vorige stap werd overgezet naar het gehele lichaam CTA-beeld via affine-registratie; En (4) Verfijning door het gebruik van het vervormbaar oppervlak model. De gemiddelde Dice-index tussen de automatische segmentatie en de referentie was $0,97 \pm 0,02$. Deze nieuwe methode verminderde de tijd nodig voor registratie en was aanvaardbaar nauwkeurig.

Het automatische bepalen van de grootte van de aortaklep ring en de optimale hoek van de C-arm röntgen projectie zijn essentieel om de juiste prothese voor de aortaklep te selecteren en te plaatsen bij de TAVR procedure. In de klinische praktijk is een multi-planaire reconstructie van de beeldgegevens nodig om de grootte en de afmeting van de aortaklep ring te bepalen. In hoofdstuk 5 presenteerden we een volledig automatische methode om de grootte en de optimale projectie hoek van de aortaklep ring te kwantificeren. De methode is gebaseerd op de segmentatie van de aortaklep ring door een atlas gebaseerd algoritme en de berekening van de hoek door middel van hoofdcomponentanalyse. 26 patiënten werden

gebruikt in een retrospectieve validatie studie. De fout van de automatische methode werd vastgesteld voor de klinische parameters: $0,1 \pm 0,4$ cm² voor het oppervlak, $0,1 \pm 0,5$ mm voor de straal, $0,7 \pm 2,3$ mm voor de diameter van de lange as, $0,3 \pm 1,5$ mm voor de diameter van de korte as en $1,8 \pm 5,5$ mm voor de omtrek; De correlatiecoëfficiënten tussen de automatische metingen en de referentiestandaard waren 0,92 voor de oppervlakte, 0,91 voor de straal, 0,85 voor de lange as diameter, 0,82 voor de korte as diameter en 0,82 voor de omtrek (respectievelijk $p < 0,001$). De gemiddelde fout van de optimale projectie hoek was $6,4^\circ$ in de craniale / caudale richting. De gemiddelde rekeningtijd voor elke patiënt was ongeveer 60 seconden, terwijl het een arts ongeveer 600 seconden zou kosten om de aortaklep ring handmatig te kwantificeren. Als zodanig kan de ontwikkelde methode nauwkeurige resultaten leveren, de analysetijd verminderen en de handmatige interactie minimaliseren.

Kwantificatie van de aortaklep verkalking speelt een belangrijke rol in de prognose van hart- en vaatziekten. De mate van verkalking is ook gerelateerd aan het voorkomen van kleplekken na TAVI. Om de aanwezigheid en omvang van de aortaklep verkalking te bepalen, is in Hoofdstuk 6 een volledig automatische aanpak ontwikkeld. De kalk op de klep werd gesegmenteerd door het drempelen van het beeld na de segmentatie van de aortawortel en de reconstructie van het dubbel-schuine aanzicht van de aortaklep. Daarna werd het kalkvolume score berekend. Om de geautomatiseerde scores te valideren, werden 68 CTA-datasets van patiënten met het vermoeden van coronaire hartziekte gebruikt. De referentiestandaard was het kalkvolume score die half automatisch door een cardioloog werd verkregen met een ander, handmatige kalk annotatie software. De nauwkeurigheid van onze aanpak werd vastgesteld door deze te vergelijken met de referentienorm. Het mediane verschil was $1,82$ mm³ (25ste-75ste percentiel: 0 tot $5,08$ mm³), met een Spearman rangcorrelatiecoëfficiënt van 0,81 ($p < 0,001$). De Bland-Altman analyse toonde aan dat het systematisch verschil tussen de automatische en de referentiestandaard $-1,1$ mm³ was met een grenswaarde van $-16,2$ en $+14,1$ mm³. De specificiteit van onze automatische aanpak was 82,4%; De gevoeligheid was 85,3%. De gemiddelde verwerkingstijd was 90 seconden. Hiermee hebben we aangetoond dat een nieuwe, volledig automatische aanpak voor het kwantificeren van kalk van de aortaklep haalbaar is.

De aorta is de hoofdvoorziening van bloed in het menselijk lichaam en speelt een sleutelrol in het controleren van de vaatweerstand en de hartslag. CT beeldvorming is belangrijk bij de diagnose en preoperatieve planning van patiënten met een aorta ziekte. Om een aorta ziekte te kunnen bekijken met behulp van CT, zijn afbeeldingen van dezelfde patiënt op verschillende

tijdstippen nodig, evenals gestandaardiseerde meetprotocollen en geautomatiseerde kwantificatietools om systematische en willekeurige fouten te minimaliseren. In hoofdstuk 7 introduceerden we een automatisch aorta verwijding kwantificering methode. Deze methode werkt als volgt: eerst wordt de thoracale aorta automatisch gesegmenteerd uit het initiële CTA-beeld. Vervolgens wordt het vervolgbeeld automatisch uitgelijnd op het basisbeeld door middel van rigide en affine beeldregistratie. Daarna wordt de contour van de thoracale aorta in het opvolgende CTA-beeld met de contour in het initiële CTA-beeld uitgelijnd door de initiële contour te vervormen. Tenslotte worden de meetposities langs de thoracale aorta handmatig gedefinieerd en worden de maximale diameters op deze locaties in het initiële en de vervolgfbeeldingen berekend. In een validatie studie met CT data van 29 patiënten waren de intraclass correlaties van de maximale diameters hoger dan 0,90; De gemiddelde verschillen tussen de manuele meting en de automatische meting van verschillende herkenningspunten waren allemaal lager dan 2 mm, behalve bij de middelste aorta-boog en de sinotubulaire aansluiting.

Samengevat presenteerde dit proefschrift verschillende volledig automatische algoritmes voor de preoperatieve planning van de TAVR procedures, inclusief de grootte van de vasculaire toegang en de aortawortel, de locatie definitie van de aortaklep ring, de bepaling van de optimale hoek van de C- Arm röntgenprojectie en de kwantificering van de aortaklep kalk score. Ook werd een algoritme ontwikkeld voor de automatische kwantificatie van thoracale aorta verwijding. Voor al deze ontwikkelingen werd een klinisch aanvaardbare nauwkeurigheid aangetoond vergeleken met expert getekende referentienormen, terwijl de analyse tijd en inspanning aanzienlijk werden verminderd.

9.2 Discussie en toekomstig werk

TAVR is een innovatieve cardiovasculaire interventieprocedure die in de afgelopen jaren is ontwikkeld. De succesvolle planning van TAVR vereist nauwkeurige en reproduceerbare metingen van de vasculaire toegang en aortawortel. Als een 3D-modaliteit met hoge resolutie, biedt CT een uitgebreide visualisatie en nauwkeurige kwantificering van de vasculaire toegang en aortawortel.

In dit proefschrift wordt volautomatische preoperatieve planning door CT-beelden besproken en is aangetoond dat ze accuraat zijn. De uitgevoerde validatiestudie voor de aortawortel was echter beperkt: de grootte van de aortaklep ring werd gekwantificeerd en gevalideerd, maar geen andere belangrijke oriëntatie vlakken werden gevalideerd. Hoewel de aortaklep ring

parameters de belangrijkste zijn voor de prothese selectie, kunnen andere oriëntatie vlakken zoals het sinotubulaire knooppunt, het linker ventrikel uitstromingskanaal en de sinus van valsalva extra nuttige informatie verschaffen.

In de huidige studie werden alleen diastolische beelden gemeten, terwijl in de klinische beeldvorming de hele hartcyclus nuttig kan zijn. Er wordt nog onderzocht welke fasen geschikt zijn voor aortaklep ring meting en andere oriëntatie vlakken. Een verdere beperking van dit werk is het feit dat we de robuustheid van de gepresenteerde benaderingen niet kunnen onderzoeken met betrekking tot alle belangrijke CT-leveranciers. Afbeeldingen van meerdere leveranciers zijn in onze studie opgenomen, maar er zijn nog enkele leveranciers niet getest. Daarom kan toekomstig werk de huidige studie verder aanvullen door zich te concentreren op andere oriëntatie vlakken, beelden van meerdere hartfasen en de robuustheid tussen verschillend CT-leveranciers.

Aangezien bioprothetische klep ongeveer 10-20 jaar meegaat, hebben de reeds behandelde patiënten de mogelijkheid om een "klep in de klep" behandeling te ondergaan. Omdat een tweede hartoperatie voor een patiënt vrij risicovol kan zijn, kan TAVR een goed alternatief bieden. In die gevallen verschijnt de vorige bioprothetische klep als een heldere structuur binnen de aortawortel in het CT-beeld. Dit zal de meting van de aortaklep ring en de andere oriëntatie vlakken moeilijker maken. In de toekomst is het belangrijk om te testen of onze automatische algoritmen voor preoperatieve planning kunnen worden gegeneraliseerd naar "ventiel-in-vent" procedures. Naast vervanging van de aortaklep is het ook belangrijk om de preoperatieve planning van andere hartkleppen te automatiseren tijdens de trans-katheter klep vervanging, zoals de mitraalklep, de pulmonaalklep en de tricuspidaalklep. De minimale invasieve operatie van deze kleppen is pas in de afgelopen jaren succesvol geïmplementeerd. Er zijn nog steeds onzekerheden en moeilijkheden voor de artsen zonder ervaring om peroperatieve planning te doen. In het bijzonder; de mitraalklep heeft een andere anatomische structuur dan de andere kleppen, aangezien het slechts twee klepdelen heeft, terwijl de anderen drie hebben. Als zodanig is een alternatieve segmentatie- en kwantificeringsbenadering van deze andere kleppen nodig voor de prothese selectie en het plaatsen van deze kleppen.

Dit proefschrift richt zich vooral op metingen op basis van beeldsegmentatie. Voor preoperatieve planning van TAVR is deze kwantificatie vanuit anatomisch perspectief belangrijk, maar er zijn ook andere problemen die aandacht verdienen om complicaties te verminderen.

Aortaklep lekken is een van de belangrijkste factoren die het uiteindelijke resultaat van TAVR beïnvloeden. Het kan worden veroorzaakt door onjuiste grootte, verkeerde plaatsing of onvolledige expansie van de prothese tijdens TAVR. Simulatie van de prothese-implantatieprocedure kan bijdragen aan het voorspellen van aortaklep lekken na de TAVR en heeft derhalve de mogelijkheid om de selectie, plaatsing en expansie van de prothese te verbeteren. Bovendien kan het ontwerp van de prothese worden verbeterd door de mechanische parameters tijdens simulatie aan te passen. De gepersonaliseerde aortawortel modellen beschreven in hoofdstuk 4 kunnen gebruikt worden als input voor dergelijke simulatiemodellen, wat uiteindelijk kan leiden tot de vermindering van het sterftcijfer van TAVR. Niet alleen voor de aortaklep, de simulatie van trans-katheter vervanging zal ook nuttig zijn voor de andere kleppen.

Wat betreft de directe evaluatie van het aortaklep lekken bij patiënten, speelt echocardiografie een belangrijke rol. Echocardiografie kan de hemodynamische verandering tijdens de TAVR visualiseren door meerdere modaliteiten te gebruiken zoals Doppler en Transoesofagale echocardiografie, waardoor het mechanisme van het aortaklep lekken, zoals de onder expansie of verkeerde plaatsing van de prothese, wordt getoond. De ernst van aortaklep lekken kan ook gekwantificeerd worden en gebruikt worden om klinische beslissingen te nemen. De combinatie van meerdere beeldmodaliteiten maakt TAVR een betrouwbare techniek.

Bibliography

- Abdel-Wahab, Mohamed et al. 2014. “Comparison of Balloon-Expandable vs Self-Expandable Valves in Patients Undergoing Transcatheter Aortic Valve Replacement: The CHOICE Randomized Clinical Trial.” *Jama* 311(15): 1503–14.
- Achenbach, Stephan et al. 2012. “SCCT Expert Consensus Document on Computed Tomography Imaging before Transcatheter Aortic Valve Implantation (TAVI)/transcatheter Aortic Valve Replacement (TAVR).” *Journal of Cardiovascular Computed Tomography* 6(6): 366–80.
- Adalsteinsson, David, and James A Sethian. 1995. “A Fast Level Set Method for Propagating Interfaces.” *Journal of computational physics* 118(2): 269–77.
- Agarwal, Shikhar et al. 2015. “Transcatheter Aortic Valve Replacement: Current Perspectives and Future Implications.” *Heart (British Cardiac Society)* 101(3): 169–77.
- Agatston, Arthur S et al. 1990. “Quantification of Coronary Artery Calcium Using Ultrafast Computed Tomography.” *Journal of the American College of Cardiology* 15(4): 827–32.
- Bapat, Vinayak et al. 2016. “Transcatheter Aortic Valve Replacement Using Transaortic Access: Experience from the Multicenter, Multinational, Prospective ROUTE Registry.” *JACC: Cardiovascular Interventions* 9(17): 1815–22.
- Bax, Jeroen J. et al. 2014. “Open Issues in Transcatheter Aortic Valve Implantation. Part 1: Patient Selection and Treatment Strategy for Transcatheter Aortic Valve Implantation.” *European heart journal* 35(38): 2627–38.
- Bertaso, Angela G. et al. 2012. “Aortic Annulus Dimension Assessment by Computed Tomography for Transcatheter Aortic Valve Implantation: Differences between Systole and Diastole.” *International Journal of Cardiovascular Imaging* 28(8): 2091–98.
- Bettinger, Nicolas et al. 2015. “TCT-327 Calcium Volume Score on Contrast-Enhanced Computed Tomography Prior to Transcatheter Aortic Valve Replacement: What’s the Most Accurate Threshold Cutoff?” *Journal of the American College of Cardiology* 15(66): B131.
- Biesdorf, Andreas et al. 2012. “Segmentation and Quantification of the Aortic Arch Using Joint 3D Model-Based Segmentation and Elastic Image Registration.” *Medical Image Analysis* 16(6): 1187–1201. <http://dx.doi.org/10.1016/j.media.2012.05.010>.

- Binder, Ronald K. et al. 2012. "Prediction of Optimal Deployment Projection for Transcatheter Aortic Valve Replacement: Angiographic 3-Dimensional Reconstruction of the Aortic Root versus Multidetector Computed Tomography." *Circulation: Cardiovascular Interventions* 5(2): 247–52.
- Blanke, Philipp et al. 2012. "Conformational Pulsatile Changes of the Aortic Annulus: Impact on Prosthesis Sizing by Computed Tomography for Transcatheter Aortic Valve Replacement." *JACC: Cardiovascular Interventions* 5(9): 984–94.
- Bleiziffer, S et al. 2013. "Which Way in? The Necessity of Multiple Approaches to Transcatheter Valve Therapy." *Current cardiology reviews* 9(4): 268–73.
- Carabello, Blase A. 2002. "Evaluation and Management of Patients with Aortic Stenosis." *Circulation* 105(15): 1746–50.
- Cribier, Alain G. 2014. "The Odyssey of TAVR from Concept to Clinical Reality." *Texas Heart Institute Journal* 41(2): 125–30.
- Cueff, Caroline et al. 2010. "Measurement of Aortic Valve Calcification Using Multislice Computed Tomography: Correlation with Haemodynamic Severity of Aortic Stenosis and Clinical Implication for Patients with Low Ejection Fraction." *Heart: hrt-2010*.
- Davidson, Michael J, Frederick G P Welt, and Andrew C Eisenhauer. 2011. "Percutaneous Balloon-Expandable Aortic Valve Implantation: Transfemoral." *Operative Techniques in Thoracic and Cardiovascular Surgery* 16(1): 30–40.
- Davies, Ryan R. et al. 2002. "Yearly Rupture or Dissection Rates for Thoracic Aortic Aneurysms: Simple Prediction Based on Size." *Annals of Thoracic Surgery* 73(1): 17–28.
- Delgado, Victoria et al. 2010. "Multimodality Imaging in Transcatheter Aortic Valve Implantation: Key Steps to Assess Procedural Feasibility." *EuroIntervention* 6(5): 643–52.
- . 2011. "Automated Assessment of the Aortic Root Dimensions with Multidetector Row Computed Tomography." *The Annals of thoracic surgery* 91(3): 716–23.
- Deza, Michel Marie, and Elena Deza. 2009. "Encyclopedia of Distances." In *Encyclopedia of Distances*, Springer, 1–583.

- Dijkstra, Edsger W. 1959. "A Note on Two Problems in Connexion with Graphs." *Numerische mathematik* 1(1): 269–71.
- Dugas, Alexandre et al. 2012. "Reproducibility of Abdominal Aortic Aneurysm Diameter Measurement and Growth Evaluation on Axial and Multiplanar Computed Tomography Reformations." *Cardiovascular and interventional radiology* 35(4): 779–87.
- Ecabert, Olivier et al. 2011. "Segmentation of the Heart and Great Vessels in CT Images Using a Model-Based Adaptation Framework." *Medical Image Analysis* 15(6): 863–76. <http://dx.doi.org/10.1016/j.media.2011.06.004>.
- Elattar, M a et al. 2014. "Automatic Segmentation of the Aortic Root in CT Angiography of Candidate Patients for Transcatheter Aortic Valve Implantation." *Medical & biological engineering & computing* 52(7): 611–18. <http://www.ncbi.nlm.nih.gov/pubmed/24903606>.
- Elattar, Mustafa et al. 2016. "Automatic Aortic Root Landmark Detection in CTA Images for Preprocedural Planning of Transcatheter Aortic Valve Implantation." *International Journal of Cardiovascular Imaging* 32(3): 501–11.
- Entezari, Pegah et al. 2013. "Analysis of the Thoracic Aorta Using a Semi-Automated Post Processing Tool." *European Journal of Radiology* 82(9): 1558–64. <http://dx.doi.org/10.1016/j.ejrad.2013.03.024>.
- Erbel, R. et al. 2014a. "2014 ESC Guidelines on the Diagnosis and Treatment of Aortic Diseases: Document Covering Acute and Chronic Aortic Diseases of the Thoracic and Abdominal Aorta of the Adult. The Task Force for the Diagnosis and Treatment of Aortic Diseases of the European." *European Heart Journal* 35(41): 2873–2926.
- . 2014b. "2014 ESC Guidelines on the Diagnosis and Treatment of Aortic Diseases: Document Covering Acute and Chronic Aortic Diseases of the Thoracic and Abdominal Aorta of the Adult * The Task Force for the Diagnosis and Treatment of Aortic Diseases of the European." *European Heart Journal* 35(41): 2873–2926.
- Ewe, See Hooi et al. 2011. "Location and Severity of Aortic Valve Calcium and Implications for Aortic Regurgitation after Transcatheter Aortic Valve Implantation." *The American journal of cardiology* 108(10): 1470–77.

- El Faquir, Nahid et al. 2016. "Definition of the Aortic Valve Plane by Means of a Novel Dedicated Software Program: Proof of Concept and Validation with Multi Slice Computed Tomography." *International Journal of Diagnostic Imaging* 3(1): p63.
- Foldyna, Borek et al. 2015. "CT Evaluation prior to Transapical Aortic Valve Replacement: Semi-Automatic versus Manual Image Segmentation." *The international journal of cardiovascular imaging* 31(6): 1233–42.
- Gao, Xinpei et al. 2014. "Automatic Extraction of Arterial Centerline from Whole-Body Computed Tomography Angiographic Datasets." In *Computing in Cardiology 2014*, IEEE, 697–700.
- Gao, Xinpei, Pieter Kitslaar, Arthur J H A Scholte, et al. 2016. "Automatic Aortic Root Segmentation in CTA Whole-Body Dataset." In *SPIE Medical Imaging*, International Society for Optics and Photonics, 97850F–97850F.
- Gao, Xinpei, Pieter H Kitslaar, Ricardo P J Budde, et al. 2016. "Automatic Detection of Aorto-Femoral Vessel Trajectory from Whole-Body Computed Tomography Angiography Data Sets." *The international journal of cardiovascular imaging* 32(8): 1311–22.
- Goenka, Ajit H., Paul Schoenhagen, Michael A. Bolen, and Milind Y. Desai. 2014. "Multidimensional MDCT Angiography in the Context of Transcatheter Aortic Valve Implantation." *American Journal of Roentgenology* 203(4): 749–58.
- Goldstein, Steven a et al. 2015. "Multimodality Imaging of Diseases of the Thoracic Aorta in Adults: From the American Society of Echocardiography and the European Association of Cardiovascular Imaging." *Journal of the American Society of Echocardiography : official publication of the American Society of Echocardiography* 28(2): 119–82.
- de Graaf, Fleur R, Joanne D Schuijf, Joëlla E van Velzen, Lucia J Kroft, et al. 2010. "Diagnostic Accuracy of 320-Row Multidetector Computed Tomography Coronary Angiography in the Non-Invasive Evaluation of Significant Coronary Artery Disease." *European heart journal*: ehp571.
- de Graaf, Fleur R, Joanne D Schuijf, Joëlla E van Velzen, Mark J Boogers, et al. 2010. "Diagnostic Accuracy of 320-Row Multidetector Computed Tomography Coronary Angiography to Noninvasively Assess in-Stent Restenosis." *Investigative radiology* 45(6): 331–40.

- Grbic, Sasa et al. 2012. "Complete Valvular Heart Apparatus Model from 4D Cardiac CT." *Medical Image Analysis* 16(5): 1003–14. <http://dx.doi.org/10.1016/j.media.2012.02.003>.
- . 2013. "ADVANCED INTERVENTION PLANNING FOR TRANSCATHETER AORTIC VALVE IMPLANTATIONS (TAVI) FROM CT USING VOLUMETRIC MODELS Imaging and Computer Vision , Corporate Technology , Princeton , USA Computer Aided Medical Procedures , Technical University Munich , Ger." : 1416–19.
- Gülsün, M Akif, and Hüseyin Tek. 2008. "Robust Vessel Tree Modeling." In *Medical Image Computing and Computer-Assisted Intervention--MICCAI 2008*, Springer, 602–11.
- Gurvitch, Ronen et al. 2010. "Multislice Computed Tomography for Prediction of Optimal Angiographic Deployment Projections during Transcatheter Aortic Valve Implantation." *JACC: Cardiovascular Interventions* 3(11): 1157–65.
- Hall, John E. 2015. *Guyton and Hall Textbook of Medical Physiology*. Elsevier Health Sciences.
- Hanneman, Kate et al. 2015. "Pre-and Postoperative Imaging of the Aortic Root." *RadioGraphics* 36(1): 19–37.
- De Heer, Linda M. et al. 2011. "Aortic Root Dimension Changes during Systole and Diastole: Evaluation with ECG-Gated Multidetector Row Computed Tomography." *International Journal of Cardiovascular Imaging* 27(8): 1195–1204.
- Hiratzka, L. F. et al. 2010. "2010 ACCF/AHA/AATS/ACR/ASA/SCA/SCAI/SIR/STS/SVM Guidelines for the Diagnosis and Management of Patients With Thoracic Aortic Disease: A Report of the American College of Cardiology Foundation/American Heart Association Task Force on Practice Guidelines." *Circulation* 121(13): e266–369.
- Ho, Siew Yen. 2009. "Structure and Anatomy of the Aortic Root." *European Heart Journal-Cardiovascular Imaging* 10(1): i3–10.
- Iglesias, Juan Eugenio, and Mert R. Sabuncu. 2015. "Multi-Atlas Segmentation of Biomedical Images: A Survey." *Medical Image Analysis* 24(1): 205–19.
- Ihara, Tsutomu et al. 2013. "Three-Dimensional Workstation Is Useful for Measuring the Correct Size of Abdominal Aortic Aneurysm Diameters." *Annals of vascular surgery* 27(2): 154–61.

- Ionasec, Razvan Ioan et al. 2010. "Patient-Specific Modeling and Quantification of the Aortic and Mitral Valves from 4-D Cardiac CT and TEE." *Medical Imaging, IEEE Transactions on* 29(9): 1636–51.
- Jilaihawi, Hasan et al. 2014. "A Revised Methodology for Aortic-Valvar Complex Calcium Quantification for Transcatheter Aortic Valve Implantation." *European Heart Journal-Cardiovascular Imaging* 15(12): 1324–32.
- Kamperidis, Vasileios et al. 2014. "Prognostic Value of Aortic and Mitral Valve Calcium Detected by Contrast Cardiac Computed Tomography Angiography in Patients with Suspicion of Coronary Artery Disease." *The American journal of cardiology* 113(5): 772–78. <http://www.scopus.com/inward/record.url?eid=2-s2.0-84893959286&partnerID=tZOtx3y1>.
- Kasel, Albert M. et al. 2013. "Standardized Imaging for Aortic Annular Sizing: Implications for Transcatheter Valve Selection." *JACC: Cardiovascular Imaging* 6(2): 249–62.
- Kauffmann, Claude et al. 2011. "Clinical Validation of a Software for Quantitative Follow-up of Abdominal Aortic Aneurysm Maximal Diameter and Growth by CT Angiography." *European Journal of Radiology* 77(3): 502–8.
- . 2012. "Measurements and Detection of Abdominal Aortic Aneurysm Growth: Accuracy and Reproducibility of a Segmentation Software." *European Journal of Radiology* 81(8): 1688–94.
- Kirişli, H. A. et al. 2010. "Evaluation of a Multi-Atlas Based Method for Segmentation of Cardiac CTA Data: A Large-Scale, Multicenter, and Multivendor Study." *Medical Physics* 37(12): 6279–91.
- Kirişli, H a et al. 2010. "Evaluation of a Multi-Atlas Based Method for Segmentation of Cardiac CTA Data: A Large-Scale, Multicenter, and Multivendor Study." *Medical physics* 37(12): 6279–91.
- Kitslaar, Pieter H. et al. 2015. "Segmentation of Branching Vascular Structures Using Adaptive Subdivision Surface Fitting." In , 94133Z. <http://proceedings.spiedigitallibrary.org/proceeding.aspx?doi=10.1117/12.2082222>.
- Klein, S et al. 2010. "<emphasis Emphasistype='mono'>elastix</emphasis>: A Toolbox for Intensity-Based Medical Image Registration." *IEEE Transactions on Medical Imaging* 29(1): 196–205.

- Krishnaswamy, Amar et al. 2014. "Predicting Vascular Complications during Transfemoral Transcatheter Aortic Valve Replacement Using Computed Tomography: A Novel Area-Based Index." *Catheterization and Cardiovascular Interventions* 84(5): 844–51.
- Kurra, Vikram et al. 2009. "Prevalence of Significant Peripheral Artery Disease in Patients Evaluated for Percutaneous Aortic Valve Insertion: Preprocedural Assessment with Multidetector Computed Tomography." *Journal of Thoracic and Cardiovascular Surgery* 137(5): 1258–64.
- . 2010. "Pre-Procedural Imaging of Aortic Root Orientation and Dimensions. Comparison Between X-Ray Angiographic Planar Imaging and 3-Dimensional Multidetector Row Computed Tomography." *JACC: Cardiovascular Interventions* 3(1): 105–13. <http://dx.doi.org/10.1016/j.jcin.2009.10.014>.
- Lardizabal, Joel A et al. 2013. "The Transaortic Approach for Transcatheter Aortic Valve Replacement: Initial Clinical Experience in the United States." *Journal of the American College of Cardiology* 61(23): 2341–45.
- Leipsic, Jonathon et al. 2011. "Multidetector Computed Tomography in Transcatheter Aortic Valve Implantation." *JACC: Cardiovascular Imaging* 4(4): 416–29.
- Lesage, David, Elsa D. Angelini, Isabelle Bloch, and Gareth Funka-Lea. 2009. "A Review of 3D Vessel Lumen Segmentation Techniques: Models, Features and Extraction Schemes." *Medical Image Analysis* 13(6): 819–45.
<http://dx.doi.org/10.1016/j.media.2009.07.011>.
- Loop, Charles. 1987. "Smooth Subdivision Surfaces Based on Triangles."
- Lorensen, William E., and Harvey E. Cline. 1987. "Marching Cubes: A High Resolution 3D Surface Construction Algorithm." *Proceedings of the 14th annual conference on Computer graphics and interactive techniques - SIGGRAPH '87* 21(4): 163–69.
- Lou, Junyang et al. 2015. "Manual, Semiautomated, and Fully Automated Measurement of the Aortic Annulus for Planning of Transcatheter Aortic Valve Replacement (TAVR/TAVI): Analysis of Interchangeability." *Journal of Cardiovascular Computed Tomography* 9(1): 42–49.
- Lu, T.-L. C. et al. 2010. "Variability of Ascending Aorta Diameter Measurements as Assessed with Electrocardiography-Gated Multidetector Computerized Tomography and

- Computer Assisted Diagnosis Software.” *Interactive CardioVascular and Thoracic Surgery* 10(2): 217–21.
- Mack, Michael J. 2012. “Access for Transcatheter Aortic Valve Replacement: Which Is the Preferred Route? ** Editorials Published in JACC: Cardiovascular Interventions Reflect the Views of the Authors and Do Not Necessarily Represent the Views of JACC: Cardiovascular Interventions.”
- . 2015. “5-Year Outcomes of Transcatheter Aortic Valve Replacement or Surgical Aortic Valve Replacement for High Surgical Risk Patients with Aortic Stenosis (PARTNER 1): A Randomised Controlled Trial.” *The Lancet* 385(9986): 2477–84.
- Mann, Douglas L, Douglas P Zipes, Peter Libby, and Robert O Bonow. 2014. *Braunwald’s Heart Disease: A Textbook of Cardiovascular Medicine*. Elsevier Health Sciences.
- Mao, Song Shou et al. 2008. “Normal Thoracic Aorta Diameter on Cardiac Computed Tomography in Healthy Asymptomatic Adults: Impact of Age and Gender.” *Academic radiology* 15(7): 827–34.
- Metz, C T et al. 2009. “Coronary Centerline Extraction from CT Coronary Angiography Images Using a Minimum Cost Path Approach.” *Medical physics* 36(12): 5568–79.
- Müller-Eschner, M. et al. 2013. “Accuracy and Variability of Semiautomatic Centerline Analysis versus Manual Aortic Measurement Techniques for TEVAR.” *European Journal of Vascular and Endovascular Surgery* 45(3): 241–47.
<http://dx.doi.org/10.1016/j.ejvs.2012.12.003>.
- Nishimura, Rick A. 2002. “Aortic Valve Disease.” *Circulation* 106(7): 770–72.
- Nkomo, Vuyisile T et al. 2006. “Burden of Valvular Heart Diseases: A Population-Based Study.” *The Lancet* 368(9540): 1005–11.
- Okuyama, Kazuaki et al. 2014. “Transfemoral Access Assessment for Transcatheter Aortic Valve Replacement: Evidence-Based Application of Computed Tomography over Invasive Angiography.” *Circulation: Cardiovascular Imaging* 8(1).
- . 2015. “Transfemoral Access Assessment for Transcatheter Aortic Valve Replacement CLINICAL PERSPECTIVE.” *Circulation: Cardiovascular Imaging* 8(1): e001995.

- Owens, David S et al. 2012. "Aortic Valve Calcium Independently Predicts Coronary and Cardiovascular Events in a Primary Prevention Population." *JACC: Cardiovascular Imaging* 5(6): 619–25.
- Park, Joo Young, Tim McInerney, Demetri Terzopoulos, and Myoung Hee Kim. 2001. "A Non-Self-Intersecting Adaptive Deformable Surface for Complex Boundary Extraction from Volumetric Images." *Computers and Graphics (Pergamon)* 25(3): 421–40.
- Queirós, Sandro et al. 2016. "Automatic 3D Aortic Annulus Sizing by Computed Tomography in the Planning of Transcatheter Aortic Valve Implantation." *Journal of Cardiovascular Computed Tomography* 11(1): 25–32.
- Quint, Leslie E. et al. 2013. "Proximal Thoracic Aortic Diameter Measurements at CT: Repeatability and Reproducibility according to Measurement Method." *The International Journal of Cardiovascular Imaging* 29(2): 479–88.
- Rengier, Fabian et al. 2009. "Centerline Analysis of Aortic CT Angiographic Examinations: Benefits and Limitations." *American Journal of Roentgenology* 192(5): 255–63.
- Rueckert, Daniel et al. 1999. "Nonrigid Registration Using Free-Form Deformations: Application to Breast MR Images." *IEEE transactions on medical imaging* 18(8): 712–21.
- Rutten, Annemarieke, Ivana Isgum, and Mathias Prokop. 2008. "Coronary Calcification: Effect of Small Variation of Scan Starting Position on Agatston, Volume, and Mass Scores 1." *Radiology* 246(1): 90–98.
- Samim, Mariam et al. 2013. "Automated 3D Analysis of Pre-Procedural MDCT to Predict Annulus Plane Angulation and C-Arm Positioning: Benefit on Procedural Outcome in Patients Referred for TAVR." *JACC: Cardiovascular Imaging* 6(2): 238–48.
<http://dx.doi.org/10.1016/j.jcmg.2012.12.004>.
- Sampson, Uchechukwu K A et al. 2014. "Global and Regional Burden of Aortic Dissection and Aneurysms: Mortality Trends in 21 World Regions, 1990 to 2010." *Global Heart* 9(1): 171–80.
- Sawaya, Fadi et al. 2012. "Aortic Stenosis: A Contemporary Review." *Am J Med Sci* 343(6): 490–96.

- Schaap, Michiel et al. 2009. "Standardized Evaluation Methodology and Reference Database for Evaluating Coronary Artery Centerline Extraction Algorithms." *Medical Image Analysis* 13(5): 701–14.
- Schoenhagen, Paul, Samir R Kapadia, et al. 2011. "Computed Tomography Evaluation for Transcatheter Aortic Valve Implantation (TAVI): Imaging of the Aortic Root and Iliac Arteries." *Journal of cardiovascular computed tomography* 5(5): 293–300.
- Schoenhagen, Paul, Jörg Hausleiter, et al. 2011. "Computed Tomography in the Evaluation for Transcatheter Aortic Valve Implantation (TAVI)." *Cardiovascular diagnosis and therapy* 1(1): 44–56.
- Shahzad, Rahil et al. 2013. "Automatic Segmentation, Detection and Quantification of Coronary Artery Stenoses on CTA." *The international journal of cardiovascular imaging*. <http://www.ncbi.nlm.nih.gov/pubmed/23925713>.
- Shapiro, Samuel Sanford, and Martin B Wilk. 1965. "An Analysis of Variance Test for Normality (Complete Samples)." *Biometrika* 52(3–4): 591–611.
- Shlens, Jonathon. 2014. "A Tutorial on Principal Component Analysis." *arXiv preprint arXiv:1404.1100*.
- Sinning, J.-M. et al. 2013. "Evaluation and Management of Paravalvular Aortic Regurgitation after Transcatheter Aortic Valve Replacement." *Journal of the American College of Cardiology* 62(1): 11–20.
<http://www.embase.com/search/results?subaction=viewrecord&from=export&id=L369182754%5Cnhttp://dx.doi.org/10.1016/j.jacc.2013.02.088>.
- Steigner, Michael L et al. 2010. "Iodinated Contrast Opacification Gradients in Normal Coronary Arteries Imaged with Prospectively ECG-Gated Single Heart Beat 320-Detector Row Computed Tomography." *Circulation: Cardiovascular Imaging* 3(2): 179–86.
- Stortecky, Stefan et al. 2014. "Accuracy and Reproducibility of Aortic Annulus Sizing Using a Dedicated Three-Dimensional Computed Tomography Reconstruction Tool in Patients Evaluated for Transcatheter Aortic Valve Replacement." *EuroIntervention* 10(3): 339–46.

- Thévenaz, Philippe, and Michael Unser. 2000. "Optimization of Mutual Information for Multiresolution Image Registration." *IEEE transactions on image processing* 9(12): 2083–99.
- Toggweiler, Stefan et al. 2013. "Management of Vascular Access in Transcatheter Aortic Valve Replacement: Part 2: Vascular Complications." *JACC: Cardiovascular Interventions* 6(8): 767–76.
- Tzikas, Apostolos et al. 2010. "Optimal Projection Estimation for Transcatheter Aortic Valve Implantation Based on Contrast-Aortography: Validation of a Prototype Software." *Catheterization and Cardiovascular Interventions* 76(4): 602–7.
- Underwood, M J et al. 2000. "The Aortic Root: Structure, Function, and Surgical Reconstruction." *Heart* 83(4): 376 LP-380.
- Vahl, Torsten P, Susheel K Kodali, and Martin B Leon. 2016. "Transcatheter Aortic Valve Replacement 2016." *Journal of the American College of Cardiology* 67(12): 1472–87.
- van't Klooster, Ronald et al. 2012. "Automatic Lumen and Outer Wall Segmentation of the Carotid Artery Using Deformable Three-Dimensional Models in MR Angiography and Vessel Wall Images." *Journal of Magnetic Resonance Imaging* 35(1): 156–65.
- Wächter, Irina et al. 2010. "Patient Specific Models for Planning and Guidance of Minimally Invasive Aortic Valve Implantation." In *International Conference on Medical Image Computing and Computer-Assisted Intervention*, Springer, 526–33.
- Watanabe, Yusuke et al. 2013. "Automated 3-Dimensional Aortic Annular Assessment by Multidetector Computed Tomography in Transcatheter Aortic Valve Implantation." *JACC: Cardiovascular Interventions* 6(9): 955–64.
- Wendler, Olaf, and Rafal Dworakowski. 2014. "TAVI in Patients Unsuitable for Surgery: A Prognostic Benefit for All?" *Journal of the American College of Cardiology* 63(9): 912–13.
- Yang, Guanyu et al. 2012. "Automatic Centerline Extraction of Coronary Arteries in Coronary Computed Tomographic Angiography." *International Journal of Cardiovascular Imaging* 28(4): 921–33.
- Zajarias, Alan, and Alain G Cribier. 2009. "Outcomes and Safety of Percutaneous Aortic Valve Replacement." *Journal of the American College of Cardiology* 53(20): 1829–36.

Zheng, Yefeng et al. 2012. “Automatic Aorta Segmentation and Valve Landmark Detection in C-Arm CT for Transcatheter Aortic Valve Implantation.” *IEEE Transactions on Medical Imaging* 31(12): 2307–21.

10

Acknowledgements

About the author

Publications

Acknowledgements

The work in this thesis started from Oct 26th, 2012, under the supervision of Prof. dr. ir. Johan H. C. Reiber, Prof. dr. ir. Boudewijn P.F. Lelieveldt and Dr. ir. Jouke Dijkstra, located in the Department of Applied Research, Medis medical imaging systems bv, the Netherlands, and the Division of Imaging Processing (LKEB), Department of Radiology, Leiden University Medical Center.

Dear Hans, thanks for your enormous help, support and encouragement. I learnt how to do research, how to collaborate with others from you. You always notice the important point and have solution for all kinds of situations.

Dear Boudewijn, I want to express my respect to your generous, decent and honest character.

Dear Jouke, your nice advices always appeared at the best moment.

The technical side of the work is also helped with two persons: Pieter Kitslaar and Shengxian (Sanven) Tu.

Dear Pieter, thank you for knowledge of CT images, programming, and encouragement, the skill to communicate and help in moving. Also, patience to listen to questions from me and give reasonable suggestions.

Dear Sanven, you are the one helped me to set up the base of work and life in Netherlands, give smart and critical advice. Your serious attitude, efficiency in work, quick reaction and hard-working are really impressvie.

For the validation of the methods, I was helped by multiple physicians.

Ricardo, thanks for your selfless support. I understand that you are already busy with your clinical work, but you always answer my questions after that. And you also inspired me a lot from clinical side.

Sara, I admire your board clinical knowledge, high efficiency, always help me with datasets, contours. We discuss with coffee and apple dessert, adding as much sugar as possible, which is really good time for me.

Also thanks to Mohamed, Arthur and Michiel, Bo Xu and Liang Xu, Martin and Tomas.

I would like to express my thankfulness to people in Medis. Yingguang, it is nice to know you here to share feelings about PhD and life. And thanks to Joan for advices in statistical analysis and dutch life. Also thanks to David, for very useful clinical feedbacks. Shufang, nice to have

you to spend the shopping and dinner times together. Kees, for advices about both research and development. Jasper, for help in algorithms. Linna, I enjoyed small shopping with you. Paulo, for help in all IT issues. And Bob, Daniel, EelcoG, EelcoV, Kevin, Gert-Jan, Gerhard, Guido, Marcel, MarcoG, MarcoL, Sylvia, Yuko, and all the others if I forgot to mention, really nice to meet you here.

Besides, I am also grateful to people in LKEB. Alex, I remember your help in my paper and your nice coffee. Patrick, for your coffee in the morning and reminder during lunch. Niels, I had interesting and friendly discussions with you about daily life. Jeroen, thanks for explanation in general PhD related questions. Qian, Shan, Yuchuan, Nancy, Qing, Zhuo, and Zhiwei: Qian, for nice advices; Yuchuan, your knowledge about registration, generous dinner, excellent cooking skills are really impressive, also your hard-working, always being so helpful and decent. Shan, thank you for nice lunch and dinner times, wish you all the best in UK. Nancy, thanks for the mature advices about life. Qing, you are always a great supporter. Zhuo, discussion with you broaden my mind in research and life. Zhiwei, your sunny smile is nice. Also thanks to others I met, Baldur for your help in correcting gramma in my paper; Denis, for help in Elastix; Leo, for casual discussions from music to politics; Marius, for advices in registration; Rahil, for the advice in algorithm; Zhenia, for downloading papers for me. Ahmed, Berend, Els, Floris, Michiel, Oleh, Pauline, Rob, Walid, and all the others if I forgot to mention, it is really nice to meet you here.

Finally, thanks to my friends here and in China, my parents. Father and mother, you are the best.

Xinpei Gao

Leiden, November 2017

About the author

Xinpei Gao was born in Jiangsu, China on 1987. After high school, she started studying the department of Biomedical Engineering in Southeast University in Nanjing, China. The department aims to train students in both biomedical and engineering fields. She received the bachelor degree in June 2009. In the same year, she was recommended to be a master student in the same department. During her master period, she also did internship in China Academy of Science (CAS), Suzhou Institute of Biomedical Engineering and Technology (SIBET). After graduation, she worked as a PhD student at Applied research department of Medis BV., and Division of image processing (LKEB), Radiology, Leiden University Medical Center. She developed clinical applications for pre-operative planning of aorta-related disease in CTA images which end up in this thesis.

List of publications

Journal papers

Xinpei Gao, Pieter Kitslaar, Ricardo P.J. Budde, Shengxian Tu, Michiel A. de Graaf, Liang Xu, Bo Xu, Arthur J.H.A. Scholte, Jouke Dijkstra, Johan H.C. Reiber, Automatic detection of aorto-femoral vessel trajectory from whole-body computed tomography angiography data sets, *The international journal of cardiovascular imaging*. DOI: 10.1007/s10554-016-0901-5

Xinpei Gao, Sara Boccalini, Pieter Kitslaar, Ricardo P.J. Budde, Shengxian Tu, Michiel A. de Graaf, Tomas Ondrus, Martin Penicka, Arthur JHA Scholte, Boudewijn PF Lelieveldt, Jouke Dijkstra, Johan HC Reiber, Quantification of aortic annulus in computed tomography angiography: development and validation of a novel fully automatic methodology, *European Journal of Radiology*, 2017.

Xinpei Gao, Pieter Kitslaar, Michiel A. de Graaf, Alexander Broersen, Shengxian Tu, Boudewijn P.F. Lelieveldt, Arthur J.H.A. Scholte, Jouke Dijkstra, Johan H.C. Reiber, Fully automatic volume quantification of aortic valve calcium in coronary computed tomography angiography, *Cardiovascular Diagnosis and Therapy*, 2017.

Xinpei Gao, Sara Boccalini, Pieter H. Kitslaar, Ricardo P.J. Budde, Shengxian Tu, Boudewijn P.F. Lelieveldt, Jouke Dijkstra, Johan H.C. Reiber, Automatic detection of aortic dilatation in baseline and follow-up contrast enhanced computed tomography angiography – submitted to *European Radiology*.

Conference papers

Xinpei Gao, Pieter Kitslaar, Arthur J. H. A. Scholte, Boudewijn P. F. Lelieveldt, Jouke Dijkstra, Johan H. C. Reiber, "Automatic aortic root segmentation in CT: a whole-body dataset", *SPIE Medical Imaging 2016*

Xinpei Gao, Shengxian Tu, Michiel A de Graaf, Liang Xu, Pieter Kitslaar, Arthur JHA Scholte, Bo Xu, Johan HC Reiber, "Automatic Extraction of Arterial Centerline from Whole-body Computed Tomography Angiographic Datasets", *Computing in Cardiology 2014*

Abstracts

Xinpei Gao, Sara Boccalini, Pieter Kitslaar, Ricardo P J Budde, Johan HC Reiber, Validation of a novel fully automated aortic annulus measurement

algorithm in cardiac CT data sets, European Society of Cardiac Radiology annual scientific meeting 2016, **Young Abstract Presenter Programme**

Xinpei Gao, Pieter Kitslaar, Michiel de Graaf, Boudewijn P.F. Lelieveldt, Jouke Dijkstra, Johan H.C. Reiber, Aortic valve calcium measurement in contrast-enhanced cardiac CT images: Evaluation of a fully automatic method, European Congress of Radiology 2017

Sara Boccalini, **Xinpei Gao**, Pieter Kitslaar, Ricardo P J Budde, Johan HC Reiber, Automatic quantification and visualization of thoracic aorta diameters on successive CTA scans, European Society of Cardiac Radiology annual scientific meeting 2017